AD-A172 838 A HIGH FREQUENY ANALYSIS OF ELECTROMAGNETIC PLANE WAVE 1/2
SCATTERING BY A F. (U) AIR FORCE INST OF TECH
WRIGHT-PATTERSON AFB OH K D TROTT 1986
UNCLASSIFIED AFIT/CI/NR-86-186D F/G 20/6 NL

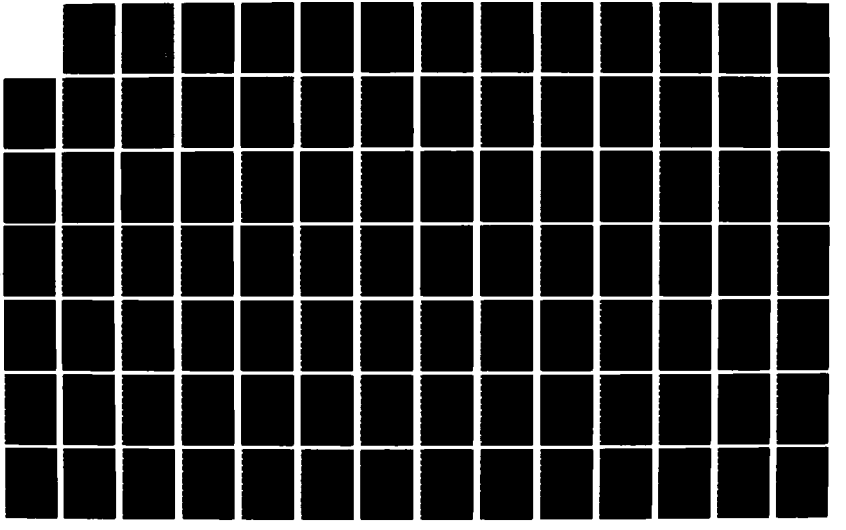

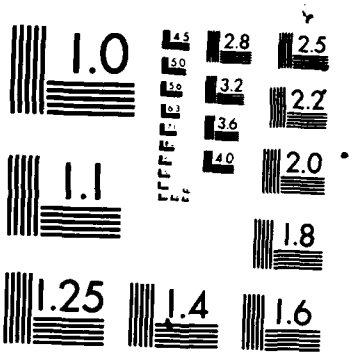

SECURITY CLASSIFICATION OF THIS PAGE *(When Data Entered)*

REPORT DOCUMENTATION PAGE

READ INSTRUCTIONS BEFORE COMPLETING FORM

1. REPORT NUMBER: AFIT/CI/NR 86-186D	2. GOVT ACCESSION NO.
3. RECIPIENT'S CATALOG NUMBER	
4. TITLE *(and Subtitle)*: A High Frequency Analysis of Electromagnetic Plane Wave Scattering By A Fully Illuminated Perfectly Conducting Semi-Infinite Cone	5. TYPE OF REPORT & PERIOD COVERED: THESIS/DISSERTATION
	6. PERFORMING ORG. REPORT NUMBER
7. AUTHOR(s): Keith Dennis Trott	8. CONTRACT OR GRANT NUMBER(s)
9. PERFORMING ORGANIZATION NAME AND ADDRESS: AFIT STUDENT AT: The Ohio State University	10. PROGRAM ELEMENT, PROJECT, TASK AREA & WORK UNIT NUMBERS
11. CONTROLLING OFFICE NAME AND ADDRESS	12. REPORT DATE: 1986
	13. NUMBER OF PAGES: 127
14. MONITORING AGENCY NAME & ADDRESS *(If different from Controlling Office)*	15. SECURITY CLASS. *(of this report)*: UNCLASS
	15a. DECLASSIFICATION/DOWNGRADING SCHEDULE

16. DISTRIBUTION STATEMENT *(of this Report)*

APPROVED FOR PUBLIC RELEASE; DISTRIBUTION UNLIMITED

17. DISTRIBUTION STATEMENT *(of the abstract entered in Block 20, If different from Report)*

18. SUPPLEMENTARY NOTES

APPROVED FOR PUBLIC RELEASE: IAW AFR 190-1

LYNN E. WOLAVER 25 Sept 86
Dean for Research and
Professional Development
AFIT/NR

19. KEY WORDS *(Continue on reverse side if necessary and identify by block number)*

20. ABSTRACT *(Continue on reverse side if necessary and identify by block number)*

ATTACHED ...

DD FORM 1 JAN 73 1473 EDITION OF 1 NOV 65 IS OBSOLETE

SECURITY CLASSIFICATION OF THIS PAGE *(When Data Entered)*

16

A HIGH FREQUENCY ANALYSIS OF ELECTROMAGNETIC PLANE WAVE SCATTERING BY A FULLY ILLUMINATED PERFECTLY CONDUCTING SEMI-INFINITE CONE

Keith Dennis Trott

Captain, U.S.A.F.

Doctor of Philosophy (Ph.D.)

The Ohio State University

1986

Professor P.H. Pathak, Advisor

127 pp.

A uniform high frequency asymptotic solution, based upon the physical optics (PO) approximation, is obtained in the format of the uniform theory of diffraction (UTD) to describe the fields diffracted by the tip of a semi-infinite, perfectly conducting cone when it is fully illuminated by an electromagnetic plane wave. The solution is expressed in terms of an integral, over finite limits, which can be numerically integrated without difficulty. The solution is uniform in the sense that, unlike the previous solution based upon PO which is valid only on the deep shadow side of the reflection boundary, and becomes singular at the reflection boundary, the present solution remains bounded and continuous within the transition region adjacent to the reflection boundary. Outside the transition region, the various field

terms in the integral form of the solution can be interpreted in terms of the geometrical theory of diffraction (GTD) as being associated with the total field consisting of the incident, surface reflected, and tip diffracted ray fields. It is noted that the PO approximation is based upon the use of the geometrical optics (GO) current on the cone. A correction to the PO tip diffracted field is investigated based on the behavior of the exact eigenfunction expansion near the tip; this this problem needs further study. The results computed from just the uniform asympototic PO solution compare well with previously published results for narrow angle semi–infinite cones. In addition, they compare well with measurement as well as with an independent moment method (MM) solution, for the scattering by a finite flat-backed cone. In the latter case, several higher order wave interactions are found to be significant; one such is an interaction between the tip and the base of the cone. It appears that until now, there were no expressions in the open literature to calculate this tip–base interaction even though it was suspected to be important. The present work provides the expressions necessary to calculate this interaction and also to confirm its relative importance.

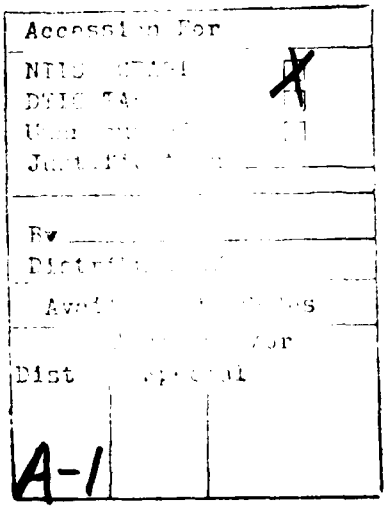

A HIGH FREQUENCY ANALYSIS OF ELECTROMAGNETIC PLANE WAVE SCATTERING BY A FULLY ILLUMINATED PERFECTLY CONDUCTING SEMI–INFINITE CONE

DISSERTATION

Presented in Partial Fulfillment of the Requirements for the Degree of Doctor of Philosophy in the Graduate School of the Ohio State University

By

Keith Dennis Trott, A.S., B.S., M.S.E.E.

* * * * *

The Ohio State University

1986

Dissertation Committee:

P.H. Pathak

L. Peters Jr.

W.D. Burnside

Approved by

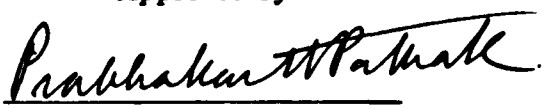

Advisor
Department of Electrical Engineering

DEDICATION

To my wife Natalie; my children Kerri, Jennifer, and Christopher;

and to my mother Kathy.

ACKNOWLEDGEMENTS

I am indebted to many people for the encouragement, support, cooperation, and guidance required to successfully complete this dissertation.

First, I would like to extend my sincere gratitude to my advisor, Dr. P.H. Pathak. His guidance throughout this project was invaluable. I would also like to thank the members of my reading committee, Dr. L. Peters Jr., and Dr. W.D. Burnside, for their suggestions and comments. I would like to express gratitude to Dr. F. Molinet (Societé Mothésim) for providing me with some of his unpublished results. These results were for the special case of axial incidence on the semi-infinite cone, and were useful in verifying my general solution. I express gratitude to Mr.(Ph.D. Candidate) Ming Cheng Liang for our many hours of discussion, and to my office mate Mr.(Ph.D. Candidate) Giancarlo Clerici, for being my sounding board. In addition, I would like to thank Dr. A.K. Dominek who assisted me in applying my theoretical results to the finite flat-backed cones so they could be compared with actual measurments.

To my wife Natalie and my son Christopher, I would like to express a heartfelt thanks for your faith in me, and your understanding of the long hours spent away from you while pursuing this goal.

Lastly, I must express my appreciation to the United States Air Force for affording me the oppurtunity to pursue this degree. Without their support, none of this would have been possible.

VITA

November 17,1952	Born- Boston, Massachusetts
1972-Present	Member of U.S.A.F.
1977	B.S. Mathematics, S.U.N.Y. at Plattsburgh Plattsburgh, New York
1981	M.S.E.E., Syracuse University Syracuse, New York
1983-Present	Special assignment at the Ohio State University pursuing a Ph.D. in Electrical Engineering

FIELDS OF STUDY

Major Field: Electrical Engineering (Electromagnetics)

Advisor:	P.H. Pathak

Studies in:

Communication Systems	F.D. Garber
Control Systems	R.J. Mayhan
Mathematics	J.T. Scheick

TABLE OF CONTENTS

DEDICATION ii

ACKNOWLEDGEMENTS iii

VITA iv

LIST OF FIGURES viii

I. INTRODUCTION 1

1.1 STATEMENT OF THE PROBLEM 1

1.2 MOTIVATION 5

1.3 DISCUSSION OF PREVIOUS RESEARCH 5

1.4 FORMAT OF THE DISSERTATION 8

II. EXACT EVALUATION OF FAR ZONE FIELDS USING PHYSICAL OPTICS 12

2.1 INTRODUCTION 12

2.2 CALCULATION OF THE SCATTERED FIELD 13

III. A UNIFORM ASYMPTOTIC ANALYSIS OF CONE TIP DIFFRACTION BASED ON PHYSICAL OPTICS 20

3.1 INTRODUCTION 20

3.2 FORMULATION OF THE NEAR FIELD PO RADIATION INTEGRAL 22
3.3 LOCATION OF THE SADDLE POINT 29
3.4 LIMITING CASES 32
3.5 UTD TIP DIFFRACTED FIELD 35
3.6 RESULTS 39

IV. VECTOR WAVE FUNCTION SOLUTION 56
4.1 INTRODUCTION 56
4.2 SOLUTION USING THE DYADIC GREEN'S FUNCTION . . 56
4.3 EXPLICIT EXPRESSIONS FOR THE FIELDS OF AN ELECTRIC CURRENT POINT SOURCE IN THE PRESENCE OF THE SEMI-INFINITE CONE 59
4.4 SPECIALIZATION TO THE CASE OF A POINT SOURCE ON THE CONE AXIS 65
4.5 FIELD BEHAVIOR NEAR THE CONE TIP 69
4.6 COMPARISON OF THE DOMINANT TIP CURRENT TO THE GO CURRENT 73
4.7 RADIATION FROM CIRCUMFERENTIAL SLOT ANTENNAS 77

V. SUMMARY AND CONCLUSIONS 83

A. EVALUATION OF TERMS IN THE UNIFORM SADDLE POINT INTEGRATION 86
A.1 INTRODUCTION 86
A.2 DERIVATION AND EVALUATION OF TERMS 86

B. VECTOR WAVE FUNCTIONS **94**

B.1 INTRODUCTION 94

B.2 GENERAL CASE 94

B.3 CONICAL VECTOR WAVE FUNCTIONS 97

C. DYADIC GREEN'S FUNCTION **101**

C.1 INTRODUCTION 101

C.2 DERIVATION OF DYADIC GREEN'S FUNCTION 101

C.3 SOLUTION WITH DYADIC GREEN'S FUNCTIONS 106

D. ASSOCIATED LEGENDRE POLYNOMIALS **108**

D.1 INTRODUCTION 108

D.2 INTEGRAL REPRESENTATION 108

D.3 ORTHOGONALITY AND NORMALIZATION 111

D.4 EIGENVALUES 113

D.5 VERIFICATION 114

REFERENCES **116**

LIST OF FIGURES

1	Geometry for Plane Wave Incidence	13
2	Geometry for Plane Wave Incidence	22
3	GTD Ray Picture	23
4	Migration of Saddle Point with ϕ' for an Observer in the Deep Shadow Side of the Reflection Boundary	30
5	Migration of Saddle Point with ϕ' for an Observer at the Reflection Shadow Boundary Corresponding to the Specular Line of Reflection	30
6	Migration of Saddle Point with ϕ' for an Observer in the Deep Lit Side of the Reflection Shadow Boundary	31
7	Comparison of H_ϕ^s for $\alpha = 5°, \beta = 0°, \phi = 0°$	41
8	Comparison of H_ϕ^s for $\alpha = 5°, \beta = 2.5°, \phi = 0°$	42
9	Comparison of H_ϕ^s for $\alpha = 15°, \beta = 0°, \phi = 0°$	43
10	Comparison of H_ϕ^s for $\alpha = 15°, \beta = 10°, \phi = 0°$	44
11	Comparison of H_ϕ^s for $\alpha = 15°, \beta = 12°, \phi = 0°$	45
12	Comparison of H_ϕ^s for $\alpha = 15°, \beta = 15°, \phi = 0°$	46
13	Comparison of H_ϕ^s for $\alpha = 15°, \beta = 0°, \phi = 45°$	47
14	Comparison of H_ϕ^s for $\alpha = 15°, \beta = 0°, \phi = 135°$	48
15	Comparison of H_ϕ^s for $\alpha = 15°, \beta = 10°, \phi = 45°$	49
16	Comparison of H_ϕ^s for $\alpha = 15°, \beta = 10°, \phi = 90°$	50
17	Comparison of H_ϕ^s for $\alpha = 15°, \beta = 10°, \phi = 135°$	51

18 Comparison of H_ϕ^s for $\alpha = 15°, \beta = 10°, \phi = 270°$ 52

19 Tip–Base Mechanism 54

20 RCS for Axial Backscatter from a Finite Flat–Backed Cone as Computed by Burnside and Peters [10] 54

21 Comparison of RCS of the Cone in Figure given by Moment Method and the Previous GTD Solution [10] 55

22 Comparison of RCS of the Cone in Figure given by Moment Method and the GTD Solution which includes the present Tip–Base Interaction 55

23 Geometry for Semi–Infinite Cone 57

24 Geometry for Application of Dipole Moment 60

25 Comparison of Radiation Pattern for Circumferential Slot at $ka = \pi$ and $\theta_0 = 165°$ from [3] 82

26 Comparison of Radiated Pattern for Circumferential Slot at $ka = 10$ and $\theta_0 = 170°$ from [35] 82

27 Geometry used in Derivation of Vector Wave Function 102

CHAPTER I

INTRODUCTION

1.1 STATEMENT OF THE PROBLEM

A uniform high frequency asymptotic solution, based upon the physical optics (PO) approximation is developed to describe the fields diffracted by the tip of a semi–infinite, perfectly conducting cone in free space when it is fully illuminated by an electromagnetic plane wave. This solution is uniform in the sense that, unlike the exact evaluation of the far zone PO integral given in Chapter II, which is valid only in the deep shadow side of the reflection boundary and becomes singular at the reflection boundary, the uniform solution presented here, remains bounded and continuous within the transition region adjacent to the reflection boundary.

This solution is derived using asymptotic methods given by Felsen and Marcuvitz [36]. The form of the solution which is found by simply applying these techniques, yields a uniform asymptotic theory (UAT) type solution. In the UAT form [40], the total field is written as

$$\mathbf{U} = \mathbf{U}^G + \mathbf{U}_k^d \tag{1.1}$$

in which the Keller diffracted field, U_k^d, is based on Keller's geometrical theory of diffraction (GTD) where one writes the total GTD field as

$$\mathbf{U}^{gtd} = \mathbf{U}^{go} + \mathbf{U}_k^d, \tag{1.2}$$

in which $\mathbf{U}^{go}$ is the geometrical optics (GO) field. It is noted that $\mathbf{U}_k^d$ becomes

singular at the incident shadow boundary (ISB) and the reflection shadow boundary (RSB). The U^G in (1.1) is a modified GO field that eliminates the singularities of U_k^d at the ISB and the RSB. In the uniform geometrical theory of diffraction (UTD) form [40], the total field is written as

$$\mathbf{U}^{utd} = \mathbf{U}^{go} + \mathbf{U}^d \tag{1.3}$$

where $\mathbf{U}^d$ is a uniform diffracted field. It is noted that $\mathbf{U}^d$ reduces to $\mathbf{U}_k^d$ away from the shadow boundary transition regions, and it compensates for the discontinuities of $\mathbf{U}^{go}$ at the shadow boundaries. Unlike UAT, the UTD compensates for the singularities of U_k^d at the ISB and RSB in a multiplicative manner because $\mathbf{U}^d$ is expressed as a product of $\mathbf{U}_k^d$ and a transition function which keeps $\mathbf{U}^d$ bounded at the ISB and RSB. From a numerical point of view, the latter is easier to implement in computer applications than the additive cancellation of the singularities in the UAT form. Outside the transition region, both the UAT and UTD forms in (1.1) and (1.3) reduce to Keller's GTD form in (1.2).

As mentioned previously, the uniform solution found for the cone starts out in a UAT form. Steps are taken to rewrite this in a UTD form. As a first step, a quasi UTD form is found for the *scattered field* that is expressed in terms of a relatively simple integral over finite limits which can be integrated numerically. The integrand is written as

$$\mathbf{I} = \mathbf{I}_{ref} + \mathbf{I}_{tran} + \mathbf{I}_{diff} \tag{1.4}$$

where the integrands denoted by $\mathbf{I}_{ref}$, $\mathbf{I}_{tran}$, and $\mathbf{I}_{diff}$ are associated with the reflected field, the transition field, and the Keller type tip diffracted field respectively. Far from the transition region, $\mathbf{I}_{tran}$ becomes small, and the remaining terms in (1.4) can be interpreted in the GTD format as being associated with the

surface reflected, and tip diffracted ray fields. This quasi UTD form also provides an additive correction for the singularities at the ISB and RSB since the singularity in $\mathbf{I}_{diff}$ is compensated for by the singularity in $\mathbf{I}_{tran}$; however, it is desirable to obtain a UTD type expression for the tip diffracted field. This has been accomplished. In the development of the latter UTD solution, the quasi UTD form for the scattered field, $\mathbf{U}^{sc}$, is rewritten in the UTD form as

$$\mathbf{U}^{sc} = \mathbf{U}_r^{go} + \mathbf{U}^d. \tag{1.5}$$

where $\mathbf{U}_r^{go}$ is the reflected component of the GO field, and $\mathbf{U}^d$ is the uniform tip diffracted field. This form gives us the UTD tip diffracted field based on the PO approximation. This UTD tip diffracted field is valid everywhere away from the tip, including the cone surface. It should be noted that this PO based tip diffracted field contains a factor which keeps $\mathbf{U}^d$ bounded at the reflection shadow boundary, and which keeps the total scattered field continuous across the reflection shadow boundary.

The present uniform solution is useful for analyzing the near axial radar cross section (RCS) of the finite flat-backed cone. In the RCS analysis of the finite flat-backed cone, the fields diffracted by the tip travel along the cone surface to the base and diffract from the edge of the base to arrive at the observation point, or travel across the base to diffract from a diametrically opposite edge of the base to arrive at the observation point, and vice versa. This tip–base interaction requires one to calculate the tip diffracted field on the illuminated surface of the cone. In general, the illuminated surface lies within the reflection boundary transition region; therefore, it becomes necessary to employ a uniform solution which, as the one developed here, remains valid within the reflection boundary transition region. It appears that until now, there were no expressions in the open literature

to calculate this tip–base interaction even though it was suspected by [10] to be important. The present work provides the expressions necessary to calculate this interaction and also to confirm its relative importance. Indeed, previous work on the axial RCS of a flat–backed cone of radius a for the range of $8 < ka < 12$, has shown an almost constant 3 dB error between calculations and measurements because the tip–base interaction could not be calculated. That error is now removed by the present work thus bringing the calculations into close agreement with the measurements.

Since this uniform solution allows one to determine the value of the field on the surface of the cone that has been diffracted by the tip; therefore, via reciprocity, if one puts an infinitesimal current element on the surface of the cone, this same UTD tip diffracted field can be used to determine the contribution to the radiated field of the current element due to that interaction. An example of how reciprocity is applied is given in Chapter IV in terms of the exact eigenfunction solution.

It is noted that the PO approximation is based upon the use of the GO current on the cone. The eigenfunction expansion is investigated and the dominant term in the eigenfunction expansion is isolated. The current from the dominant term exhibits the proper singularity at the tip. It is compared to the GO current for the case of axial incidence and it is also shown that there is a close correlation between these two expressions. This leads one to believe that a correction to the PO tip diffracted field could be constructed using an expression for the current that is the matching of the eigenfunction current near the tip to the GO current far from the tip. It is felt that this could provide a very good approximation to the actual current because the eigenfunction expansion yields the proper tip singularity, and the GO current dominates far from the tip when the cone is fully illuminated.

1.2 MOTIVATION

The right circular cone is one of the simplest canonical shapes that exhibits a tip discontinuity. Little work has been done regarding tip diffraction in the forward scatter region toward the cone surface. This information is needed to accurately study the scattering from the cone geometry, and thus motivates the present research effort.

1.3 DISCUSSION OF PREVIOUS RESEARCH

There has been a wealth of work conducted on the cone geometry; both finite and semi-infinite. The following summary is not an exhaustive one. Its goal is to give the reader an indication of the amount of interest that exists in the cone geometry.

Between 1952–1953, Siegel, et al. [1,2] published work which determined scattering from a cone and later did a comparison of theory to experiment. Their analyses were based on an eigenfunction expansion that is slowly convergent, and special summation techniques were employed.

In 1956, Bailin and Silver [3] solved the boundary value problem for spheres and cones. They also used the radial transmission eigenfunction expansion. Patterns were plotted for circumferential excitation of the semi-infinite cone. A few of their numerical results were later found to be in error by Pridmore–Brown et al. [35]. This is verified by the present work.

In 1957, Felsen [4,5] published companion articles on alternate field representations for regions bounded by spheres, cones and planes. In these papers, he uses the angular transmission eigenfunction expansion. This representation converges faster than the radial transmission version used by Siegel, et al. and Bailin and

Silver. His result gave the tip scattered field which is valid only on the shadow side of the reflection shadow boundary for wide and narrow angle cones. Moreover, his eigenfunction expansion lends itself more easily to an asymptotic high frequency analysis. In 1957, Felsen [6] extracted the asymptotic expansion of the tip diffracted wave from the semi-infinite cone from his representation.This result was also valid only on the shadow side of the reflection shadow boundary.

In 1965, Shultz, et al. [7] published work on a spherically capped finite cone for axial incidence. They used the vector wave functions. Their results are valid up to ka=3.2, where a is the radius of the cone base.

Also in 1965, Bechtel [8] published work on the finite cone. Bechtel used the geometrical theory of diffraction (GTD). The upper limit in his study was a=2.87. He neglected tip diffraction and did not account for the tip-base interaction.

In 1969, Bowman et al. [33], gave a complete overview of most of the work done on the cone geometry up to that point in time. He discussed both the acoustic and electromagnetic cases. This treatise was used to compare many of the intermediate results in this research.

In 1971, Senior and Uslenghi [9] published work on the backscatter from the finite flat-backed cone using GTD and keeping the first two terms in the asymptotic expansion. They used wedge diffraction coefficients for the higher order diffractions across the base of the flat-backed cone. There is an error, by a factor of 2, in their treatment of grazing incidence which was later corrected in 1972 by Burnside and Peters [10] who used equivalent currents and higher order diffractions to determine the axial radar cross section (RCS) of the finite flat-backed cone. This paper also uses the equivalent wedge diffraction coefficients for higher order diffractions across the base of the cone. They indicate a 3 dB discrepancy between measured and calculated data for a cone where $8 < ka < 12$, and postulated this to be caused by a

missing diffraction mechanism; namely, the tip–base interaction. Their conjecture is verified to be true in the present work.

In 1977, Kouyoumjian [11] published work on the high frequency backscatter from flat backed finite cone. This paper presents both the acoustic and electromagnetic solutions. In this paper the first attempt is made to account for the tip–base interaction. An expression is used for the tip diffraction that is not strictly valid beyond the reflection shadow boundary; however, the results are reasonably accurate for large ka but there is still more than a one dB difference for smaller ka values.

From 1977–1979, Felsen and Chan published a series of papers [12,13,14] in which the integral form of the Green's function for the cone was determined. The first of these extracted the creeping wave from two points located on the surface far from the tip. In the latter two papers, their Green's function was transformed to the time domain to investigate transient behavior.

In 1984, Wang and Mitschang [15] published a hybrid moment method (MM) and physical theory of diffraction (PTD) solution for the finite circular and elliptical cones. They commented in their study that the tip–base interaction was negligible; however, that comment is shown to be untrue in the present work.

It has come to our attention that Molinet [39] has also independently worked on the problem of scattering from the cone tip using PO and high frequency techniques from Felsen and Marcuvitz [36]. He has treated the special case of axial incidence [39]. His results, which were determined independently, were used to verify the general solution given here; however, unlike the present UTD form of the solution, he keeps his high frequency solution, also based on PO, in the form of uniform asymptotic theory (UAT).

This work is devoted to determining the value of the wave that is excited at

the tip via diffraction and travels along the cone surface until diffracted by the edge at the base of a finite cone. A uniform high frequency asymptotic solution, based upon the physical optics (PO) approximation, is obtained to describe the fields diffracted by the tip of a semi-infinite, perfectly conducting cone when it is fully illuminated by an electromagnetic plane wave. The solution is uniform in the sense that, unlike the far field solution based upon PO which is valid only in the deep shadow side of the reflection boundary, the present solution can be employed even within the transition region adjacent to the reflection boundary up to the cone surface. The results computed from the present uniform asymptotic PO solution are shown to compare well with previously published results for narrow angle semi-infinite cones [5]. In addition, the results obtained for the RCS of the finite flat-backed cone are found to compare closely with measurements and with an independent moment method (MM) solution. It should be noted that the UTD tip diffracted field on the cone surface, found in the present work, can be used in conjunction with reciprocity to determine the radiation from a source on the cone surface.

1.4 FORMAT OF THE DISSERTATION

The format for this dissertation is as follows. In Chapter II, an exact evaluation of the far zone field scattered from the cone is developed using Physical Optics (PO). If this result were generalized to the near zone, it would be a non-uniform expression since the expressions for fields are singular at the reflection shadow boundary. Furthermore, it is not valid on the lit side of the shadow boundary. The reasons for this restriction will be discussed. This is done for plane wave incidence in the special case when the cone is fully illuminated. This field expression is then used to determine the scattering cross-section, σ. It is shown that this field

expression yields the familiar radar cross section from PO, σ_{po}, as shown in [33]. Moreover, the field expression reduces to that given by Goryainov [37] for axial incidence. It appears that an explicit field expression for the case of non-axial incidence, but with full illumination, has not been published previously although the σ_{po} has been obtained previously.

In Chapter III, a uniform solution based upon PO is developed for scattering from a fully illuminated semi-infinite cone. In the PO radiation integral over the cone surface, the free-space Green's function with an exact kernel is used. The integration is performed asymptotically in the radial coordinate (r') along the cone generator using a uniform saddle point method which takes into consideration the effect of the saddle point near the end point (tip). The remaining azimuthal (ϕ') integration is then done numerically. It is found that the saddle point migrates to the end point (tip) as a function of ϕ'.

This answer is first written in a quasi uniform theory of diffraction (UTD) form. It includes a surface reflected field term, a tip diffracted field term, and a transition term which vanishes in the deep shadow region. The transition term keeps the total solution bounded and continous across the reflection boundary. In general, the transition region extends throughout the lit region for the fully illuminated cone. This quasi UTD solution was subsequently rewritten in a UTD form such that a UTD type tip diffracted field has been found using the PO approximation. One of the goals of this research is to develop an expression that can be used to calculate the contribution by the wave diffracted from the tip. In the case of finite flat-backed cone, the tip diffracted wave travels along the cone and can diffract from the edge at the base of the cone. The UTD tip diffracted field has been determined for the semi-infinite cone, but since high frequency diffraction is a local phenomena, this tip diffraction is the same for either the finite or the

semi-infinite cone.

To date there has been an almost constant 3 dB difference between analysis and experiment for axial backscatter from a moderately large ($8 < ka < 12$) flat-backed finite right circular cone in which "a" is the radius of the base and k is the free space wave number. It is shown that including the aforementioned tip–base interaction improves the results and brings the analysis in line with the experiments.

In Chapter IV, an exact eigenfunction expansion is derived for the fields using the vector wave functions **M** and **N** described in [21,32]. From this, expressions are determined for the surface current induced on the cone. When the small argument form of the Bessel function is applied to the series, it can be shown that there is a dominant term in the tip region. This term represents the tip discontinuity and models the true behavior of the current near the tip. For the case of axial incidence, the actual tip current and the GO based current are compared and it is shown that the two currents are very similar. This leads one to believe that these currents could be combined to yield a more accurate approximation to the current which could then be used to determine the tip diffracted field using the methods in Chapter III.

In addition, the vector wave functions are employed to compute the radiated fields from a circumferential slot on the cone. Bailin and Silver [3] have published patterns for several configurations. Pridmore–Brown et al. [35] have also published patterns for circumferential slots. The Pridmore–Brown paper claims that there are several discrepancies in the results of Bailin and Silver. To resolve this issue, patterns are plotted based on the present work using the same parameters. It should be noted that the present expressions using the vector wave functions are identical to those given in [3], although derived using a totally different approach.

Moreover, the present expressions appear vastly different from those in [35]. The case in point is for ka=10, and $\theta_0 = 170°$. The present plots agree with those in [35] and are very different from those in [3]. It should be noted that the present plots do agree with that in [3] for ka=π, and $\theta_0 = 165°$. One could attribute the discrepancy to the level of sophistication of computers then and now.

Appendix A gives the expressions used in the uniform saddle point approximation derived in Chapter III. The derivation of the vector wave functions and the dyadic Green's function used in the present work are detailed in Appendices B and C. An important aspect of this problem is the heavy dependence on special functions. There is also the requirement to compute the incomplete normalization integrals. Even more critical is the determination of the eigenvalues associated with the cone problem. This requires the eigenvalues that are solutions to

$$P_\gamma^m(\cos\theta_0) = 0 \quad \text{and} \tag{1.6}$$

$$\frac{d}{d\theta} P_\nu^m(\cos\theta_0) = 0. \tag{1.7}$$

For the cone problem, the eigenvalues ν and γ are non-integer; therefore, a special effort was required to derive expressions that could be programmed to yield results for any angle, order and degree. Programs were written to calculate these and were compared to published results in [16]. Integral forms for the associated Legendre polynomials found in [17] were used for these functions. These integral forms were also used to determine the eigenvalues. These eigenvalues compare very well with those published in [2,31]. Appendix D discusses the derivations of the associated Legendre polynomials used in this dissertation.

The $e^{j\omega t}$ time convention is assumed and suppressed throughout the following development.

CHAPTER II

EXACT EVALUATION OF FAR ZONE FIELDS USING PHYSICAL OPTICS

2.1 INTRODUCTION

In this chapter, the field scattered by the cone using the Physical Optics (PO) approximation is determined. The PO radiation integral which is valid in the far zone of the tip is used and the discussion is specialized to the case when the cone is fully illuminated. This is true when $\beta \leq \pi - \theta_0 = \alpha$, where the angles are shown in Figure 1.

It will be shown that the expressions for the scattered field found in this chapter are not valid at or beyond the reflection shadow boundary due to restrictions placed upon the integration techniques. The integral is over the cone surface which is described in terms of the radial (r') and azimuthal (ϕ') coordinates. The integration in (r') is over infinite limits; therefore, these restrictions are placed upon the integral to insure convergence. The integration has been performed two ways. The first approach is shown in detail within this chapter. It was also done in the reverse order holding (ϕ') fixed, integrating over (r'), then performing the integration in (ϕ') using contour integration. Both techniques yield the same answers and the same restrictions.

Since these expressions for the scattered field are valid only on the shadow side of the reflection boundary, they represent the fields diffracted by the tip. If

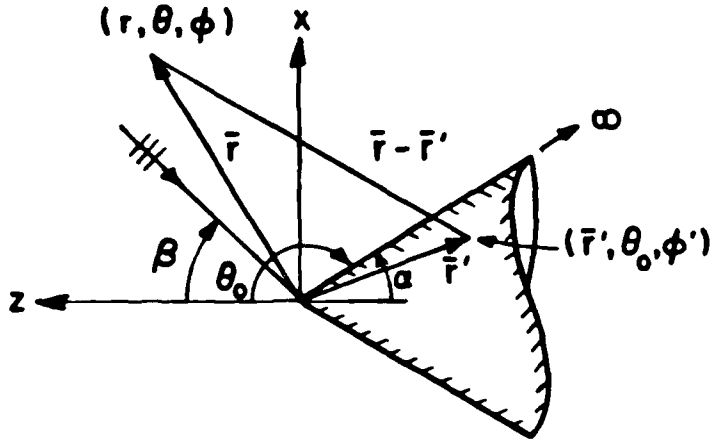

Figure 1: Geometry for Plane Wave Incidence

this were generalized to the near zone case, then this solution would be considered non-uniform since it is singular at the reflection shadow boundary.

2.2 CALCULATION OF THE SCATTERED FIELD

Figure 1 shows the geometry for a plane wave incident on the cone. The electric field associated with the incident plane wave at the conical surface is given by

$$\mathbf{E}^{i}(\mathbf{r}') = \left\{ \begin{array}{c} \hat{\theta}' \\ \hat{\phi}' \end{array} \right\} e^{jkr'(\sin\theta_0 \sin\beta \cos\phi' + \cos\theta_0 \cos\beta)} \tag{2.1}$$

where the bracketed term represents the two possible polarizations. The variables (r') and (ϕ') represent the radial and azimuthal variation of the source coordinates as shown in Figure 1. It is assumed that the plane of incidence is the x-z plane. For this configuration, the incident magnetic field $\mathbf{H}^{i}$ field is given by

$$\mathbf{H}^{i}(\mathbf{r}') = \left\{ \begin{array}{c} -\hat{\phi}' \\ \hat{\theta}' \end{array} \right\} Y_0 e^{jkr'(\sin\theta_0 \sin\beta \cos\phi' + \cos\theta_0 \cos\beta)}. \tag{2.2}$$

In the PO approximation, the radiation integral for the scattered field is evaluated after employing the geometrical optics (GO) approximation for the surface

current. This GO current is given by

$$\mathbf{J_{go}}(\mathbf{r}') = \begin{cases} 2\hat{n}' \times \mathbf{H^i}(\mathbf{r}') & \text{in the lit region, and} \\ 0 & \text{in the shadow region.} \end{cases} . \tag{2.3}$$

However, the entire cone is illuminated; therefore, there is no shadow region on the surface, and the integration is performed over the entire cone surface.

The outward normal to the cone is given by

$$\hat{n}' = -\hat{\theta}'\Big]_{\theta'=\theta_0} = -\hat{x}\cos\theta_0\cos\phi' - \hat{y}\cos\theta_0\sin\phi' + \hat{z}\sin\theta_0. \tag{2.4}$$

Therefore, the expression for the scattered electric field in the far zone of the tip is given by

$$\mathbf{E^s}(\mathbf{r}) \simeq jk\frac{e^{-jkr}}{r}\hat{r} \times \hat{r} \times \int_0^{\infty}\int_0^{2\pi} \frac{\mathbf{f}(\phi')}{2\pi} e^{jkr'q(\phi')} r' \sin\theta_0 dr' d\phi' \tag{2.5}$$

where

$$\mathbf{f}(\phi') = \begin{cases} \hat{x}\sin\theta_0 + \hat{z}\cos\theta_0\cos\phi' & \text{for } \hat{\theta}' \text{ incidence, and} \\ \hat{x}\cos\theta_0\sin\beta\sin\phi' + \hat{z}\cos\theta_0\cos\beta\sin\phi' & \text{for } \hat{\phi}' \text{ incidence} \\ \quad +\hat{y}\left(\sin\theta_0\cos\beta - \cos\theta_0\sin\beta\cos\phi'\right) & \end{cases} \tag{2.6}$$

and

$$\begin{aligned} q(\phi') &= \sin\theta_0\left[(\sin\theta\cos\phi + \sin\beta)\cos\phi' + \sin\theta\sin\phi\sin\phi'\right] \\ &\quad + \cos\theta_0\left[\cos\theta + \cos\beta\right]. \end{aligned} \tag{2.7}$$

One can rewrite this as follows:

$$q(\phi') = a\cos(\phi' - \delta) + \gamma \tag{2.8}$$

where

$$\gamma = \cos\theta_0\left[\cos\theta + \cos\beta\right] \tag{2.9}$$

$$a\cos\delta = \sin\theta_0\left(\sin\theta\cos\phi + \sin\beta\right) \quad \text{and} \tag{2.10}$$

$$a \sin\delta = \sin\theta_0 \sin\theta \sin\phi. \tag{2.11}$$

From Equations (2.10) and (2.11), it is found that

$$a = \sin\theta_0 \sqrt{\sin^2\theta + \sin^2\beta + 2\sin\theta\sin\beta\cos\phi}. \tag{2.12}$$

The expression for the scattered field becomes

$$\begin{aligned} \mathbf{E}^s(\mathbf{r}) \;\simeq\; & jk\frac{e^{-jkr}}{r}\sin\theta_0 \hat{r}\times\hat{r}\times \\ & \int_0^\infty r' e^{jk\gamma r'} \int_0^{2\pi} \frac{\mathbf{f}(\phi')}{2\pi} e^{jkar'\cos(\phi'-\delta)} d\phi' dr' \end{aligned} \tag{2.13}$$

Concentrating on the ϕ' integration, the following results [21] are used:

$$\frac{1}{2\pi j^n}\int_0^{2\pi} \cos n\phi' e^{jx\cos(\phi-\phi')} d\phi' = \cos n\phi J_n(x) \tag{2.14}$$

and

$$\frac{1}{2\pi j^n}\int_0^{2\pi} \sin n\phi' e^{jx\cos(\phi-\phi')} d\phi' = \sin n\phi J_n(x). \tag{2.15}$$

For either polarization, there will be linear combinations of the same three basic integrals. Using the above results, they are given by

$$\frac{1}{2\pi}\int_0^{2\pi} e^{jkar'\cos(\phi'-\delta)} d\phi' = J_0(kar') \tag{2.16}$$

$$\frac{1}{2\pi}\int_0^{2\pi} \cos\phi' e^{jkar'\cos(\phi'-\delta)} d\phi' = j\cos\delta J_1(kar') \tag{2.17}$$

and

$$\frac{1}{2\pi}\int_0^{2\pi} \sin\phi' e^{jkar'\cos(\phi-\delta)} d\phi' = j\sin\delta J_1(kar'). \tag{2.18}$$

Once the ϕ' integration has been performed, what remains are integrals of the form :

$$\int_0^\infty r' J_0(kar') e^{jk\gamma r'} dr' = \frac{-\gamma}{k^2(\gamma^2 - a^2)^{3/2}} \tag{2.19}$$

and

$$\int_0^\infty r' J_1(kar') e^{jk\gamma r'} dr' = \frac{a}{jk^2(\gamma^2 - a^2)^{3/2}}. \tag{2.20}$$

The answers to these were found by applying the following results [38]:

$$\int_0^\infty e^{-\alpha x} J_\nu(\beta x) x^\nu = \frac{(2\beta)^\nu \Gamma(\nu + 1/2)}{\sqrt{\pi}(\alpha^2 + \beta^2)^{\nu+1/2}} \tag{2.21}$$

and

$$\int_0^\infty e^{-\alpha x} J_\nu(\beta x) x^{\nu+1} = \frac{2\alpha(2\beta)^\nu \Gamma(\nu + 3/2)}{\sqrt{\pi}(\alpha^2 + \beta^2)^{\nu+3/2}} \tag{2.22}$$

where $Re(\alpha) > |Im(\beta)|$. It has been assumed that k is slightly lossy so this condition yields $-\gamma > a$. Substituting $\theta_0 = \pi - \alpha$ into the expressions for γ and a yields the following restriction on the integral:

$$\cos\alpha\,[\cos\theta + \cos\beta] > \sin\alpha\sqrt{\sin^2\theta + \sin^2\beta + 2\sin\theta\sin\beta\cos\phi}. \tag{2.23}$$

This expression will be discussed later after the shadow boundaries have been discussed.

Defining $E_\theta^{\theta'}$ as the θ component of the field generated by a $\hat{\theta}'$ source and so forth, then using the following identities

$$\hat{r} \times \hat{r} \times \hat{x} = -\hat{\theta}\cos\theta\cos\phi + \hat{\phi}\sin\phi \tag{2.24}$$

$$\hat{r} \times \hat{r} \times \hat{y} = -\hat{\theta}\cos\theta\sin\phi - \hat{\phi}\cos\phi \tag{2.25}$$

and

$$\hat{r} \times \hat{r} \times \hat{z} = \hat{\theta}\sin\theta, \tag{2.26}$$

then simplifying the expressions yields:

$$E_\theta^{\theta'} = j\frac{e^{-jkr}}{kr}\frac{\tan^2\alpha}{\Pi^{3/2}}\,[[1 + \cos\theta\cos\beta]\cos\phi + \sin\theta\sin\beta] \tag{2.27}$$

$$E_\phi^{\theta'} = -j\frac{e^{-jkr}}{kr}\frac{\tan^2\alpha}{\Pi^{3/2}}\,[\cos\theta + \cos\beta]\sin\phi \tag{2.28}$$

$$E_\phi^{\phi'} = j\frac{e^{-jkr}}{kr}\frac{\tan^2\alpha}{\Pi^{3/2}}\,[[1 + \cos\theta\cos\beta]\cos\phi + \sin\theta\sin\beta] \tag{2.29}$$

$$E_\theta^{\phi'} = j\frac{e^{-jkr}}{kr}\frac{\tan^2\alpha}{\Pi^{3/2}}\,[\cos\theta + \cos\beta]\sin\phi \tag{2.30}$$

where Π is given by

$$\Pi = [\cos\theta + \cos\beta]^2 - \tan^2\alpha \left[\sin^2\theta + \sin^2\beta + 2\sin\theta\sin\beta\cos\phi\right]. \qquad (2.31)$$

It should be noted that $\tan^2\theta_0$ has been replaced with $\tan^2\alpha$ in all the expressions above since $\alpha = \pi - \theta_0$.

For the sake of completeness, it is also noted that the scattered magnetic field in the far zone of the tip is given by

$$\mathbf{H}^s \simeq \hat{r} \times Y_0 \mathbf{E}^s. \qquad (2.32)$$

The field expressions will have a singularity when the denominator goes to zero. These singularities occur at the shadow boundaries. The reflection shadow boundary that corresponds to the specular line of scattering from the entire cone generator occurs in the incident plane, i.e., $\phi = 0$. Setting $\phi = 0$, Π can be written as

$$4\left[\cos^2(\frac{\theta-\beta}{2})\left[\cos^2(\frac{\theta+\beta}{2}) - \tan^2\alpha\sin^2(\frac{\theta+\beta}{2})\right]\right]. \qquad (2.33)$$

Setting this equal to zero yields a condition on $\theta + \beta$ given by

$$\theta + \beta = \pi - 2\alpha = 2\theta_0 - \pi. \qquad (2.34)$$

This is the reflection shadow boundary (RSB). The RSB also occurs elsewhere, and its position varies as a function of ϕ.

Setting $\phi = \pi$ yields the incident shadow boundary (ISB) given by

$$\theta + \beta = \pi. \qquad (2.35)$$

Going back to equation (2.23), the restriction on the integral, and setting $\phi = 0$, yields

$$\cos(\alpha + \frac{\theta+\beta}{2}) > 0 \qquad (2.36)$$

from which it is noted

$$\theta + \beta < \pi - 2\alpha. \tag{2.37}$$

Setting $\phi = \pi$, yields

$$\theta + \beta < \pi. \tag{2.38}$$

One should recognize these values as the RSB and ISB, respectively. The incident shadow boundary poses no problem in this case. However, there is a phase shift passing through the RSB and the expressions are not valid beyond this boundary. The expressions will be plotted beyond the RSB by introducing the phase shift that is caused by passing through this boundary. The plots indicate that the behavior is reasonable for axial incidence; however, it shows rapid flucuations on the lit side of the reflection shadow boundary for non-axial incidence.

As mentioned previously, these fields are only valid in the shadow region. They do not account for the surface reflected field or the transition field; therefore, the scattered field given is the tip diffracted field.

It is of interest to compute the scattering cross-section from these expressions. The scattering cross-section is defined by

$$\sigma = \lim_{r\to\infty} 4\pi r^2 \frac{|\mathbf{E}^s|^2}{|\mathbf{E}^i|^2} = \lim_{r\to\infty} 4\pi r^2 \left[|E_\theta^s|^2 + |E_\phi^s|^2\right]. \tag{2.39}$$

In either case, after simplification

$$\sigma_{po} = \frac{\lambda^2}{\pi} \frac{\tan^4\alpha}{\Pi^3} \left[[1 + \cos\theta\cos\beta] + \cos\phi\sin\theta\sin\beta\right]^2 \tag{2.40}$$

where Π is given by Equation (2.31). This expression for σ_{po} is identical to that given previously by [33]. Moreover, Goryainov has done this for axial incidence. His expressions are given in [37] by:

$$E_\theta^{\theta'} = j\frac{e^{-jkr}}{kr}\cos\phi \mathrm{L}(\theta,\alpha) \quad \text{and} \tag{2.41}$$

$$E_\phi^{\theta'} = -j\frac{e^{-jkr}}{kr}\sin\phi \mathrm{L}(\theta,\alpha) \tag{2.42}$$

where

$$L(\theta,\alpha) = \frac{\sin^2\alpha\cos\alpha}{4\cos\frac{\theta}{2}\left(\cos(\alpha+\frac{\theta}{2})\cos(\alpha-\frac{\theta}{2})\right)^{3/2}}. \tag{2.43}$$

The exact PO expressions starting with Equation (2.27), for $\hat{\theta}'$ incidence could be written as:

$$E_\theta^{\theta'} = j\frac{e^{-jkr}}{kr}\cos\phi \mathrm{T1}(\theta,\alpha,\beta) + \mathrm{T2}(\theta,\alpha,\beta) \quad \text{and} \tag{2.44}$$

$$E_\phi^{\theta'} = -j\frac{e^{-jkr}}{kr}\sin\phi \mathrm{T3}(\theta,\alpha,\beta) \tag{2.45}$$

where

$$T1(\theta,\alpha,\beta) = \frac{\tan^2\alpha}{\Pi^{3/2}}[[1+\cos\theta\cos\beta]] \tag{2.46}$$

$$T2(\theta,\alpha,\beta) = \frac{\tan^2\alpha}{\Pi^{3/2}}[\sin\theta\sin\beta] \quad \text{and} \tag{2.47}$$

$$T3(\theta,\alpha,\beta) = \frac{\tan^2\alpha}{\Pi^{3/2}}[\cos\theta+\cos\beta] \tag{2.48}$$

Evaluating the expressions for $\beta = 0$, yields

$$T2(\theta,\alpha,0) = 0 \tag{2.49}$$

and

$$T1(\theta,\alpha,0) = T3(\theta,\alpha,0) = L(\theta,\alpha). \tag{2.50}$$

That is, the expressions reduce to that given by Goryainov for axial incidence.

In some applications, the individual scattered field expressions are more useful than the composite σ_{po} expression. It is important to note that the scattered field expressions and hence σ_{po} satisfy reciprocity.

CHAPTER III

A UNIFORM ASYMPTOTIC ANALYSIS OF CONE TIP DIFFRACTION BASED ON PHYSICAL OPTICS

3.1 INTRODUCTION

The exact far zone PO integral calulated in the preceeding chapter was singular at reflection shadow boundary (RSB) and not valid on the lit side of the reflection shadow boundary. In this chapter, the solution for the scattering by a fully illuminated cone is improved by making it uniform across the reflection shadow boundary. To this end, an exact kernel for the Green's function is used in the PO radiation integral for the scattered field in which the integration is taken over the GO currents on the cone surface. This integral, which is valid in the near zone of the tip but not too close to the tip, will be approximated asymptotically in the radial coordinate (r') along the generator of the cone using the saddle point method. The saddle point can migrate to the end point of integration at the tip of the cone; therefore, special techniques are used to account for this. The integration in the remaining azimuthal coordinate (ϕ') is done numerically. This is done only for $\hat{\theta}'$ incidence. The $\hat{\phi}'$ case would follow in a similar manner.

To determine the field on the cone surface, a uniform solution is required. There are two common types of uniform solutions. These will be discussed briefly. As discussed in the Introduction, the total field in the UAT form [40] is written as

$$\mathbf{U} = \mathbf{U}^G + \mathbf{U}_k^d \tag{3.1}$$

in which the Keller diffracted field, U_k^d, is based on Keller's geometrical theory of diffraction (GTD) where one writes the total GTD field as

$$\mathbf{U}^{gtd} = \mathbf{U}^{go} + \mathbf{U}_k^d, \tag{3.2}$$

in which $\mathbf{U}^{go}$ is the geometrical optics (GO) field. It is noted that $\mathbf{U}_k^d$ becomes singular at the incident shadow boundary (ISB) and the reflection shadow boundary (RSB). The U^G in (1.1) is a modified GO field that eliminates the singularities of U_k^d at the ISB and the RSB. In the uniform geometrical theory of diffraction (UTD) form [40], the total field is written as

$$\mathbf{U}^{utd} = \mathbf{U}^{go} + \mathbf{U}^d \tag{3.3}$$

where $\mathbf{U}^d$ is a uniform diffracted field. It is noted that $\mathbf{U}^d$ reduces to $\mathbf{U}_k^d$ away from the shadow boundary transition regions, and it compensates for the discontinuities of $\mathbf{U}^{go}$ at the shadow boundaries. Unlike UAT, the UTD compensates for the singularities of U_k^d at the ISB and RSB in a multiplicative manner because $\mathbf{U}^d$ is expressed as a product of $\mathbf{U}_k^d$ and a transition function which keeps $\mathbf{U}^d$ bounded at the ISB and RSB. From a numerical point of view, the latter is easier to implement in computer applications than the additive cancellation of the singularities in the UAT form. Outside the transition region, both the UAT and UTD forms in (3.1) and (3.3) reduce to Keller's GTD form in (3.2).

The solution developed here is in terms of a finite integral. The integrands for this integral are first developed into a quasi UTD form; however, a UTD expression for the tip diffracted field is desired. To this end, knowledge of the behavior in the vicinity of the reflection shadow boundary is utilized and the quasi UTD form is rewritten in a UTD form that isolates the UTD tip diffracted field.

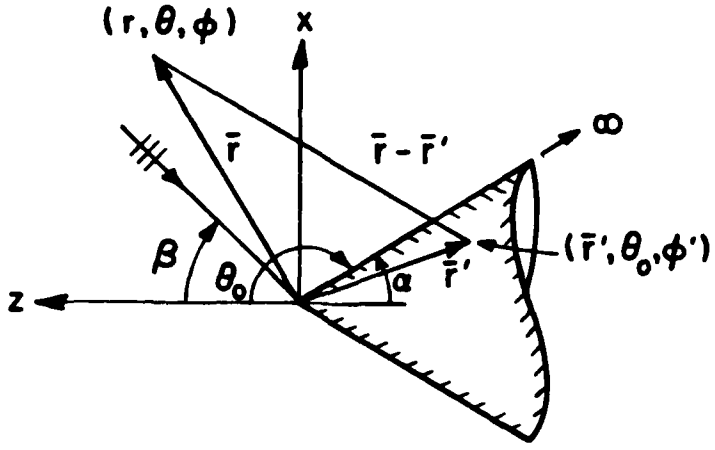

Figure 2: Geometry for Plane Wave Incidence

3.2 FORMULATION OF THE NEAR FIELD PO RADIATION INTEGRAL

The expression for the GO current for the case being considered is given by

$$\mathbf{J_{go}}(r', \phi') = 2Y_0 e^{jkr' \cos\gamma}(\hat{x} \sin\alpha - \hat{z} \cos\alpha \cos\phi') \tag{3.4}$$

where

$$\cos\gamma = \sin\alpha \sin\beta \cos\phi' - \cos\alpha \cos\beta. \tag{3.5}$$

The magnetic vector potential $\mathbf{A}$ defined by $\mathbf{H^s} = \nabla \times \mathbf{A}$ associated with this $\mathbf{J_{go}}$ is given by

$$\mathbf{A}(\mathbf{r}) = \int_0^{2\pi} d\phi' \int_0^{\infty} \mathbf{J_{go}}(r', \phi') \frac{e^{-jkR}}{4\pi R} r' \sin\alpha dr' \tag{3.6}$$

with

$$R = |\mathbf{r} - \mathbf{r}'| = \sqrt{r^2 + r'^2 - 2rr' \cos\varsigma} \tag{3.7}$$

and

$$\cos\varsigma = \sin\alpha \sin\theta \cos(\phi - \phi') - \cos\alpha \cos\theta \tag{3.8}$$

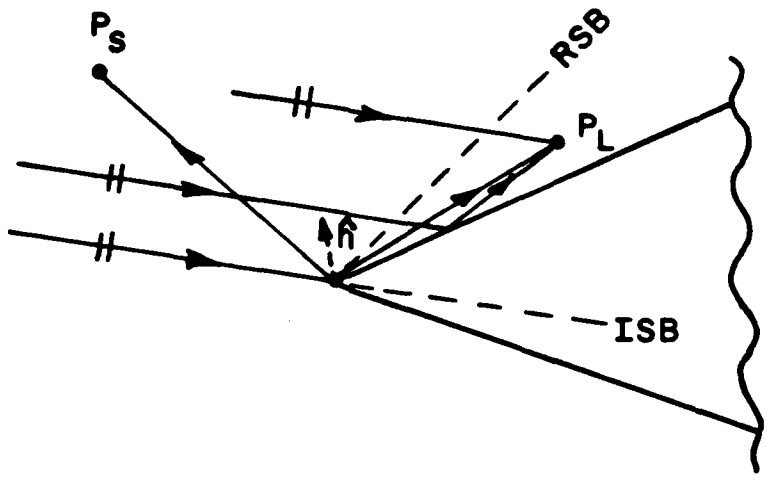

Figure 3: GTD Ray Picture

Using the fact that $\mathbf{H}^s = \nabla \times \mathbf{A}$ the scattered magnetic field is given by

$$\mathbf{H}^s(\mathbf{r}) = \nabla \times \int_0^{2\pi} d\phi' \int_0^{\infty} \mathbf{J_{go}}(r', \phi') \frac{e^{-jkR}}{4\pi R} r' \sin\alpha dr' \tag{3.9}$$

Since the curl is operating on the unprimed or observation coordinates, one can move this operation under the integral. Only the Green's function is a function of r; therefore, after applying a vector identity,

$$\nabla \times \left(\mathbf{J_{go}}(r', \phi') G_0(R)\right) = \nabla G_0(R) \times \mathbf{J_{go}}(r', \phi') \tag{3.10}$$

where

$$G_0(R) = \frac{e^{-jkR}}{4\pi R} \tag{3.11}$$

and

$$\nabla G_0(R) = \frac{d}{dR} G_0(R) \nabla R = -(jk + \frac{1}{R}) \frac{e^{-jkR}}{R} \hat{R} \tag{3.12}$$

since

$$\nabla R = \hat{R} \tag{3.13}$$

Substituting into (3.9), one obtains

$$\mathbf{H}^s(\mathbf{r}) = \int_0^{2\pi} d\phi' \int_0^{\infty} \mathbf{f}(r', \phi') e^{jkq(r', \phi')} dr' \tag{3.14}$$

where

$$\mathbf{f}(r', \phi') = -r' \frac{Y_0 \sin\alpha}{2\pi R} (jk + \frac{1}{R}) \hat{R} \times (\hat{x} \sin\alpha - \hat{z} \cos\alpha \cos\phi') \tag{3.15}$$

and

$$q(r', \phi') = r' \cos\gamma - \sqrt{r^2 + r'^2 - 2rr' \cos\varsigma}. \tag{3.16}$$

Concentrating on the inner integral on r' in Equation (3.9), one finds that

$$\mathbf{I}(r', \phi') = \int_0^{\infty} \mathbf{f}(r', \phi') e^{jkq(r', \phi')} dr'. \tag{3.17}$$

The function f is slowly varying in the interval and the exponential function is oscillatory with a stationary phase point. It is therefore clear that the dominant contribution to the integral in (3.17) comes from the stationary point at $r' = r_s$ and from the end point or cone tip at $r' = 0$. Rather than use the stationary phase method, it is more convenient to employ the saddle point technique to evaluate not only the leading terms but also the higher order terms corresponding to the end point and saddle (stationary) contributions which are important in this case. It is noted that it is usually more difficult to obtain higher order terms from the stationary phase approximation. The saddle point method requires one to integrate along the steepest descent path through the saddle point. Transforming to the steepest descent path as in [36] requires the following definitions:

$$q(r', \phi') = q(r_s, \phi') - s^2 \tag{3.18}$$

and

$$G(s) = \mathbf{f}(r', \phi') \frac{dr'}{ds} \tag{3.19}$$

where, in addition, one defines

$$s_a \equiv \pm|\sqrt{q(r_s,\phi') - q(0,\phi')}| \qquad r_s \lesseqgtr 0. \tag{3.20}$$

G has not been written as a vector for convenience even though it is defined in terms of a vector function in that it is not relevant to the derivation.

Next, G(s) is written as in [36] as

$$G(s) = G(0) + (G(s) - G(0)). \tag{3.21}$$

So the integral **I** becomes

$$\mathbf{I} = e^{jkq(r_s,\phi')}\left\{G(0)\int_{s_a}^{\infty} e^{-jks^2}ds + \int_{s_a}^{\infty}\frac{(G(s)-G(0))}{-2jks}\frac{d}{ds}e^{-jks^2}ds\right\}. \tag{3.22}$$

Integrating by parts once more (again assuming k lossy), yields

$$\begin{aligned}\mathbf{I} \;=\; & e^{jkq(r_s,\phi')}\left\{G(0)\int_{s_a}^{\infty} e^{-jks^2}ds + \frac{(G(s_a)-G(0))}{2jks_a}e^{-jks_a{}^2}\right.\\ & \left.+\frac{1}{2jk}\int_{s_a}^{\infty}\frac{d}{ds}\left[\frac{G(s)-G(0)}{s}\right]e^{-jks^2}ds\right\}.\end{aligned} \tag{3.23}$$

A new function H(s) is defined by

$$H(s) = \frac{d}{ds}\left[\frac{G(s)-G(0)}{s}\right] \tag{3.24}$$

and written

$$H(s) = H(0) + (H(s) - H(0)) \tag{3.25}$$

as done before with G(s). Putting this into the integral yields

$$\begin{aligned}\mathbf{I} \;=\; & e^{jkq(r_s,\phi')}\left\{G(0)\int_{s_a}^{\infty} e^{-jks^2}ds + \frac{G(s_a)-G(0)}{2jks_a}e^{-jks_a{}^2}\right.\\ & \left.+\frac{1}{2jk}H(0)\int_{s_a}^{\infty}e^{-jks^2}ds + \frac{1}{2jk}\int_{s_a}^{\infty}\left[\frac{H(s)-H(0)}{-2jks}\right]\frac{d}{ds}e^{-jks^2}ds\right\}\end{aligned} \tag{3.26}$$

Integrating by parts again and ignoring the unintegrated term yields

$$\mathbf{I} \simeq e^{jkq(r_s,\phi')} \left\{ \left[G(0) + \frac{H(0)}{2jk} \right] \int_{s_a}^{\infty} e^{-jks^2} ds + \frac{e^{-jks_a{}^2}}{2jk} \frac{G(s_a) - G(0)}{s_a} + \frac{e^{-jks_a{}^2}}{(2jk)^2} \frac{H(s_a) - H(0)}{s_a} \right\} \tag{3.27}$$

The integral from s_a to ∞ is known as a transition function. It can be written in terms of the Fresnel integral. In the uniform theory of diffraction (UTD) format, one finds that

$$\int_X^{\infty} e^{-jt^2} dt = \sqrt{\frac{\pi}{j}} U(-X) + \frac{F(X^2)}{2jX} e^{-jX^2} \tag{3.28}$$

where U(X) is the unit step function given by

$$U(X) = \begin{cases} 1 & \text{for X>0, and} \\ 0 & \text{for X<0} \end{cases} \tag{3.29}$$

and from [19]

$$F(X) \equiv 2j\sqrt{X} e^{jX} \int_{\sqrt{X}}^{\infty} e^{-jt^2} dt. \tag{3.30}$$

After a change of variables, the transition function is written as

$$\int_{s_a}^{\infty} e^{-jks^2} dt = \sqrt{\frac{\pi}{jk}} U(-\sqrt{k} s_a) + \frac{F(ks_a{}^2)}{2jks_a} e^{-jks_a{}^2}. \tag{3.31}$$

Our expression has several terms of the form:

$$e^{jk(q(r_s,\phi') - s_a{}^2)} \tag{3.32}$$

but, by definition

$$q(r_s, \phi') - s_a{}^2 = q(0, \phi') = -r. \tag{3.33}$$

Substituting and rearranging terms in (3.27) yields

$$\begin{aligned} \mathbf{I}(r, \phi', k) \simeq\ & e^{jkq(r_s,\phi')} U(-\sqrt{k} s_a) \sqrt{\frac{\pi}{jk}} \left[G(0) + \frac{H(0)}{2jk} \right] \\ & + e^{-jkr} \frac{\left[1 - F(ks_a{}^2) \right]}{2jks_a} \left\{ G(s_a) - G(0) + \frac{H(s_a) - H(0)}{2jk} \right\} \\ & + e^{-jkr} \frac{F(ks_a{}^2)}{2jks_a} \left\{ G(s_a) + \frac{H(s_a)}{2jk} \right\}. \end{aligned} \tag{3.34}$$

The derivation of the following terms is shown in Appendix A.

$$G(s_a) = 0 \tag{3.35}$$

$$H(s_a) = \frac{s_a G'(s_a) + G(0)}{{s_a}^2} \tag{3.36}$$

Using these relations in the expression yields a more physically revealing form of the integrand which is given by

$$\begin{aligned}
\mathbf{I}(r, \phi', k) \simeq\ & e^{jkq(r_s,\phi')} U(-\sqrt{k}s_a) \sqrt{\frac{\pi}{jk}} \left[G(0) + \frac{H(0)}{2jk} \right] \\
& + e^{-jkr} \left[\frac{G(0)}{2jks_a} \left[F(k{s_a}^2) - \left(1 - \frac{1}{2jk{s_a}^2} \right) \right] - \frac{H(0)}{2jk} \frac{(1 - F(k{s_a}^2))}{2jks_a} \right] \\
& + e^{-jkr} \frac{G'(s_a)}{(2jks_a)^2}
\end{aligned} \tag{3.37}$$

Note that different wave components can be identified as follows:

$$\mathbf{I} = \mathbf{I}_{ref} + \mathbf{I}_{tran} + \mathbf{I}_{diff} \tag{3.38}$$

where

$$\mathbf{I}_{ref} = e^{jkq(r_s,\phi')} U(-\sqrt{k}s_a) \sqrt{\frac{\pi}{jk}} \left[G(0) + \frac{H(0)}{2jk} \right] \tag{3.39}$$

$$\mathbf{I}_{tran} = e^{-jkr} \left[\frac{G(0)}{2jks_a} \left[F(k{s_a}^2) - \left(1 - \frac{1}{2jk{s_a}^2} \right) \right] - \frac{H(0)}{2jk} \frac{(1 - F(k{s_a}^2))}{2jks_a} \right] \tag{3.40}$$

$$\mathbf{I}_{diff} = e^{-jkr} \frac{G'(s_a)}{(2jks_a)^2}. \tag{3.41}$$

The reflected field component, $\mathbf{I}_{ref}$, containing the step function, corresponds to the surface reflected field. It vanishes in the shadow region bounded by the RSB and exists only in the lit region beyond the RSB when $s_a < 0$. The higher order term is required because the first order term vanishes at the tip. There is a tip-diffracted or end point term, $\mathbf{I}_{diff}$. This term is the same term that was found

in the non-uniform solution. It represents the field diffracted from the tip. Lastly, there is the transition term, $\mathbf{I}_{tran}$. This factor keeps the total solution uniform across the RSB, and it reduces to zero in the deep shadow region. Moreover, the combination of all three components provides continuity across the RSB.

The scattered magnetic field is then given by

$$\mathbf{H}^s \simeq \int_0^{2\pi} \left[\mathbf{I}_{ref} + \mathbf{I}_{tran} + \mathbf{I}_{diff}\right] d\phi' \tag{3.42}$$

or more specifically

$$\begin{aligned}\mathbf{H}^s(\mathbf{r},\phi,k) \simeq \int_0^{2\pi} \Bigg[& e^{jkq(r_s,\phi')} U(-\sqrt{k}s_a)\sqrt{\frac{\pi}{jk}}\left[G(0) + \frac{H(0)}{2jk}\right] \\ & + e^{-jkr}\left[\frac{G(0)}{2jks_a}\left[F(ks_a{}^2) - \left(1 - \frac{1}{2jks_a{}^2}\right)\right] - \frac{H(0)}{2jk}\frac{\left(1 - F(ks_a{}^2)\right)}{2jks_a}\right] \\ & + e^{-jkr}\frac{G'(s_a)}{(2jks_a)^2}\Bigg] d\phi'. \end{aligned} \tag{3.43}$$

This expression will not yield the desired expression for the UTD tip diffracted field as yet. One problem is that, in this form, there is no term that exists on the lit side, that can be attributed to the tip. Before the modification is undertaken, it will be shown that this solution is uniform across the reflection boundary. In addition, the behavior far from the reflection shadow boundary in the deep shadow will be investigated. The transition term plays an important role because, in general, the reflection boundary transition region extends into almost the entire region in which the reflected field is present. Once this is completed, the expression will be rewritten and the UTD tip diffracted field identified. It will be shown that this new form yields the same limits as the quasi UTD form near the reflection shadow boundary, and far from the reflection shadow boundary. It also approximates the quasi UTD solution everywhere within the transition region.

In the next section, the expression for the saddle point contribution will be

determined. It will be shown that the saddle point migrates as a function of ϕ', and the implications of this behavior will be discussed.

3.3 LOCATION OF THE SADDLE POINT

The saddle point r_s is where the derivative of the phase function in the integrand of (3.17) goes to zero where the phase function is given by

$$q(r', \phi') = r' \cos\gamma - \sqrt{r^2 + r'^2 - 2rr' \cos\varsigma} \tag{3.44}$$

Then, its derivative is

$$\frac{d}{dr'} q(r', \phi') = \cos\gamma - \frac{r' - r\cos\varsigma}{\sqrt{r^2 + r'^2 - 2rr'\cos\varsigma}}. \tag{3.45}$$

Setting this equal to zero yields

$$r_s = r(\cos\varsigma \pm \cos\gamma \frac{\sin\varsigma}{\sin\gamma}) \tag{3.46}$$

Substituting this result into Equation (3.45), it can be seen that the + sign satisfies the original equation; therefore,

$$r_s = r(\cos\varsigma + \cos\gamma \frac{\sin\varsigma}{\sin\gamma}). \tag{3.47}$$

Figures 4 thru 6 show plots of the migration of the saddle point as a function of ϕ' for an observer located in specific regions.

In the lit side of the reflection shadow boundary, the saddle point r_s becomes positive for some ϕ'; however, it is always negative on the shadow side of the reflection shadow boundary. This ties in to the existence of the reflected field. Recall that

$$s_a = \pm|\sqrt{q(r_s, \phi') - q(0, \phi')}| \qquad r_s \lessgtr 0 \tag{3.48}$$

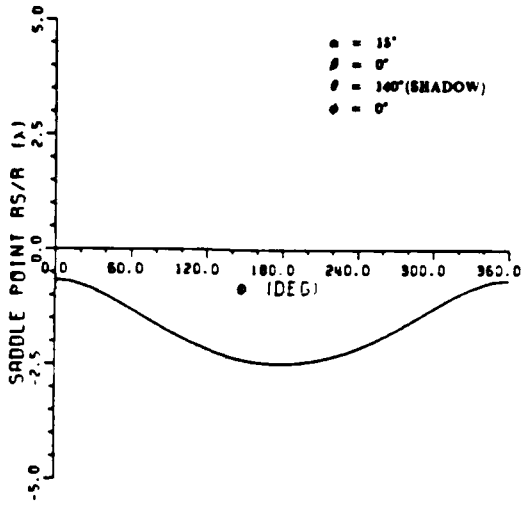

Figure 4: Migration of Saddle Point with ϕ' for an Observer in the Deep Shadow Side of the Reflection Boundary

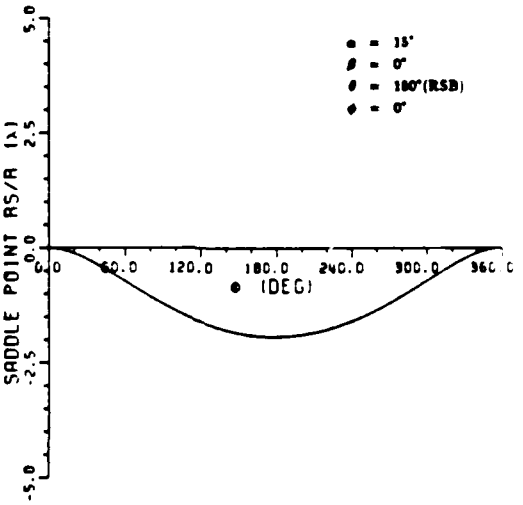

Figure 5: Migration of Saddle Point with ϕ' for an Observer at the Reflection Shadow Boundary Corresponding to the Specular Line of Reflection

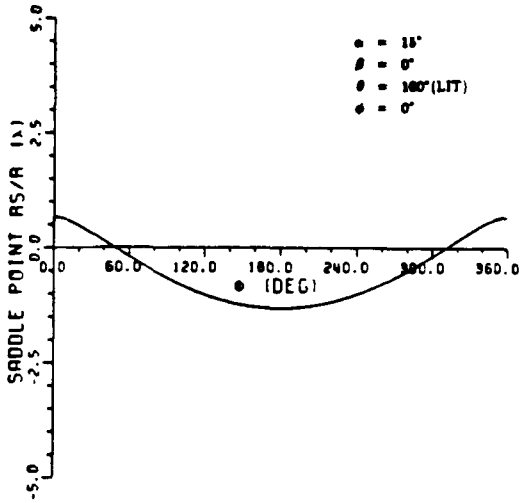

Figure 6: Migration of Saddle Point with ϕ' for an Observer in the Deep Lit Side of the Reflection Shadow Boundary

and that the reflected field has a unit step function, $U(-\sqrt{k}s_a)$. When $r_s < 0$, then $s_a > 0$ and there is no reflected field. This follows since $r_s < 0$ occurs in the shadow side of the reflection shadow boundary. When $r_s > 0$, then $s_a < 0$, and there can be a reflected field component. It is worth noting that even in the lit side of the reflection shadow boundary, r_s is not always greater than zero, and that it varies as a function of ϕ'. That is, the reflected field exists only for certain aspects. Also, the saddle point approaches the end point which therefore requires a more careful treatment of the integral in (3.17). That is the reason why the asymptotic approximation to the integration in (3.17) was performed as shown in the previous section.

This saddle point migration was also observed by Molinet [39] in his research.

In the next section, the behavior of the integral at the reflection shadow boundary and in the deep shadow side of the reflection boundary will be investigated.

3.4 LIMITING CASES

Two limiting cases are investigated for the result in (3.37). Near the RSB, and in the deep shadow side of the reflection shadow boundary.

Substituting the actual expression for H from (3.24) into the integral in (3.34), and recalling that $G(s_a) = 0$, yields the following in ϕ':

$$\begin{aligned}\mathbf{I}(r,\phi',k) \simeq\ & e^{jkq(r_s,\phi')}U(-\sqrt{k}s_a)\sqrt{\frac{\pi}{jk}}\left[G(0)+\frac{G''(0)}{4jk}\right] \\ & +e^{-jkr}\left[\frac{G(0)}{2jks_a}\left[F(ks_a{}^2)-\left(1-\frac{1}{2jks_a{}^2}\right)\right]-\frac{G''(0)}{4jk}\frac{(1-F(ks_a{}^2))}{2jks_a}\right] \\ & +e^{-jkr}\frac{G'(s_a)}{(2jks_a)^2}. \end{aligned} \tag{3.49}$$

This is the expression from which uniformity is proven. The small and large argument forms of the transition function F(X) are given in [19] as,

$$F(X)\approx\begin{cases} 1-\frac{1}{2jX} & \text{for X>>1, and} \\ \sqrt{\pi jX}e^{jX} & \text{for X<<1.}\end{cases} \tag{3.50}$$

Near the shadow boundary, $X \to 0$; therefore, the small argument form of the transition function is used. In terms of specific components, the expression becomes

$$\mathbf{I}_{ref} = e^{jkq(r_s,\phi')}U(-\sqrt{k}s_a)\sqrt{\frac{\pi}{jk}}\left[G(0)+\frac{G''(0)}{4jk}\right] \tag{3.51}$$

$$\begin{aligned}\mathbf{I}_{tran} = e^{-jkr}\Bigg[&\frac{G(0)}{2jks_a}\left[\sqrt{\pi jk}|s_a|e^{jks_a{}^2}-\left(1-\frac{1}{2jks_a{}^2}\right)\right] \\ &-\frac{G''(0)}{4jk}\frac{\left[1-\sqrt{\pi jk}|s_a|e^{jks_a{}^2}\right]}{2jks_a}\Bigg]\end{aligned} \tag{3.52}$$

$$\mathbf{I}_{diff} = e^{-jkr}\frac{G'(s_a)}{(2jks_a)^2} \tag{3.53}$$

Next, G is expanded in a Taylor series about s_a. This is given by

$$G(s) = G(s_a) + (s - s_a)G'(s_a) + \frac{(s - s_a)^2}{2}G''(s_a) + \frac{(s - s_a)^3}{6}G'''(s_a) + \ldots \quad (3.54)$$

from which

$$G'(s) = G'(s_a) + (s - s_a)G''(s_a) + \frac{(s - s_a)^2}{2}G'''(s_a) + \ldots \quad (3.55)$$

$$G''(s) = G''(s_a) + (s - s_a)G'''(s_a) + \ldots \quad (3.56)$$

Recall that $G(s_a) = 0$; therefore, evaluating at $s = 0$ yields

$$G(0) = -s_a G'(s_a) + \frac{{s_a}^2}{2}G''(s_a) + \ldots \quad (3.57)$$

$$G'(0) = G'(s_a) - s_a G''(s_a) + \ldots \quad (3.58)$$

$$G''(0) = G''(s_a) + \ldots \quad (3.59)$$

Substituting these into Equations (3.51) and noting that ${s_a}^2 - r = q(0) + {s_a}^2 = q(r_s)$, yields

$$\mathbf{I}_{ref} = e^{jkq(r_s,\phi')}U(-\sqrt{k}s_a)\sqrt{\frac{\pi}{jk}}\left[\frac{G''(s_a)}{4jk} + o(s_a)\right] \quad (3.60)$$

$$\mathbf{I}_{tran} = e^{-jkr}\left[\frac{G'(s_a)}{2jk} - \frac{G'(s_a)}{(2jks_a)^2}\right] + e^{jkq(r_s,\phi')}\frac{1}{2}\sqrt{\frac{\pi}{jk}}\frac{G''(s_a)}{4jk}\mathrm{sgn}(s_a) \quad (3.61)$$

$$\mathbf{I}_{diff} = e^{-jkr}\frac{G'(s_a)}{(2jks_a)^2}. \quad (3.62)$$

Approaching from the shadow side of the reflection shadow boundary, $s_a \rightarrow 0^+$ $(s_a > 0)$, the integrand becomes

$$\mathbf{I}(r, \phi, k) = \mathbf{I}_{tran} + \mathbf{I}_{diff} \quad (3.63)$$

$$= \frac{1}{2}e^{jkq(r_s,\phi')}\sqrt{\frac{\pi}{jk}}\frac{G''(s_a)}{4jk} + e^{-jkr}\frac{G'(s_a)}{2jk} \quad (3.64)$$

Approaching from the lit side of the reflection shadow boundary, $s_a \rightarrow 0^-$ ($s_a < 0$), the integrand becomes

$$\begin{aligned} \mathbf{I}(r,\phi,k) &= \mathbf{I}_{ref} + \mathbf{I}_{tran} + \mathbf{I}_{diff} \\ &= e^{jkq(r_s,\phi')}\sqrt{\frac{\pi}{jk}}\frac{G''(s_a)}{4jk}\left(1-\frac{1}{2}\right) + e^{-jkr}\frac{G'(s_a)}{2jk} \\ &= \frac{1}{2}e^{jkq(r_s,\phi')}\sqrt{\frac{\pi}{jk}}\frac{G''(s_a)}{4jk} + e^{-jkr}\frac{G'(s_a)}{2jk} \end{aligned} \tag{3.65}$$

This requires that the limit as $s_a \rightarrow 0$ be taken, which means that $r_s \rightarrow 0$. This occurs at the reflection shadow boundary, where $\varsigma + \gamma = \pi$. In addition, $q(r_s,\phi') = -r$ at the reflection shadow boundary

From the above, it has been shown that the integrand in ϕ', and hence the integral over ϕ', is continuous across the reflection shadow boundary and the solution is uniform.

Far from the RSB the large argument form of the transition function is used. The behavior far from the RSB on the shadow side of the RSB will be investigated. In this case, one finds that

$$\mathbf{I}_{ref} = 0 \tag{3.66}$$

$$\mathbf{I}_{tran} = 0 \tag{3.67}$$

$$\mathbf{I}_{diff} = e^{-jkr}\frac{G'(s_a)}{(2jks_a)^2}. \tag{3.68}$$

The above results follow because on the shadow side of the reflection boundary, $s_a > 0$ and the step function term containing the reflected field vanishes because there is no reflected field in this region. In the transition term, there are $1 - F(ks_a{}^2)$ factors. Using the large argument form of the transition function, these asymptotically go to zero. Therefore, $\mathbf{I}$ reduces to the tip–diffracted term alone such that

$$\mathbf{I}(r,\phi,k) = \mathbf{I}_{diff}. \tag{3.69}$$

As previously mentioned, once integrated, this yields the same value for tip diffracted fields as the exact evaluation of the far zone PO integral. Note that on the lit side of the RSB, the argument of the transition function F is never sufficiently large; thus, unlike the shadow side, the transition region extends over the entire lit side of the RSB.

3.5 UTD TIP DIFFRACTED FIELD

The UTD tip diffracted field contains a factor (transition function) which keeps it bounded at the RSB. In the quasi UTD form from the previous section, the singularities at the GO boundaries were corrected additively. This is similar to the way that the relevant singularities cancel at the RSB in the UAT form described in the beginning of the chapter. Molinet [39], has independently worked the problem of scattering from a cone using the PO approximation. This was done for the special case of axial incidence, and he basically writes his high frequency solution in the form of the uniform asymptotic theory (UAT) [40] which follows from the use of asymptotic methods discussed in Felsen and Marcuvitz [36]. The additive correction in the UAT form requires special treatment to overcome the numerical difficulties encountered in programming this type of solution. The current UTD expression does not encounter this difficulty. In addition, it enables the isolation of a uniform tip diffracted field. The tip diffracted field is extremely useful for both the scattering and the antenna problems.

The UTD form for the scattered field is given by

$$\mathbf{U}^{sc} \approx \mathbf{U}_r^{go} + \mathbf{U}^d \tag{3.70}$$

where, for the cone, the first term is the GO reflected field component, and the second term is the tip diffracted field component. It can be seen that in order to

get the expressions from the previous section in this form, one must first recognize from (3.70) and (3.39) that

$$\mathbf{U}_r^{go} = \mathbf{I}_{ref} = e^{jkq(r_s,\phi')}U(-\sqrt{k}s_a)\sqrt{\frac{\pi}{jk}}\left[G(0) + \frac{H(0)}{2jk}\right] \tag{3.71}$$

$$\mathbf{U}^d = \mathbf{I}_{tran} + \mathbf{I}_{diff} = e^{-jkr}\left[\frac{G(0)}{2jks_a}\left[F(ks_a{}^2) - \left(1 - \frac{1}{2jks_a{}^2}\right)\right]\right. \tag{3.72}$$

$$\left. - \frac{H(0)}{2jk}\frac{(1 - F(ks_a{}^2))}{2jks_a}\right] + e^{-jkr}\frac{G'(s_a)}{(2jks_a)^2} \tag{3.73}$$

where it was previously given that

$$\mathbf{I}_{tran} = e^{-jkr}\left[\frac{G(0)}{2jks_a}\left[F(ks_a{}^2) - \left(1 - \frac{1}{2jks_a{}^2}\right)\right] - \frac{H(0)}{2jk}\frac{(1 - F(ks_a{}^2))}{2jks_a}\right] \tag{3.74}$$

$$\mathbf{I}_{diff} = e^{-jkr}\frac{G'(s_a)}{(2jks_a)^2}. \tag{3.75}$$

One can futher recognize that the terms in $\mathbf{I}_{tran}$ are important only near the reflection shadow boundary; whereas, they are negligible away from the reflection boundary. Near the boundary, s_a is small and the Taylor series expansion for G(0) and H(0) can be used.

Having the expressions in terms of the end point, rather than the saddle point also gives an even clearer picture of the mechanisms involved. The scattered field will have two identifiable sources; the end point (tip) diffracted field, associated with the UTD tip diffracted field, and the surface reflected field. Once the expressions are derived, it will be shown that they reduce to the same limits as the quasi UTD expression from the previous section.

Recall that $H(0) = \frac{1}{2}G''(0)$ and that

$$G(0) = -s_aG'(s_a) + \frac{s_a{}^2}{2}G''(s_a) + \ldots \tag{3.76}$$

$$G'(0) = G'(s_a) - s_aG''(s_a) + \ldots \tag{3.77}$$

$$G''(0) = G''(s_a) + \ldots. \tag{3.78}$$

Substituting this into the expression for $\mathbf{I}_{tran}$ in (3.74) yields

$$\begin{aligned}\mathbf{I}_{tran} &= e^{-jkr}\left[\frac{G''(s_a)}{4jk}\frac{F(ks_a{}^2)}{2jks_a}+\left[1-F(ks_a{}^2)\right]\left(\frac{G'(s_a)}{2jk}-s_a\frac{G''(s_a)}{4jk}\right)\right] \\ &\quad -e^{-jkr}\frac{G'(s_a)}{(2jks_a)^2}\end{aligned} \tag{3.79}$$

The last term cancels $\mathbf{I}_{diff}$; therefore,

$$\begin{aligned}\mathbf{U}^d &= \mathbf{I}_{tran}+\mathbf{I}_{diff} = e^{-jkr}\left[\frac{G''(s_a)}{4jk}\frac{F(ks_a{}^2)}{2jks_a}\right. \\ &\quad \left.+\left[1-F(ks_a{}^2)\right]\left(\frac{G'(s_a)}{2jk}-s_a\frac{G''(s_a)}{4jk}\right)\right]\end{aligned} \tag{3.80}$$

Once again, the small and large argument forms of the transition function F(X) are given below:

$$F(X)\approx\begin{cases}1-\frac{1}{2jX} & \text{for X>>1, and}\\ \sqrt{\pi jX}e^{jX} & \text{for X<<1.}\end{cases} \tag{3.81}$$

Far from the reflection shadow boundary,

$$F(ks_a{}^2)\approx 1-\frac{1}{2jks_a{}^2} \tag{3.82}$$

Assuming the observation point is on the shadow side, then the reflected field, $\mathbf{U}_r^{go}$, is zero, and all that remains is $\mathbf{U}^d$. Inserting the large argument form shown above into $\mathbf{U}^d$ yields

$$\begin{aligned}\mathbf{U}^d &= e^{-jkr}\left[\frac{G''(s_a)}{4jk}\left[\frac{1}{2jks_a}-\frac{1}{(2jk)^2s_a{}^3}\right]+\left[\frac{1}{2jks_a{}^2}\right]\left(\frac{G'(s_a)}{2jk}-s_a\frac{G''(s_a)}{4jk}\right)\right] \\ &= e^{-jkr}\left[\frac{G'(s_a)}{(2jks_a)^2}+o(k^{-3})\right] \\ &\approx e^{-jkr}\frac{G'(s_a)}{(2jks_a)^2}\end{aligned} \tag{3.83}$$

which is the same limit as in the previous section. As before, this is also the value for the tip diffracted fields that the exact evaluation of far zone PO integral yields in this region.

Close to the reflection shadow boundary, the small argument of the transition function is used. That is

$$F(ks_a{}^2) \approx \sqrt{\pi jk}|s_a|e^{jks_a{}^2} \tag{3.84}$$

Hence, for ka$\rightarrow$ 0

$$1 - F(ks_a{}^2) \approx 1 \tag{3.85}$$

$$\frac{F(ks_a{}^2)}{2jks_a} \approx \frac{1}{2}e^{jks_a{}^2}\sqrt{\frac{\pi}{jk}}\mathrm{sgn}(s_a) \tag{3.86}$$

Therefore, noting that $s_a{}^2 - r = q(0) + s_a{}^2 = q(r_s)$, then

$$\mathbf{U}^d \approx \frac{1}{2}e^{jkq(r_s,\phi')}\sqrt{\frac{\pi}{jk}}\frac{G''(s_a)}{4jk}\mathrm{sgn}(s_a) \tag{3.87}$$

$$+e^{-jkr}\frac{G'(s_a)}{2jk} \tag{3.88}$$

and

$$\mathbf{U}_r^{go} \approx e^{jkq(r_s,\phi')}\sqrt{\frac{\pi}{jk}}\frac{G''(s_a)}{4jk}U(-\sqrt{k}s_a) \tag{3.89}$$

Approaching from the shadow side of the reflection shadow boundary, $s_a \rightarrow 0^+$ ($s_a > 0$), the integrand becomes

$$\mathbf{U}^{sc} = \mathbf{U}^d \tag{3.90}$$

$$= \frac{1}{2}e^{jkq(r_s,\phi')}\sqrt{\frac{\pi}{jk}}\frac{G''(s_a)}{4jk} + e^{-jkr}\frac{G'(s_a)}{2jk} \tag{3.91}$$

Approaching from the lit side of the reflection shadow boundary, $s_a \rightarrow 0^-$ ($s_a < 0$), the integrand becomes

$$\mathbf{U}^{sc} = \mathbf{U}_r^{go} + \mathbf{U}^d$$

$$= e^{jkq(r_s,\phi')}\sqrt{\frac{\pi}{jk}}\frac{G''(s_a)}{4jk}\left(1 - \frac{1}{2}\right) + e^{-jkr}\frac{G'(s_a)}{2jk}$$

$$= \frac{1}{2}e^{jkq(r_s,\phi')}\sqrt{\frac{\pi}{jk}}\frac{G''(s_a)}{4jk} + e^{-jkr}\frac{G'(s_a)}{2jk} \tag{3.92}$$

Again, this is the same limit as before. Also, as before, this requires that the limit as $s_a \rightarrow 0$ be taken, which means that $r_s \rightarrow 0$. This occurs at the reflection shadow boundary, where $\varsigma + \gamma = \pi$. In addition, $q(r_s, \phi') = -r$ at the reflection shadow boundary

Investigation of $\mathbf{U}^d$ shows that it is a function of only the end point. For unit amplitude plane wave incidence, using the tip as the phase reference, U^i(tip)=1. Therefore, letting the point Q be the tip, yields the usual form given by

$$\mathbf{U}^d = U^i(Q)\mathbf{D}_T e^{-jkr} \tag{3.93}$$

where

$$\mathbf{D}_T = \left[\frac{G''(s_a)}{4jk}\frac{F(ks_a{}^2)}{2jks_a} + \left[1 - F(ks_a{}^2)\right]\left(\frac{G'(s_a)}{2jk} - s_a\frac{G''(s_a)}{4jk}\right)\right]. \tag{3.94}$$

One should recall that G' and G'' are vector quantities, but for convenience, were not written in vector notation; therefore, $\mathbf{D}_T$ is a vector quantity. This is used to determine the contribution from tip–base interaction for the finite cone. It can also be used, via reciprocity, to determine the radiation from an infinitesimal current element on the cone surface due to this interaction.

The scattered magnetic field is then given by

$$\mathbf{H}^s \simeq \int_0^{2\pi}\left[\mathbf{U}_r^{go} + \mathbf{U}^d\right] d\phi' \tag{3.95}$$

Moreover, The magnetic field from the tip is then given by

$$\mathbf{H}_{tip} \simeq \int_0^{2\pi}\mathbf{D}_T e^{-jkr} d\phi' \tag{3.96}$$

where $\mathbf{D}_T$ was given in (3.94).

3.6 RESULTS

In this section, plots of the scattered field for various cone configurations will be shown. In addition, the uniform PO solution is compared to the far zone PO

solution for the scattered field from Chapter II. Both will be compared to Felsen's small angle cone result [5].

Theory is compared to experiment. The tip–base interaction shown in Figure 19 is included in the computation of the RCS for a finite flat–backed in the result given by Burnside and Peters [10], and it is shown that this mechanism corrects the previous discrepancy between calculation and measurement.

Let us begin with the comparisons. The H_ϕ^s component found in terms of both the uniform and exact far zone PO solutions are plotted in Figures 7 thru 18 with Felsen's small angle cone result. There is reasonable agreement over most of the shadow side of the reflection boundary between Felsen's result [5] and the uniform PO solution for the case of axial incidence. The agreement is excellent for small cone angles where Felsen's result [5] is the most accurate; however, the agreement holds up even for cone angles up to 15°. When the incidence is nonaxial, the agreement between the present result and the one obtained using the result in [5] is still good for the narrow angle cone, but is 1 or 2 dB worse than that for axial incidence in the case of wider angle cones. The present uniform PO solution and the far zone PO solution are valid when the cone is fully illuminated. This is true when the incidence angle is smaller than the internal cone angle. Numerical results were also obtained for incidence angles that were at or near this limit to see how the uniform solution behaved. As long as one is a few degrees away from this boundary, the results look fine compared to those far from this boundary; however, when evaluated right on this boundary, as shown in Figure 12, the curve shows an unexpected drop of approximately 8 dB at the cone surface. One would not expect the field to vary this much in the span of 1°; therefore, it is assumed that this is a numerical problem; however, this could also be a result of grazing incidence when the incident field lies along this boundary.

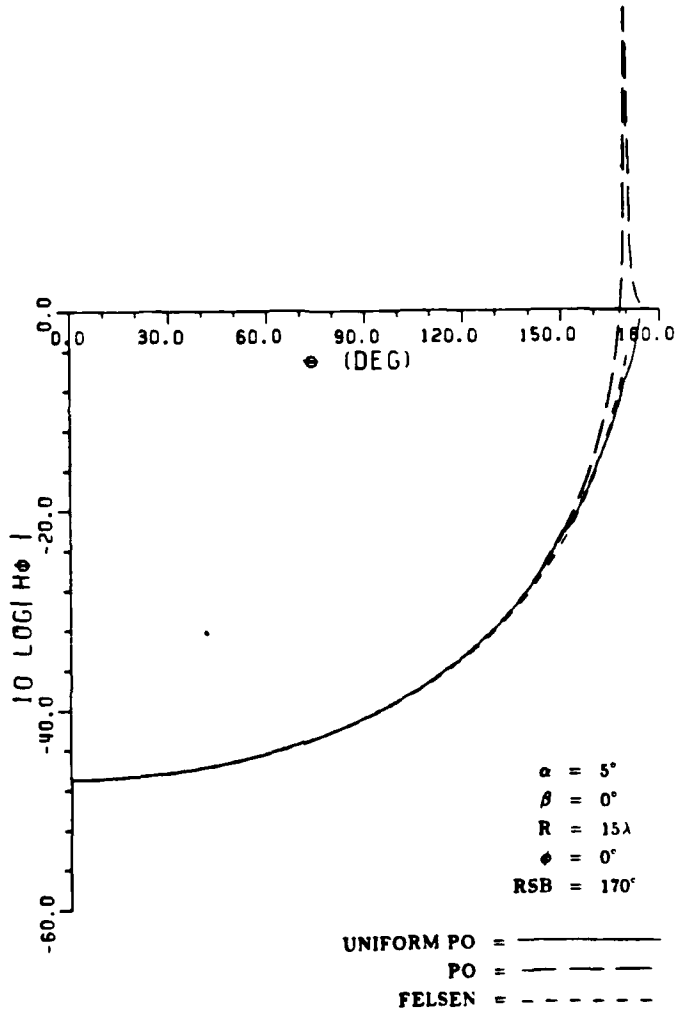

Figure 7: Comparison of H_ϕ^s for $\alpha = 5°$, $\beta = 0°$, $\phi = 0°$

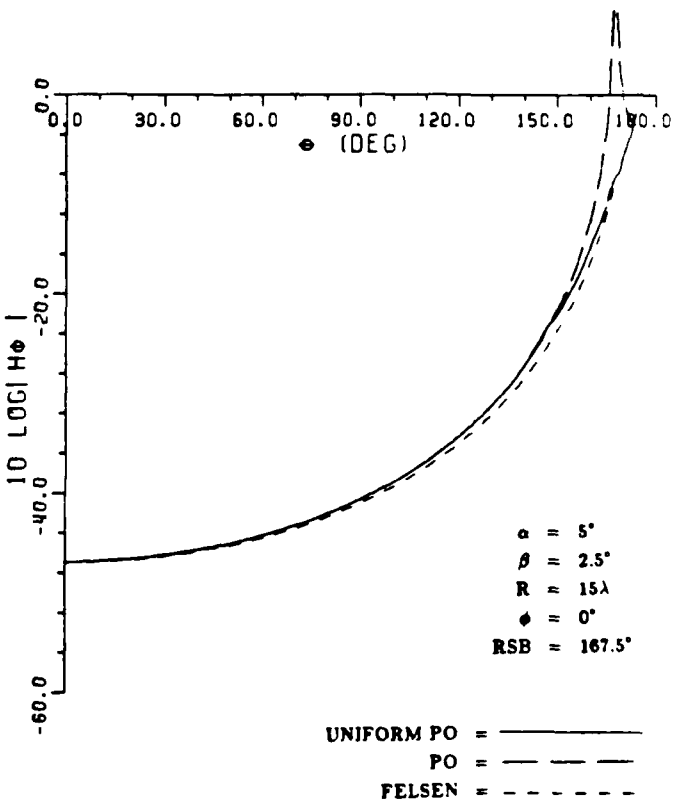

Figure 8: Comparison of H_ϕ^s for $\alpha = 5°$, $\beta = 2.5°$, $\phi = 0°$

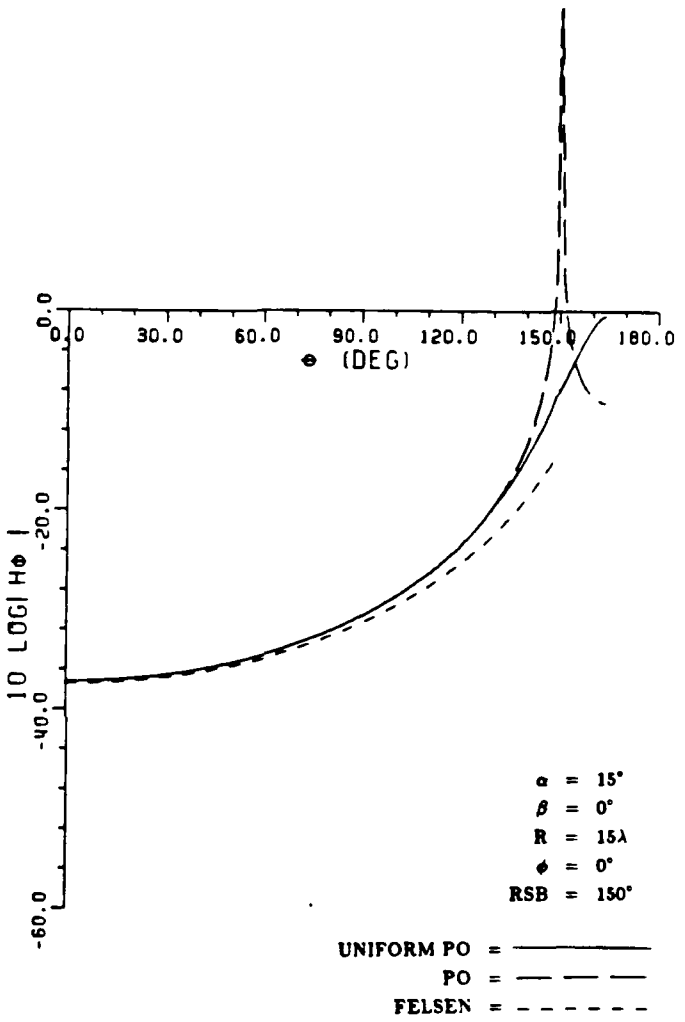

Figure 9: Comparison of H_{ϕ}^{s} for $\alpha = 15°$, $\beta = 0°$, $\phi = 0°$

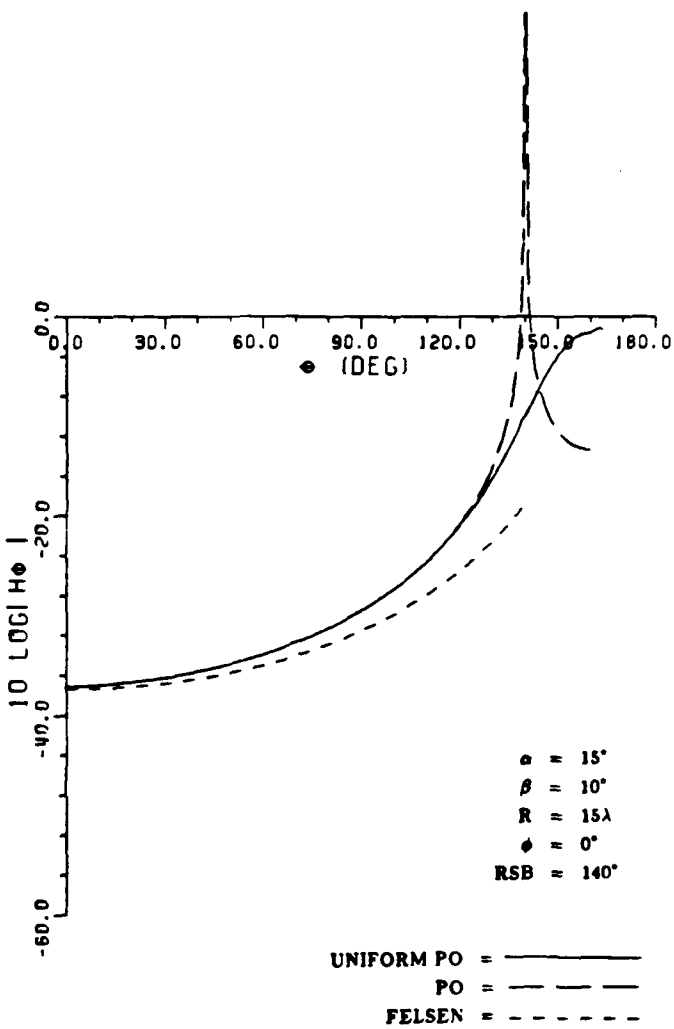

Figure 10: Comparison of H_ϕ^s for $\alpha = 15°$, $\beta = 10°$, $\phi = 0°$

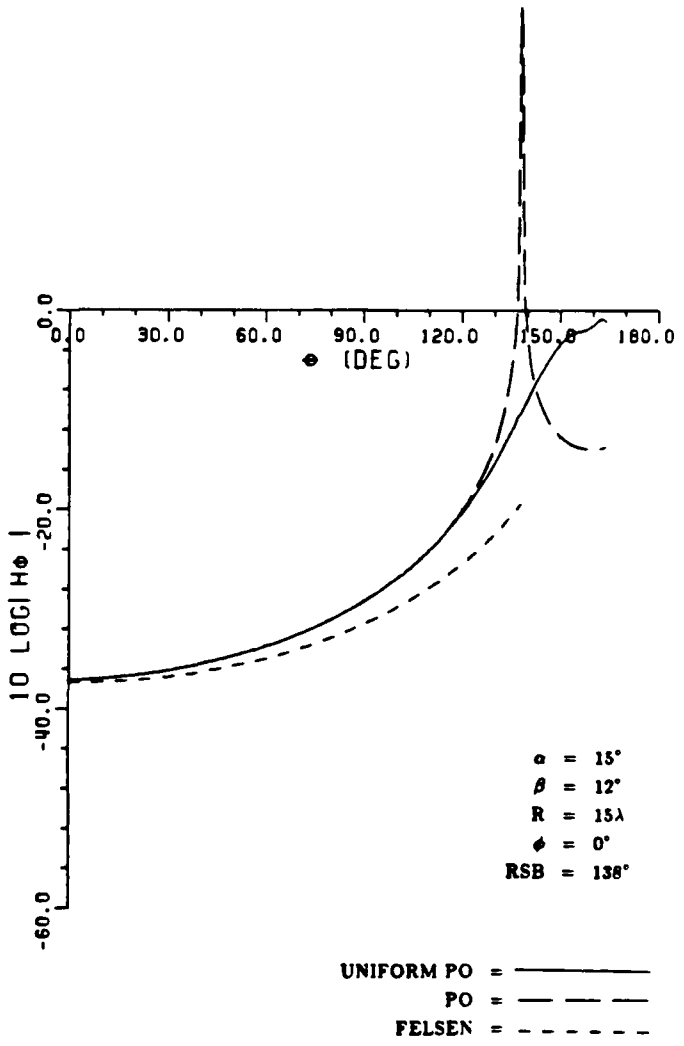

Figure 11: Comparison of H_ϕ^s for $\alpha = 15°$, $\beta = 12°$, $\phi = 0°$

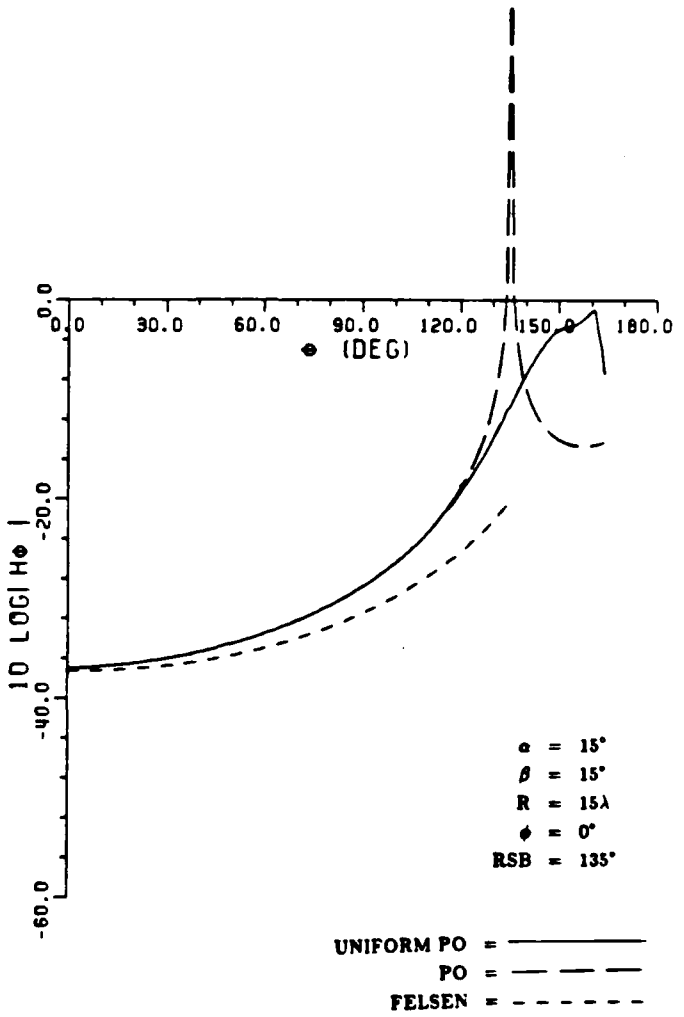

Figure 12: Comparison of H_ϕ^s for $\alpha = 15°$, $\beta = 15°$, $\phi = 0°$

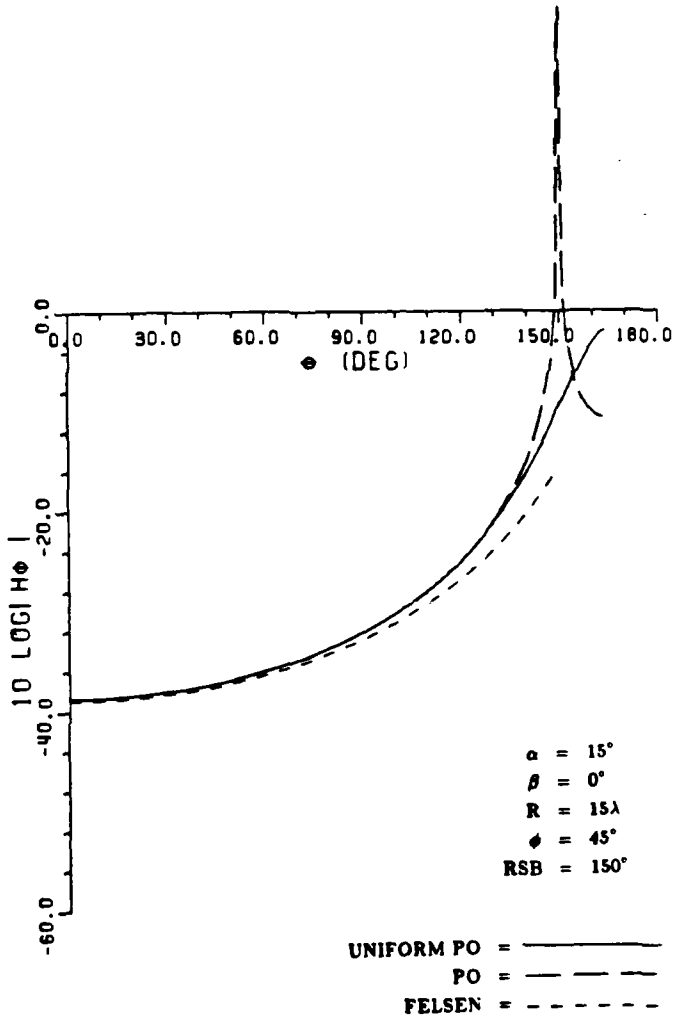

Figure 13: Comparison of H_ϕ^s for $\alpha = 15°$, $\beta = 0°$, $\phi = 45°$

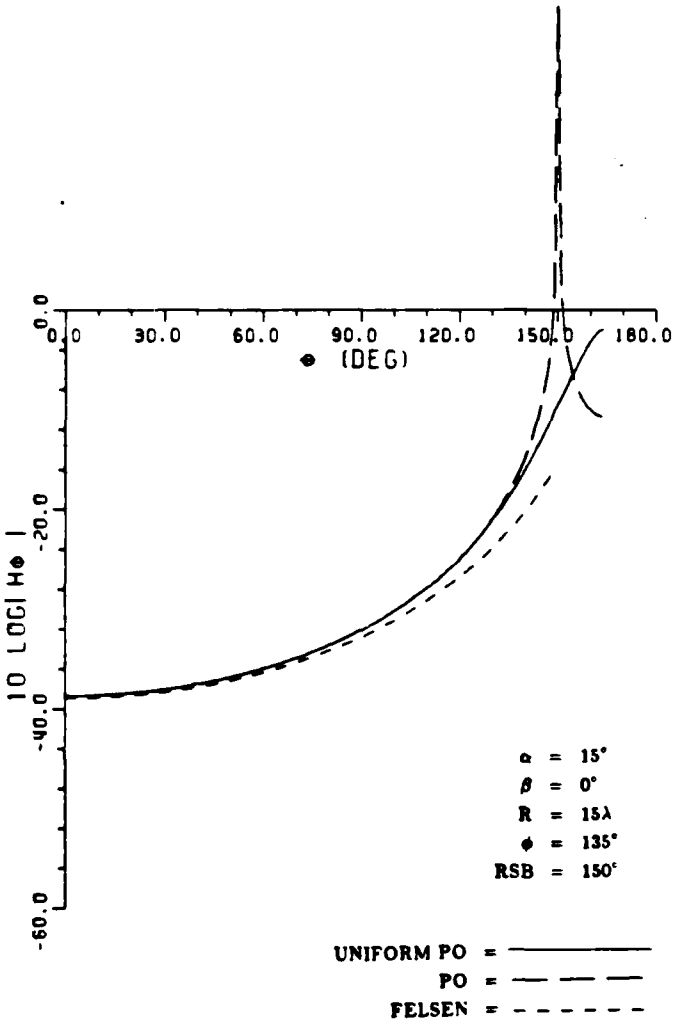

Figure 14: Comparison of H_ϕ^s for $\alpha = 15°$, $\beta = 0°$, $\phi = 135°$

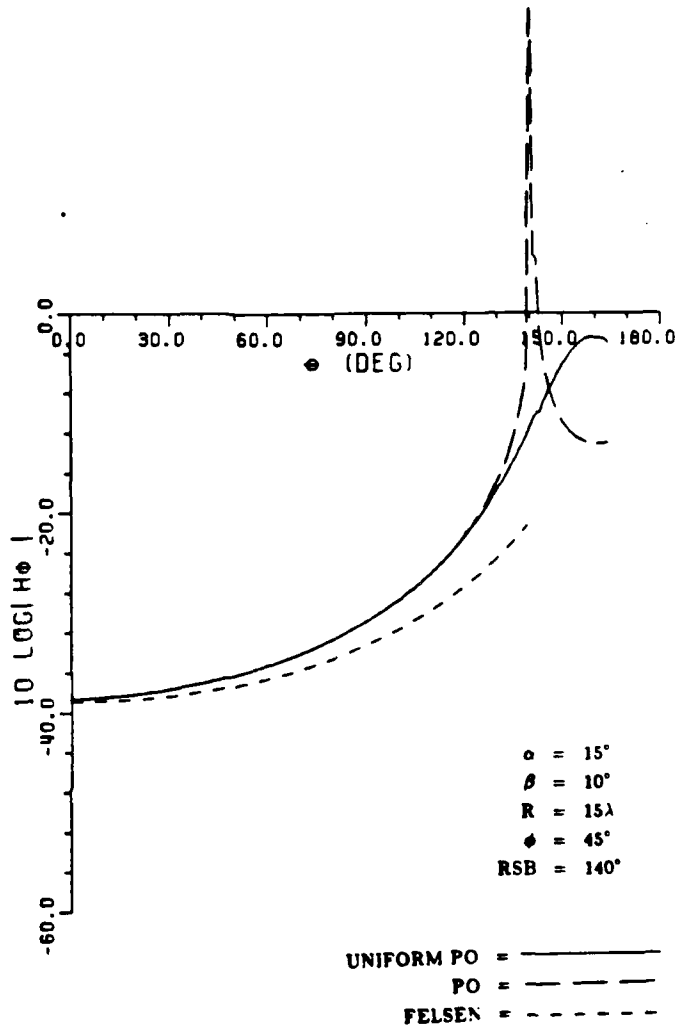

Figure 15: Comparison of H_ϕ^s for $\alpha = 15°$, $\beta = 10°$, $\phi = 45°$

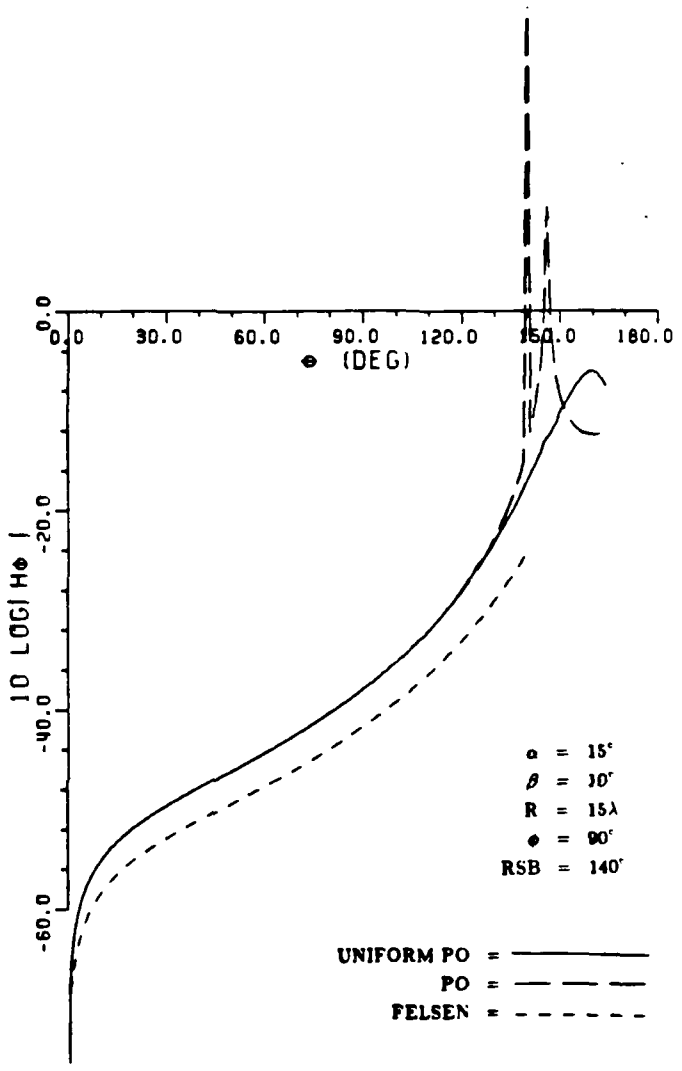

Figure 16: Comparison of H_ϕ^s for $\alpha = 15°$, $\beta = 10°$, $\phi = 90°$

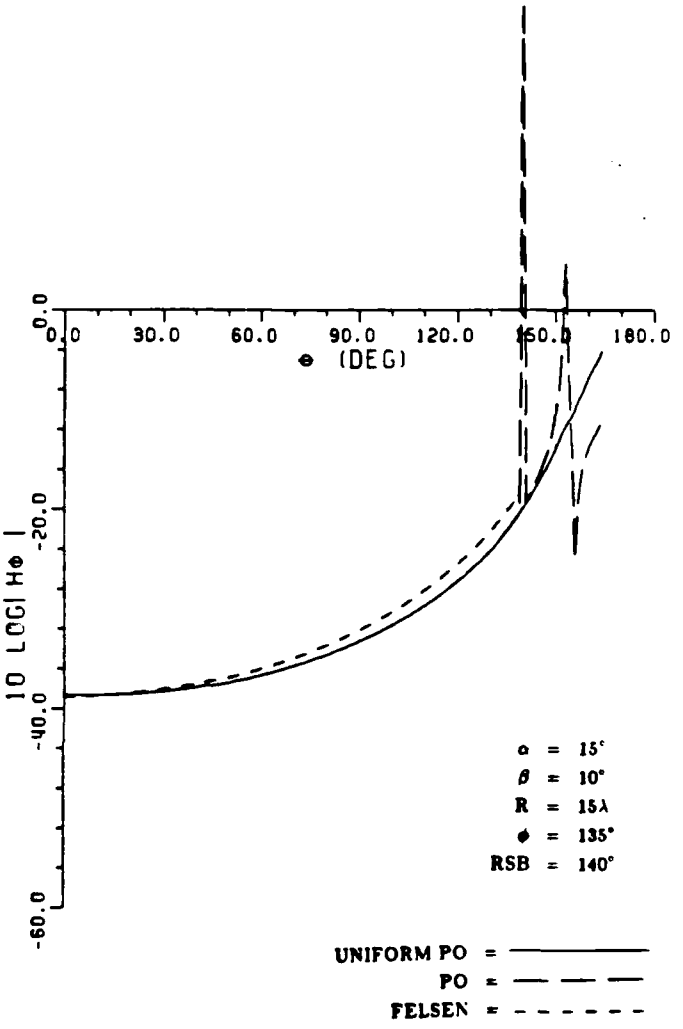

Figure 17: Comparison of H_ϕ^s for $\alpha = 15°$, $\beta = 10°$, $\phi = 135°$

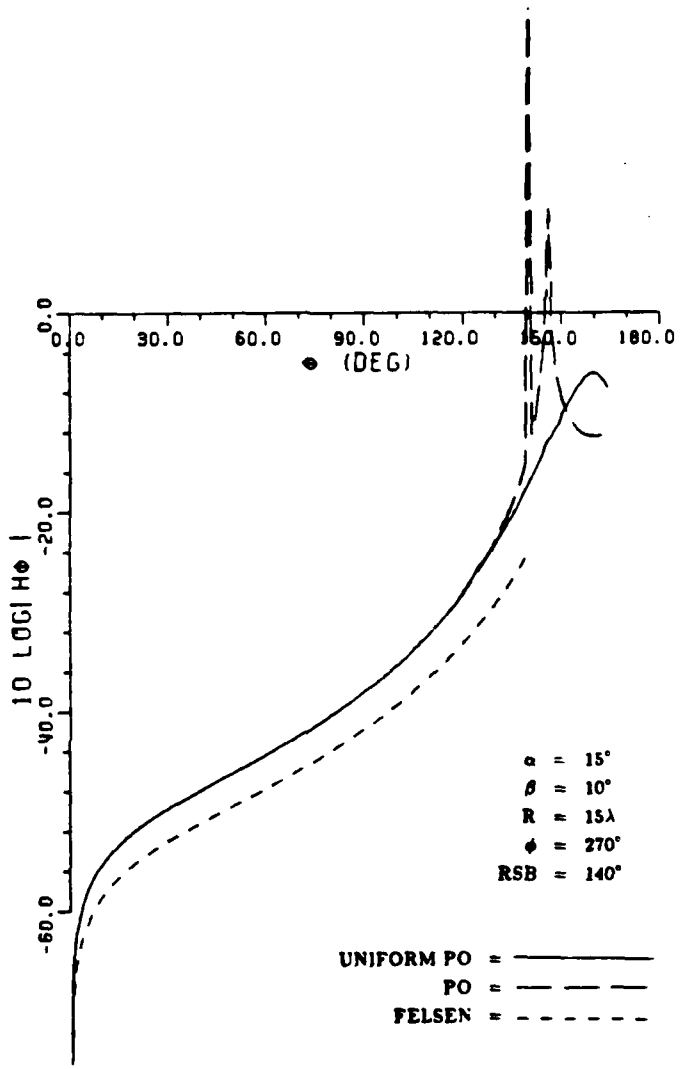

Figure 18: Comparison of H_ϕ^s for $\alpha = 15°$, $\beta = 10°$, $\phi = 270°$

The UTD tip diffracted field is used to determine the tip–base interaction shown in Figure 19. The tip–base interaction is included in the GTD analysis conducted in [10]. In Figure 20, the plots of Burnside and Peter's [10] GTD solution for the RCS of the flat–backed cone are compared to measurement. In Figure 21, the GTD solution in [10] is compared with a moment method (MM) solution for the finite flat–backed right circular cone. It is noted that the MM solution shows essentially the same behavior as the measurements; furthermore, the GTD solution in [10] is in error, with respect to both measurements and the MM solution, by approximately 3 dB over the entire frequency range $8 < ka < 12$. In Figure 22, the comparison of the GTD solution in [10] which is modified to include the tip–base interaction based on the current work is shown; indeed, it is evident from this figure that the inclusion of the tip–base interaction essentially removes the error which results if the latter interaction is not included. The ripple in the MM solution is probably caused by the interference between the direct tip and base diffraction contributions. It is noted that the direct diffraction by the tip is not included in Figures 20 and 21 or in the modification of the GTD result of [10] shown in Figure 22.

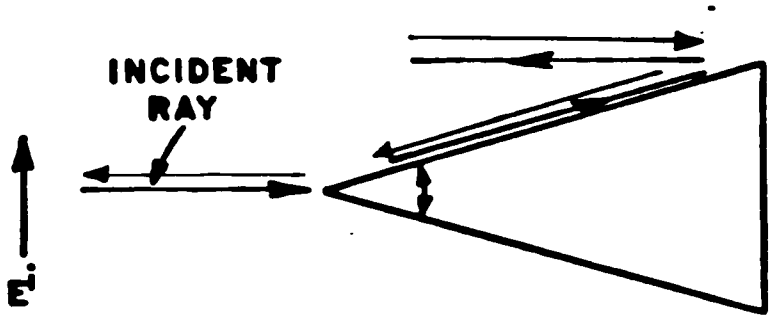

Figure 19: Tip–Base Mechanism

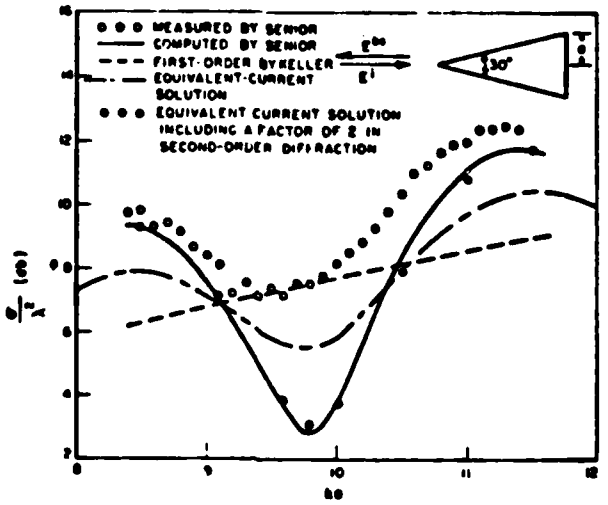

Figure 20: RCS for Axial Backscatter from a Finite Flat–Backed Cone as Computed by Burnside and Peters [10]

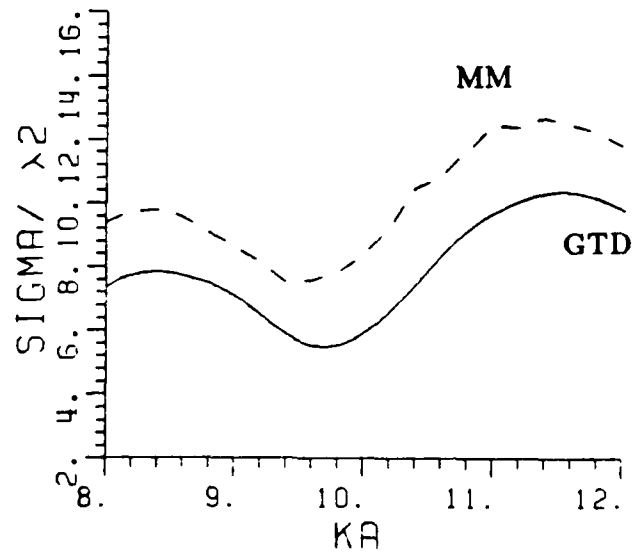

Figure 21: Comparison of RCS of the Cone in Figure given by Moment Method and the Previous GTD Solution [10]

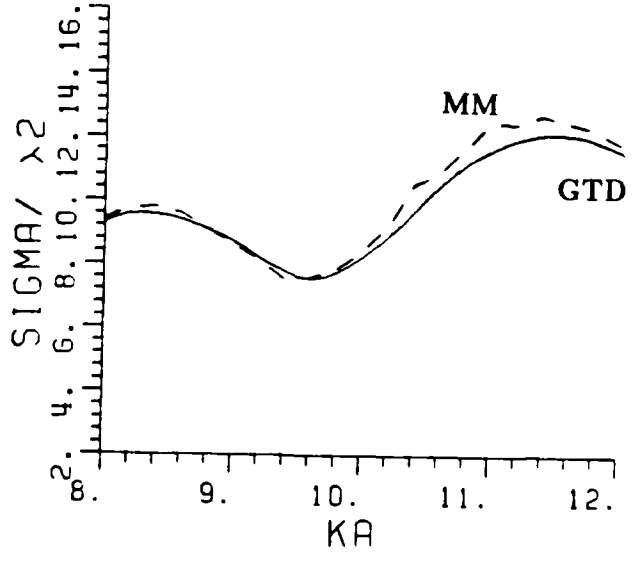

Figure 22: Comparison of RCS of the Cone in Figure given by Moment Method and the GTD Solution which includes the present Tip-Base Interaction

CHAPTER IV

VECTOR WAVE FUNCTION SOLUTION

4.1 INTRODUCTION

In this chapter, the eigenfunction expansion of the dyadic Green's function for the semi-infinite cone, derived in Appendix C, is used to describe the fields of an arbitrary electric point source. The expansion is then specialized to the case where an electric current point source is located on the forward axis of the cone. The resulting expressions are investigated as the observation point nears the tip. Lastly, the problem of the radiation by circumferential slot antennas on the cone is solved.

4.2 SOLUTION USING THE DYADIC GREEN'S FUNCTION

The geometry for the semi-infinite cone is shown in Figure 23.

Beginning with expression (C.34) in Appendix C, where $\mathbf{E}$ and $\mathbf{H}$ are the total electric and magnetic fields, and $\overline{\overline{\Gamma}}$ is the dyadic Green's function, and substituting the expression for the equivalent electric surface current, $\mathbf{J_s}$, which is given in terms of the magnetic field at the surface by $\mathbf{J_s}(\mathbf{R}') = \hat{n}' \times \mathbf{H}(\mathbf{R}')$ yields

$$\left.\begin{array}{ll} \text{R in V} & \mathbf{E}(\mathbf{R}) \\ \text{R not in V} & 0 \end{array}\right\} = j\omega\mu \int_V \mathbf{J_v}(\mathbf{R}') \cdot \overline{\overline{\Gamma}}(\mathbf{R}', \mathbf{R}) dV'$$

$$+ j\omega\mu \oint_S \hat{n}' \times \mathbf{H}(\mathbf{R}') \cdot \overline{\overline{\Gamma}}(\mathbf{R}', \mathbf{R}) dS' + \oint_S \mathbf{K_s}(\mathbf{R}') \cdot (\nabla' \times \overline{\overline{\Gamma}}(\mathbf{R}', \mathbf{R})) dS' \qquad (4.1)$$

where V is the volume enclosed by the surface S, and the vector $\mathbf{R}'$ is the source

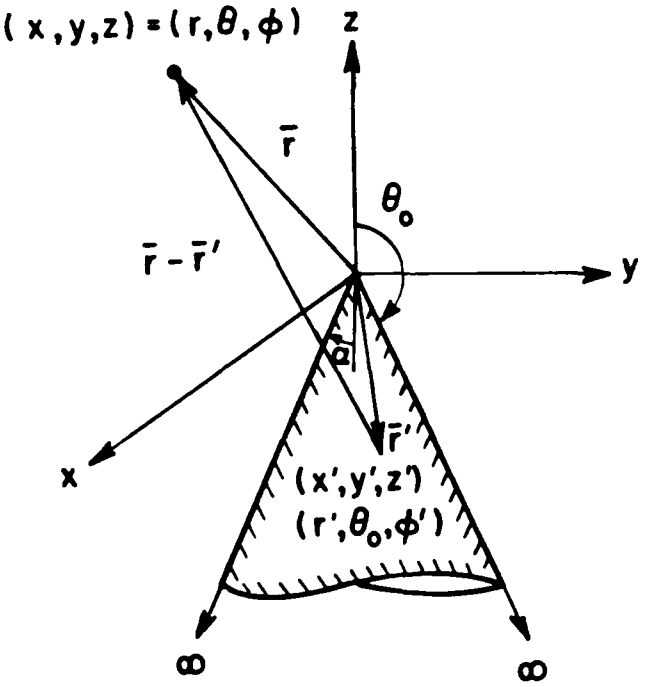

Figure 23: Geometry for Semi-Infinite Cone

vector given by $\mathbf{R}' = (R', \theta', \phi')$ and $\mathbf{R}$ is the observation vector given by $\mathbf{R} = (R, \theta, \phi)$.

The Green's function has been chosen such that

$$\hat{n}' \times \overline{\overline{\Gamma}}(\mathbf{R}', \mathbf{R})\Big]_{\theta=\theta_0} = -\hat{\theta} \times \overline{\overline{\Gamma}}(\mathbf{R}', \mathbf{R})\Big]_{\theta=\theta_0} = 0. \tag{4.2}$$

The eigenfunction expansion of the dyadic Green's function for the cone, in terms of the vector wave functions, which meets these conditions is derived in Appendix C. It is given by

$$\overline{\overline{\Gamma}}(\mathbf{R}, \mathbf{R}') = \begin{cases} \sum_p \frac{\mathbf{M}_p^{(1)}(\mathbf{R})\mathbf{M}_p^{(4)}(\mathbf{R}')}{\Omega_p} + \sum_q \frac{\mathbf{N}_q^{(1)}(\mathbf{R})\mathbf{N}_q^{(4)}(\mathbf{R}')}{\Upsilon_q} & R < R' \\ \sum_p \frac{\mathbf{M}_p^{(4)}(\mathbf{R})\mathbf{M}_p^{(1)}(\mathbf{R}')}{\Omega_p} + \sum_q \frac{\mathbf{N}_q^{(4)}(\mathbf{R})\mathbf{N}_q^{(1)}(\mathbf{R}')}{\Upsilon_q} & R > R' \end{cases} \tag{4.3}$$

Since p and q are distinct, application of Equation (4.2) yields

$$\hat{\theta} \times \mathbf{M}_p^{(1)}(\mathbf{R})\Big]_{\theta=\theta_0} = \hat{\theta} \times \mathbf{N}_q^{(1)}(\mathbf{R})\Big]_{\theta=\theta_0} = 0. \tag{4.4}$$

where $p = \begin{matrix} e \\ o \end{matrix} m\nu$ and $q = \begin{matrix} e \\ o \end{matrix} m\gamma$. Evaluating these, it is seen that

$$\hat{\theta} \times \mathbf{M}_p^{(1)}(\mathbf{R})\Big]_{\theta_0} = 0 \tag{4.5}$$

which requires

$$\frac{d}{d\theta} P_\nu^m(\cos\theta)\Big]_{\theta=\theta_0} = 0, \tag{4.6}$$

and

$$\hat{\theta} \times \mathbf{N}_q^{(1)}(\mathbf{R})\Big]_{\theta=\theta_0} = 0 \tag{4.7}$$

which requires

$$P_\gamma^m(\cos\theta_0) = 0. \tag{4.8}$$

Commuting the dot and cross products in the first surface integral yields

$$\hat{n'} \times \mathbf{H}(\mathbf{R'}) \cdot \overline{\overline{\Gamma}}(\mathbf{R'}, \mathbf{R}) = -\mathbf{H}(\mathbf{R'}) \cdot \hat{n'} \times \overline{\overline{\Gamma}}(\mathbf{R'}, \mathbf{R}), \tag{4.9}$$

but from Equation (4.2), $\hat{n'} \times \overline{\overline{\Gamma}}(\mathbf{R'}, \mathbf{R}) = 0$; therefore, the first surface integral goes to zero. In other words, the Green's function accounts for the presence of the cone. Moreover, the cone is assumed to be a perfect conductor; therefore, the equivalent magnetic surface current, $\mathbf{K_s}$, is given by $\mathbf{K_s} \equiv 0$. This eliminates the second surface integral.

Once these preliminary steps are carried out, all that remains is

$$\mathbf{E}(\mathbf{R}) = jkZ_c \int_V \mathbf{J_v}(\mathbf{R'}) \cdot \overline{\overline{\Gamma}}(\mathbf{R'}, \mathbf{R}) dV'. \tag{4.10}$$

This can be rewritten in a different form. It can be shown that for a vector–dyadic pair

$$\mathbf{a} \cdot \overline{\overline{f}} = \widetilde{\overline{\overline{f}}} \cdot \mathbf{a} \tag{4.11}$$

Letting $\mathbf{a} = \mathbf{J_v}(\mathbf{R'})$ and $\overline{\overline{f}} = \overline{\overline{\Gamma}}(\mathbf{R'}, \mathbf{R})$, and recalling that

$$\widetilde{\overline{\overline{\Gamma}}}(\mathbf{R'}, \mathbf{R}) = \overline{\overline{\Gamma}}(\mathbf{R}, \mathbf{R'}) \tag{4.12}$$

the electric field can then be written as

$$\mathbf{E}(\mathbf{R}) = jkZ_c \int_V \overline{\overline{\Gamma}}(\mathbf{R},\mathbf{R}') \cdot \mathbf{J_v}(\mathbf{R}')dV' \tag{4.13}$$

where $\omega\mu = kZ_c$, $k = \omega\sqrt{\mu\epsilon}$, and $Z_c = \sqrt{\frac{\mu}{\epsilon}}$.

Using $\mathbf{R}''$ as a dummy variable of integration, and defining $\mathbf{J_v}(\mathbf{R}'')$ in terms of a point electric current source at $\mathbf{R}'$, the volume current source can be written as

$$\mathbf{J_v}(\mathbf{R}'') = \mathbf{p_e}(\mathbf{R}'')\delta(\mathbf{R}'' - \mathbf{R}'). \tag{4.14}$$

Inserting this expression into Equation (4.13) with $\mathbf{R}''$ yields

$$\mathbf{E}(\mathbf{R}) = jkZ_c \int_V \overline{\overline{\Gamma}}(\mathbf{R},\mathbf{R}'') \cdot \mathbf{p_e}(\mathbf{R}'')\delta(\mathbf{R}'' - \mathbf{R}')dV'' \tag{4.15}$$

Applying the sifting property of the delta function yields

$$\mathbf{E}(\mathbf{R}) = jkZ_c\overline{\overline{\Gamma}}(\mathbf{R},\mathbf{R}') \cdot \mathbf{p_e}(\mathbf{R}') \tag{4.16}$$

which yields an expression for the electric field in terms of a point current source of strength $\mathbf{p_e}$ at $\mathbf{R}'$.

Once the $\mathbf{E}$ field has been determined, it is an easy task to determine the $\mathbf{H}$ field and then the surface currents that will be present on the cone. For the sake of completeness, it is noted that

$$\mathbf{H}(\mathbf{R}) = -\nabla \times \overline{\overline{\Gamma}}(\mathbf{R},\mathbf{R}') \cdot \mathbf{p_e}(\mathbf{R}'). \tag{4.17}$$

4.3 EXPLICIT EXPRESSIONS FOR THE FIELDS OF AN ELECTRIC CURRENT POINT SOURCE IN THE PRESENCE OF THE SEMI-INFINITE CONE

It is still assumed that the plane of incidence is the x–z plane. This can be done without any loss of generality since the cone geometry is very symmetric.

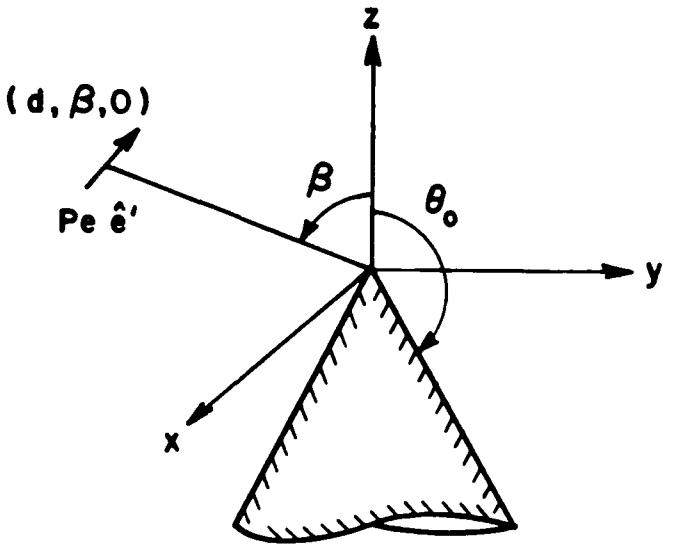

Figure 24: Geometry for Application of Dipole Moment

If another aspect were desired, one could just rotate the coordinate system. The choice of the x–z plane as the plane of incidence simplifies the expressions.

In general, the strength of the electric current point source can be written as

$$\mathbf{p_e} = p_e \hat{e'} \tag{4.18}$$

Two orientations of the current will be dealt with. They are $\hat{e'} = \hat{\theta'}$ and $\hat{e'} = \hat{\phi'}$. Any arbitrary polarization of the incident field arriving from a distant source can be expressed as a linear combination of these. Figure 24 shows the geometry and the location of the point source.

The point source is placed such that $R' = d > R$; therefore, the representation of the Green's function that is valid for $R < R'$ is used because, eventually, the field near the cone tip is desired. The source position vector is given by $\mathbf{R'} = (d, \beta, 0)$ since the plane of incidence is assumed to be the x–z plane. The incidence angle β is chosen such that $0 \leq \beta < \theta_0 = \pi - \alpha$, where α is the cone half-angle. The selection of the required θ_0 or α is needed to solve the eigenvalue problem for ν

and γ.

The fields due to point sources which are oriented transverse to $\hat{R}'$ can be found by letting $\mathbf{p_e} = p_e\hat{\theta}'$ and $\mathbf{p_e} = p_e\hat{\phi}'$ and by letting $p_e = 1$ for convenience. The θ' and ϕ' in the superscripts show which point source orientation generates the corresponding fields and currents. This yields

$$\mathbf{E}^{\theta'}(\mathbf{R}) = jkZ_c\overline{\overline{\Gamma}}(\mathbf{R},\mathbf{R}')\cdot\hat{\theta}' \tag{4.19}$$

and

$$\mathbf{E}^{\phi'}(\mathbf{R}) = jkZ_c\overline{\overline{\Gamma}}(\mathbf{R},\mathbf{R}')\cdot\hat{\phi}' \tag{4.20}$$

Each case separately is worked separately. In the $\hat{\theta}'$ case

$$\mathbf{E}^{\theta'}(\mathbf{R}) = jkZ_c\left[\sum_p \frac{\mathbf{M}_p^{(1)}(\mathbf{R})\mathbf{M}_p^{(4)}(\mathbf{R}')}{\Omega_p}\cdot\hat{\theta}' + \sum_q \frac{\mathbf{N}_q^{(1)}(\mathbf{R})\mathbf{N}_q^{(4)}(\mathbf{R}')}{\Upsilon_q}\cdot\hat{\theta}'\right]_{(d,\beta,0)} \tag{4.21}$$

This yields

$$\mathbf{M}_p^{(4)}(\mathbf{R}')\cdot\hat{\theta}'\Big]_{(d,\beta,0)} = m\frac{P_\nu^m(\cos\beta)}{\sin\beta}h_\nu^{(2)}(kd) = \mathbf{M}_{om\nu}^{(4)}(\mathbf{R}')\cdot\hat{\theta}' \tag{4.22}$$

and

$$\mathbf{N}_q^{(4)}(\mathbf{R}')\cdot\hat{\theta}'\Big]_{(d,\beta,0)} = \frac{(kdh_\gamma^{(2)}(kd))'}{kd}\frac{d}{d\beta}P_\gamma^m(\cos\beta) = \mathbf{N}_{em\gamma}^{(4)}(\mathbf{R}')\cdot\hat{\theta}' \tag{4.23}$$

so for the θ' polarization

$$p = om\nu \tag{4.24}$$

$$q = em\gamma \tag{4.25}$$

Therefore, the electric field in this case is given by

$$\begin{aligned}\mathbf{E}^{\theta'}(\mathbf{R}) \;=\; & jkZ_c\left[\sum_p \frac{\mathbf{M}_{om\nu}^{(1)}(\mathbf{R})}{\Omega_p}h_\nu^{(2)}(kd)m\frac{P_\nu^m(\cos\beta)}{\sin\beta}\right.\\ & \left.+\sum_q \frac{\mathbf{N}_{em\gamma}^{(1)}(\mathbf{R})}{\Upsilon_q}\frac{(kdh_\gamma^{(2)}(kd))'}{kd}\frac{d}{d\beta}P_\gamma^m(\cos\beta)\right].\end{aligned} \tag{4.26}$$

$\mathbf{E}^{\phi'}(\mathbf{R})$ is found in a similar manner. Applying Equation (4.20) yields

$$\mathbf{E}^{\phi'}(\mathbf{R}) = jkZ_c \left[\sum_p \frac{\mathbf{M}_p^{(1)}(\mathbf{R})\mathbf{M}_p^{(4)}(\mathbf{R}')}{\Omega_p} \cdot \hat{\phi}' + \sum_q \frac{\mathbf{N}_q^{(1)}(\mathbf{R})\mathbf{N}_q^{(4)}(\mathbf{R}')}{\Upsilon_q} \cdot \hat{\phi}' \right]_{(d,\beta,0)} \tag{4.27}$$

Performing the indicated dot products yields

$$\mathbf{M}_p^{(4)}(\mathbf{R}') \cdot \hat{\phi}' \Big]_{(d,\beta,0)} = -h_\nu^{(2)}(kd) \frac{d}{d\beta} P_\nu^m(\cos\beta) = \mathbf{M}_{emv}^{(4)}(\mathbf{R}') \cdot \hat{\phi}' \tag{4.28}$$

and

$$\mathbf{N}_q^{(4)}(\mathbf{R}') \cdot \hat{\phi}' \Big]_{(d,\beta,0)} = m \frac{P_\gamma^m(\cos\beta)}{\sin\beta} \frac{(kdh_\gamma^{(2)}(kd))'}{kd} = \mathbf{N}_{omv}^{(4)}(\mathbf{R}') \cdot \hat{\phi}' \tag{4.29}$$

so for the ϕ' polarization

$$p = emv \tag{4.30}$$

$$q = omv \tag{4.31}$$

Therefore, the electric field in this case is given by

$$\begin{aligned} \mathbf{E}^{\phi'}(\mathbf{R}) \;=\; & jkZ_c \left[\sum_p \frac{\mathbf{M}_{emv}^{(1)}(\mathbf{R})}{\Omega_p} (-h_\nu^{(2)}(kd)) \frac{d}{d\beta} P_\nu^m(\cos\beta) \right. \\ & \left. + \sum_q \frac{\mathbf{N}_{omv}^{(1)}(\mathbf{R})}{\Upsilon_q} \frac{(kdh_\gamma^{(2)}(kd))'}{kd} m \frac{P_\gamma^m(\cos\beta)}{\sin\beta} \right]. \end{aligned} \tag{4.32}$$

Therefore, it is seen that the location and direction of the sources determines the modes which are summed. As seen in the $\mathbf{E}^{\theta'}$ case, the non-zero values of $\mathbf{M} \cdot \hat{\theta}'$ and $\mathbf{N} \cdot \hat{\theta}'$ determined the specific behavior of p and q. As was said earlier, the choice of the plane of incidence made the expressions simpler; however, no generality was lost as a result.

Equations (4.26) and (4.32) contain similar expressions involving the Legendre functions. To simplify, write

$$S(\alpha, m, \theta) = m \frac{P_\alpha^m(\cos\theta)}{\sin\theta} \tag{4.33}$$

and

$$T(\alpha, m, \theta) = \frac{d}{d\theta} P_\alpha^m(\cos\theta). \tag{4.34}$$

These can be inserted into the previous equations for $\mathbf{E}^{\theta'}(\mathbf{R})$ and $\mathbf{E}^{\phi'}(\mathbf{R})$.

Using recursion formulas found in [18], S and T can be written as

$$S(\alpha, m, \theta) = \frac{P_\alpha^{m+1}(\cos\theta) + (\alpha - m + 1)(\alpha + m) P_\alpha^{m-1}(\cos\theta)}{2\cos\theta} \tag{4.35}$$

and

$$T(\alpha, m, \theta) = \frac{P_\alpha^{m-1}(\cos\theta)(\alpha - m + 1)(\alpha + m) - P_\alpha^{m+1}(\cos\theta)}{2} \tag{4.36}$$

Recalling the relationship between $\mathbf{M}$ and $\mathbf{N}$, and applying Maxwell's equations to the expressions for the $\mathbf{E}$ fields yields

$$\begin{aligned} \mathbf{H}^{\theta'}(\mathbf{R}) &= -k \left[\sum_p \frac{\mathbf{N}_{om\nu}^{(1)}(\mathbf{R})}{\Omega_p} h_\nu^{(2)}(kd) S(\nu, m, \beta) \right. \\ &\quad \left. + \sum_q \frac{\mathbf{M}_{em\gamma}^{(1)}(\mathbf{R})}{\Upsilon_q} \frac{(kdh_\gamma^{(2)}(kd))'}{kd} T(\gamma, m, \beta) \right] \end{aligned} \tag{4.37}$$

$$\begin{aligned} \mathbf{H}^{\phi'}(\mathbf{R}) &= -k \left[\sum_p \frac{\mathbf{N}_{em\nu}^{(1)}(\mathbf{R})}{\Omega_p} (-h_\nu^{(2)}(kd)) T(\nu, m, \beta) \right. \\ &\quad \left. + \sum_q \frac{\mathbf{M}_{om\gamma}^{(1)}(\mathbf{R})}{\Upsilon_q} \frac{(kdh_\gamma^{(2)}(kd))'}{kd} S(\gamma, m, \beta) \right] \end{aligned} \tag{4.38}$$

Evaluating the $\mathbf{H}$ fields on the surface of the cone at $\mathbf{R_0} = (R_0, \theta_0, \phi)$, and calculating the surface current $\mathbf{J_s}(\mathbf{R_0})$ given by $\hat{n} \times \mathbf{H}(\mathbf{R_0})$ where $\hat{n} = -\hat{\theta}$, yields

$$\begin{aligned} \mathbf{J}_\mathbf{s}^{\theta'}(\mathbf{R_0}) &= k \left[\sum_p \frac{\hat{\theta} \times \mathbf{N}_{om\nu}^{(1)}(\mathbf{R_0})}{\Omega_p} h_\nu^{(2)}(kd) S(\nu, m, \beta) \right. \\ &\quad \left. + \sum_q \frac{\hat{\theta} \times \mathbf{M}_{em\gamma}^{(1)}(\mathbf{R_0})}{\Upsilon_q} \frac{(kdh_\gamma^{(2)}(kd))'}{kd} T(\gamma, m, \beta) \right] \end{aligned} \tag{4.39}$$

$$\mathbf{J}_s^{\phi'}(\mathbf{R_0}) = k\left[\sum_p \frac{\hat{\theta}\times\mathbf{N}_{em\nu}^{(1)}(\mathbf{R_0})}{\Omega_p}(-h_\nu^{(2)}(kd))T(\nu,m,\beta) + \sum_q \frac{\hat{\theta}\times\mathbf{M}_{om\gamma}^{(1)}(\mathbf{R_0})}{\Upsilon_q}\frac{(kdh_\gamma^{(2)}(kd))'}{kd}S(\gamma,m,\beta)\right] \quad (4.40)$$

where

$$\hat{\theta}\times\mathbf{N}_{om\nu}^{(1)}(\mathbf{R_0}) = \hat{R}\left\{j_\nu'(kR_0)+\frac{j_\nu(kR_0)}{kR_0}\right\}m\frac{P_\nu^m(\cos\theta_0)}{\sin\theta_0}\cos m\phi - \hat{\phi}\nu(\nu+1)\frac{j_\nu(kR_0)}{kR_0}P_\nu^m(\cos\theta_0)\sin m\phi \quad (4.41)$$

$$\hat{\theta}\times\mathbf{M}_{em\gamma}^{(1)}(\mathbf{R_0}) = -\hat{R}\frac{d}{d\theta}P_\gamma^m(\cos\theta_0)j_\gamma(kR_0)\cos m\phi \quad (4.42)$$

$$\hat{\theta}\times\mathbf{N}_{em\nu}^{(1)}(\mathbf{R_0}) = -\hat{R}\left\{j_\nu'(kR_0)+\frac{j_\nu(kR_0)}{kR_0}\right\}m\frac{P_\nu^m(\cos\theta_0)}{\sin\theta_0}\sin m\phi - \hat{\phi}\nu(\nu+1)\frac{j_\nu(kR_0)}{kR_0}P_\nu^m(\cos\theta_0)\cos m\phi \quad (4.43)$$

$$\hat{\theta}\times\mathbf{M}_{om\gamma}^{(1)}(\mathbf{R_0}) = -\hat{R}\frac{d}{d\theta}P_\gamma^m(\cos\theta_0)j_\gamma(kR_0)\sin m\phi. \quad (4.44)$$

From Appendix B,

$$\Omega_{m\nu} = \frac{2\pi}{jk\epsilon_m}\nu(\nu+1)I_{m\nu} \quad (4.45)$$

$$\Upsilon_{m\gamma} = \frac{2\pi}{jk\epsilon_m}\gamma(\gamma+1)I_{m\gamma} \quad (4.46)$$

where the normalization integral, $I_{m\alpha}$, is given by

$$I_{m\alpha} = \int_0^{\theta_0}[P_\alpha^m(\cos\theta)]^2\sin\theta d\theta. \quad (4.47)$$

Substituting Equations (4.41)-(4.46) into Equations (4.39) and (4.40) the component surface currents are given by

$$J_{sR}^{\theta'\phi'}(\mathbf{R_0}) =$$

$$\frac{jk^2}{2\pi}\left[\sum_p \frac{\epsilon_m h_\nu^{(2)}(kd)}{\nu(\nu+1)I_{m\nu}} \left\{ \begin{array}{c} \mathrm{S}(\nu,\mathrm{m},\beta)\cos m\phi \\ \mathrm{T}(\gamma,\mathrm{m},\beta)\sin m\phi \end{array} \right\} \left\{ j_\nu'(kR_0) + \frac{j_\nu(kR_0)}{kR_0} \right\} \frac{mP_\nu^m(\cos\theta_0)}{\sin\theta_0}\right.$$

$$\left. - \sum_q \frac{\epsilon_m j_\gamma(kR_0)}{\gamma(\gamma+1)I_{m\gamma}} \left\{ \begin{array}{c} \mathrm{T}(\nu,\mathrm{m},\beta)\cos m\phi \\ \mathrm{S}(\gamma,\mathrm{m},\beta)\sin m\phi \end{array} \right\} \left\{ h_\gamma^{(2)'}(kd) + \frac{h_\gamma^{(2)}(kd)}{kd} \right\} \frac{d}{d\theta} P_\gamma^m(\cos\theta_0) \right] \tag{4.48}$$

$$J_{s\phi}^{\theta'\phi'}(\mathbf{R_0}) = \frac{jk^2}{2\pi} \sum_p \frac{\epsilon_m}{I_{m\nu}} \left\{ \begin{array}{c} -\mathrm{S}(\nu,\mathrm{m},\beta)\sin m\phi \\ \mathrm{T}(\nu,\mathrm{m},\beta)\cos m\phi \end{array} \right\} h_\nu^{(2)}(kd) \frac{j_\nu(kR_0)}{kR_0} P_\nu^m(\cos\theta_0) \tag{4.49}$$

The expressions for the surface current can vary as either a function of the azimuthal angle ϕ, or the radial distance from the cone tip R_0.

In the next section, the case for which the dipole moments are on the cone axis are shown; in other words, for axial incidence. The recursion formulas will be especially useful in this case.

4.4 SPECIALIZATION TO THE CASE OF A POINT SOURCE ON THE CONE AXIS

In this section, the surface currents for the case when the electric current point source is on the cone axis are determined. The source on the cone axis is chosen to be oriented transverse to the cone axis so it could have $\hat{\theta}'$ and $\hat{\phi}'$, or $\hat{x}$ and $\hat{y}$ components. In this case $\beta = 0$. We will be starting with Equations (4.48) and (4.49) for the currents. The value of m can be determined by investigating Equations (4.35) and (4.36) for $\beta = 0$. In both cases note that

$$P_\alpha(1) = 1 \tag{4.50}$$

this implies that

$$P_\alpha^m(1) = 0 \quad m > 0. \tag{4.51}$$

Looking at Equations (4.35) and (4.36), both S and T have a term of the form $P_\alpha^{m-1}(1)$. Cleary this will be zero when $m - 1 > 0$, or $m > 1$. Therefore,

$$S(\alpha, m, 0) = T(\alpha, m, 0) = \begin{cases} \frac{1}{2}\alpha(\alpha+1) & m = 1 \\ 0 & m \neq 1 \end{cases} \tag{4.52}$$

The following representations for the current due to an axially positioned point source are given by

$$\begin{aligned} \mathbf{J}_s^{\theta'}(\mathbf{R_0}) &= k\left[\sum_\nu \frac{\hat{\theta} \times \mathbf{N}_{o1\nu}^{(1)}(\mathbf{R_0})}{\Omega_{1\nu}} h_\nu^{(2)}(kd) \frac{\nu(\nu+1)}{2}\right. \\ &\left. + \sum_\gamma \frac{\hat{\theta} \times \mathbf{M}_{e1\gamma}^{(1)}(\mathbf{R_0})}{\Upsilon_{1\gamma}} \frac{(kdh_\gamma^{(2)}(kd))'}{kd} \frac{\gamma(\gamma+1)}{2}\right] \end{aligned} \tag{4.53}$$

and

$$\begin{aligned} \mathbf{J}_s^{\phi'}(\mathbf{R_0}) &= k\left[\sum_\nu \frac{\hat{\theta} \times \mathbf{N}_{e1\nu}^{(1)}(\mathbf{R_0})}{\Omega_{1\nu}} (-h_\nu^{(2)}(kd)) \frac{\nu(\nu+1)}{2}\right. \\ &\left. + \sum_\gamma \frac{\hat{\theta} \times \mathbf{M}_{o1\gamma}^{(1)}(\mathbf{R_0})}{\Upsilon_{1\gamma}} \frac{(kdh_\gamma^{(2)}(kd))'}{kd} \frac{\gamma(\gamma+1)}{2}\right] \end{aligned} \tag{4.54}$$

Evaluating the previous expressions for $m = 1$ yields

$$\Omega_{1\nu} = \frac{\pi}{jk}\nu(\nu+1)I_{1\nu} \tag{4.55}$$

$$\Upsilon_{1\gamma} = \frac{\pi}{jk}\gamma(\gamma+1)I_{1\gamma} \tag{4.56}$$

from which

$$\frac{\nu(\nu+1)}{2}\frac{1}{\Omega_{1\nu}} = \frac{jk}{2\pi I_{1\nu}} \tag{4.57}$$

$$\frac{\gamma(\gamma+1)}{2}\frac{1}{\Upsilon_{1\gamma}} = \frac{jk}{2\pi I_{1\gamma}} \tag{4.58}$$

where $I_{1\alpha}$ is given as in Appendix B as

$$I_{1\alpha} = \int_0^{\theta_0} [P_\alpha^1(\cos\theta)]^2 \sin\theta d\theta. \tag{4.59}$$

For ν,

$$\int_0^{\theta_0} [P_\nu^1(\cos\theta)]^2 \sin\theta d\theta = \frac{-\sin\theta_0}{2\nu+1} P_\nu^1(\cos\theta_0) \frac{\partial^2}{\partial\nu\partial\theta} P_\nu^1(\cos\theta_0) \tag{4.60}$$

and for γ,

$$\int_0^{\theta_0} [P_\gamma^1(\cos\theta_0)]^2 \sin\theta d\theta = \frac{\sin\theta_0}{2\gamma+1} \frac{\partial}{\partial\gamma} P_\gamma^1(\cos\theta_0) \frac{\partial}{\partial\theta} P_\gamma^1(\cos\theta_0). \tag{4.61}$$

Recall from Appendix D, that for m=1

$$\mathrm{L}_\nu^1(\theta_0) = \frac{\partial^2}{\partial\nu\partial\theta} P_\nu^1(\cos\theta_0) \tag{4.62}$$

$$L_\gamma^1(\theta_0) = \frac{\partial}{\partial\gamma} P_\gamma^1(\cos\theta_0) \tag{4.63}$$

When these functions are evaluated on the cone surface, there will be some factors that cancel. Prior to the cancellation, the component expressions for the current are given by

$$J_{sR}^{\theta'\phi'}(\mathbf{R_0}) = \frac{jk^2}{2\pi} \left\{ \begin{array}{c} \cos\phi \\ \sin\phi \end{array} \right\} \Psi_R \tag{4.64}$$

$$J_{s\phi}^{\theta'\phi'}(\mathbf{R_0}) = \frac{jk^2}{2\pi} \left\{ \begin{array}{c} -\sin\phi \\ \cos\phi \end{array} \right\} \Psi_\phi \tag{4.65}$$

where

$$\Psi_R = \left[\sum_\nu \frac{1}{I_{1\nu}} h_\nu^{(2)}(kd) \left\{ j_\nu'(kR_0) + \frac{j_\nu(kR_0)}{kR_0} \right\} \frac{P_\nu^1(\cos\theta_0)}{\sin\theta_0} \right.$$
$$\left. - \sum_\gamma \frac{1}{I_{1\gamma}} \left\{ h_\gamma^{(2)\prime}(kd) + \frac{h_\gamma^{(2)}(kd)}{kd} \right\} j_\gamma(kR_0) \frac{d}{d\theta} P_\gamma^1(\cos\theta_0) \right] \tag{4.66}$$

and

$$\Psi_\phi = \sum_\nu \frac{\nu(\nu+1)}{I_{1\nu}} h_\nu^{(2)}(kd) \frac{j_\nu(kR_0)}{kR_0} P_\nu^1(\cos\theta_0). \tag{4.67}$$

After cancellation,

$$J_{sR}^{\theta' \phi'}(\mathbf{R_0}) = \frac{-jk^2}{2\pi \sin\theta_0} \left\{ \begin{array}{c} \cos\phi \\ \sin\phi \end{array} \right\} \Lambda_R \tag{4.68}$$

and

$$J_{s\phi}^{\theta' \phi'}(\mathbf{R_0}) = \frac{-jk^2}{2\pi \sin\theta_0} \Lambda_\phi \tag{4.69}$$

where

$$\Lambda_R = \left[\sum_\nu \frac{(2\nu+1)}{\sin\theta_0} \frac{h_\nu^{(2)}(kd)}{L_\nu^1(\theta_0)} \left\{ j_\nu'(kR_0) + \frac{j_\nu(kR_0)}{kR_0} \right\} + \sum_\gamma \left\{ h_\gamma^{(2)\prime}(kd) + \frac{h_\gamma^{(2)}(kd)}{kd} \right\} \frac{(2\gamma+1) j_\gamma(kR_0)}{L_\gamma^1(\theta_0)} \right] \tag{4.70}$$

and

$$\Lambda_\phi = \sum_\nu \nu(\nu+1)(2\nu+1) \frac{h_\nu^{(2)}(kd)}{L_\nu^1(\theta_0)} \frac{j_\nu(kR_0)}{kR_0}. \tag{4.71}$$

The source can be placed in the far field. This allows the use of the large argument form of the Hankel functions given by

$$\lim_{x\to\infty} H_\nu^{(2)}(x) \to \sqrt{\frac{2j}{\pi x}} j^\nu e^{-jx} \tag{4.72}$$

which yields

$$\lim_{x\to\infty} h_\nu^{(2)}(x) \to j^{\nu+1} \frac{e^{-jx}}{x}; \tag{4.73}$$

therefore,

$$\lim_{kR\to\infty} \frac{(kRh_\nu^{(2)}(kR))'}{kR} \to j^\nu \frac{e^{-jkR}}{kR} \tag{4.74}$$

At this point, specializing the solutions to the case of plane wave incidence by moving the point source far away, it is noted that

$$E^i = jkZ_c \frac{e^{-jkd}}{4\pi d}. \tag{4.75}$$

Applying this to Equations (4.68) and (4.69) yields

$$J_{sR}^{\phi'\,\theta'}(\mathbf{R_0}) = \frac{-2Y_0}{\sin\theta_0} \left\{ \begin{array}{c} \cos\phi \\ \sin\phi \end{array} \right\} \Delta_R \tag{4.76}$$

$$J_{s\phi}^{\phi'\,\theta'}(\mathbf{R_0}) = \frac{-2Y_0}{\sin\theta_0} \left\{ \begin{array}{c} -\sin\phi \\ \cos\phi \end{array} \right\} \Delta_\phi \tag{4.77}$$

where

$$\Delta_R = \left[\sum_\nu \frac{j^{\nu+1}(2\nu+1)}{\sin\theta_0 L_\nu^1(\theta_0)} \left\{ j_\nu'(kR_0) + \frac{j_\nu(kR_0)}{kR_0} \right\} + \sum_\gamma \frac{j^\gamma(2\gamma+1)}{L_\gamma^1(\theta_0)} j_\gamma(kR_0) \right] \tag{4.78}$$

$$\Delta_\phi = \sum_\nu j^{\nu+1} \frac{\nu(\nu+1)(2\nu+1)}{L_\nu^1(\theta_0)} \frac{j_\nu(kR_0)}{kR_0}. \tag{4.79}$$

The expressions for the Δ_R and Δ_ϕ agree with those given in Bowman et al. [33].

In Equations (4.64)–(4.79), it is clear that the sum is over the eigenvalues given by solving Equations (4.6) and (4.8). All of the previous expressions are valid only for axial incidence.

In the next section, the behavior near the tip and the dominant behavior in the tip region are determined.

4.5 FIELD BEHAVIOR NEAR THE CONE TIP

Looking at Equations (4.26), (4.32), (4.37), and (4.38) from the previous section, the fields could be written simply as

$$\mathbf{E}(\mathbf{R}) = \sum_p a_p \mathbf{M}_p^{(1)}(\mathbf{R}) + \sum_q b_q \mathbf{N}_q^{(1)}(\mathbf{R}) \tag{4.80}$$

and

$$\mathbf{H}(\mathbf{R}) = jY_0 \sum_p a_p \mathbf{N}_p^{(1)}(\mathbf{R}) + jY_0 \sum_q b_q \mathbf{M}_q^{(1)}(\mathbf{R}) \tag{4.81}$$

where Y_0 is the characteristic admittance. The superscript (1) implies that the radial behavior is characterized by $j_\nu(\rho)$.

The behavior near the tip is desired. As $\rho = kR \to 0$, the small argument form of the Bessel function is used. It is given by

$$j_\nu(\rho) \approx \frac{\sqrt{\pi}\rho^\nu}{2^{\nu+1}\Gamma(\nu + 3/2)} = \alpha_\nu \rho^\nu \tag{4.82}$$

Using this representation for the Bessel functions, and writing **M** and **N** in terms of their auxiliary wave functions yields

$$\mathbf{M}_p^{(1)}(\rho) \approx \alpha_\nu \rho^\nu \mathbf{m_p} \tag{4.83}$$

$$\mathbf{N}_q^{(1)}(\rho) \approx \alpha_\gamma \rho^{\gamma-1} \gamma(\gamma+1) \left(Y_q \hat{R} + \frac{1}{\gamma} \hat{R} \times \mathbf{m_q} \right) \tag{4.84}$$

Inserting these asymptotic relationships into Equations (4.80) and (4.81) yields

$$\mathbf{E}(\mathbf{R}) \approx \sum_p \widetilde{a}_p \rho^\nu \mathbf{m_p} + \sum_q \widetilde{b}_q \rho^{\gamma-1} \gamma(\gamma+1) \left(Y_q \hat{R} + \frac{1}{\gamma} \hat{R} \times \mathbf{m_q} \right) \tag{4.85}$$

and

$$\mathbf{H}(\mathbf{R}) \approx jY_0 \sum_p \widetilde{a}_p \rho^{\nu-1} \nu(\nu+1) \left(Y_p \hat{R} + \frac{1}{\nu} \hat{R} \times \mathbf{m_q} \right) + jY_0 \sum_q \widetilde{b}_q \rho^\gamma \mathbf{m_q} \tag{4.86}$$

where

$$\widetilde{a}_p = a_p \alpha_\nu \tag{4.87}$$

$$\widetilde{b}_q = b_q \alpha_\gamma \tag{4.88}$$

We can determine a bound on the values of ν and γ by imposing the tip condition as $R \to \epsilon$ given by

$$\lim_{\epsilon \to 0} \epsilon^2 \int_\Omega \mathbf{E} \times \mathbf{H}^* \cdot \hat{R} d\Omega \to \text{bounded at the origin} \tag{4.89}$$

where Ω is a shrinking spherical volume centered at the cone tip. After performing the integration, and evaluating the limit, the powers of ν and γ for which the integral would be bounded are determined. In order to satisfy this condition

$$\nu > -\frac{1}{2} \tag{4.90}$$

and

$$\gamma > -\frac{1}{2}. \tag{4.91}$$

Closer investigation of Equation (4.85) shows the dominant behavior for the **E** field given by

$$E_R \rightarrow \rho^{\gamma-1} \tag{4.92}$$

$$E_\theta \rightarrow \rho^{\gamma-1} \tag{4.93}$$

$$E_\phi \rightarrow \rho^{\gamma-1} \tag{4.94}$$

where γ is given by Equation (4.8).

The surface current behavior is determined by working with Equation (4.86). The dominant behavior is found to be

$$J_{sR} \rightarrow \rho^{\nu-1} \tag{4.95}$$

$$J_{s\phi} \rightarrow \rho^{\nu-1} \tag{4.96}$$

where ν is given by Equation (4.6). Now, the dominant tip current will be investigated in more detail.

Returning to axial incidence case, evaluating $\hat{n} \times \mathbf{H}$ on the surface at $\mathbf{R_0} = (R_0, \theta_0, \phi)$ and substituting Equation (4.82) into Equations (4.78) and (4.79), yields

$$J_{sR}^{\theta' \atop \phi'}(\mathbf{R_0}) = \frac{-2Y_0}{\sin\theta_0} \left\{ \begin{array}{c} \cos\phi \\ \sin\phi \end{array} \right\} \Delta_{Rsa} \tag{4.97}$$

$$J_{s\phi}^{\theta' \phi'}(\mathbf{R_0}) = \frac{-2Y_0}{\sin\theta_0} \left\{ \begin{array}{c} -\sin\phi \\ \cos\phi \end{array} \right\} \Delta_{\phi sa} \tag{4.98}$$

where

$$\Delta_{Rsa} = \left[\sum_{\nu} \frac{j(j/2)^{\nu}(\nu+1)\sqrt{\pi}(kR_0)^{\nu-1}}{\sin\theta_0 \Gamma(\nu+1/2) L_{\nu}^{1}(\theta_0)} + \sum_{\gamma} (j/2)^{\gamma} \frac{\sqrt{\pi}(kR_0)^{\gamma}}{\Gamma(\gamma+1/2) L_{\gamma}^{1}(\theta_0)} \right] \tag{4.99}$$

$$\Delta_{\phi sa} = \sum_{\nu} \frac{j(j/2)^{\nu}\nu(\nu+1)\sqrt{\pi}(kR_0)^{\nu-1}}{\Gamma(\nu+1/2) L_{\nu}^{1}(\theta_0)} \tag{4.100}$$

where the "sa" means that the small argument approximation for the Bessel function has been applied.

When $90° < \theta_0 < 180°$, $0 < \nu_1 < 1$. Specifically, when θ_0 is 165°, $\nu_1 = .96714$ and $\gamma_1 = 1.03163$. Since $kR_0 << 1$, it is clear that ν_1 is the dominant eigenvalue. Therefore, the dominant term for the current with axial incidence is given by

$$J_{sR}^{\theta' \phi'}(\mathbf{R_0}) = \frac{-2jY_0}{\sin\theta_0} \left\{ \begin{array}{c} \cos\phi \\ \sin\phi \end{array} \right\} \frac{(j/2)^{\nu_1}(\nu_1+1)\sqrt{\pi}(kR_0)^{\nu_1-1}}{\sin\theta_0 \Gamma(\nu_1+1/2) L_{\nu_1}^{1}(\theta_0)} \tag{4.101}$$

$$J_{s\phi}^{\theta' \phi'}(\mathbf{R_0}) = \frac{-2jY_0}{\sin\theta_0} \left\{ \begin{array}{c} -\sin\phi \\ \cos\phi \end{array} \right\} \frac{(j/2)^{\nu_1}\nu_1(\nu_1+1)\sqrt{\pi}(kR_0)^{\nu_1-1}}{\Gamma(\nu_1+1/2) L_{\nu_1}^{1}(\theta_0)} \tag{4.102}$$

This is also true for non-axial incidence, since m=1 still produces the eigenvalue for which $\nu_1 < 1$. It must be modified to account for the fact that $\beta \neq 0$. The expressions are given by

$$J_{sR}^{\theta' \phi'}(\mathbf{R_0}) = Y_0 \frac{G(\beta)}{\nu_1 \sin^2\theta_0} \left\{ \begin{array}{c} \cos\phi \\ \sin\phi \end{array} \right\} \frac{1}{2^{\nu_1-2}} \frac{\sqrt{\pi}(jkR_0)^{\nu_1-1}}{\Gamma(\nu_1+1/2) L_{\nu_1}^{1}(\theta_0)} \tag{4.103}$$

$$J_{s\phi}^{\theta' \phi'}(\mathbf{R_0}) = Y_0 \frac{G(\beta)}{\sin\theta_0} \left\{ \begin{array}{c} -\sin\phi \\ \cos\phi \end{array} \right\} \frac{1}{2^{\nu_1-2}} \frac{\sqrt{\pi}(jkR_0)^{\nu_1-1}}{\Gamma(\nu_1+1/2) L_{\nu_1}^{1}(\theta_0)} \tag{4.104}$$

where

$$G(\beta) = \left\{ \begin{array}{c} \frac{P^1_{\nu_1}(\cos\beta)}{\sin\beta} \\ \frac{d}{d\beta}P^1_{\nu_1}(\beta) \end{array} \right\}. \tag{4.105}$$

The upper and lower terms in (4.105) are associated with the θ' and ϕ' notation from above. These expressions also agree with the expressions for the dominant behavior near the tip found in Bowman et al. [33]. In the next section, the dominant tip current is compared to the GO current for the case of axial incidence.

4.6 COMPARISON OF THE DOMINANT TIP CURRENT TO THE GO CURRENT

The dominant tip current and the GO current will be compared for the case of axial incidence. It will be shown that these currents are very similar in this case.

As mentioned previously, from Equations (4.103) and (4.104) (replacing R_0 with r' for this discussion) since $kr' << 1$, and $\nu_1 < 1$, it is clear that ν_1 is the dominant eigenvalue. The eigenvalue ν_1 is such that $\nu_1 < 1$ for cone angles in the range given by $90° < \theta_0 < 180°$; therefore, the dominant term for the current is given by

$$J^{\theta'}_{sR}{}^{\phi'}(\mathbf{r}') = Y_0 \frac{G(\beta)}{\nu_1 \sin^2\theta_0} \left\{ \begin{array}{c} \cos\phi \\ \sin\phi \end{array} \right\} \frac{1}{2^{\nu_1-2}} \frac{\sqrt{\pi}(jkr')^{\nu_1-1}}{\Gamma(\nu_1+1/2)L^1_{\nu_1}(\theta_0)} \tag{4.106}$$

and

$$J^{\theta'}_{s\phi}{}^{\phi'}(\mathbf{r}') = Y_0 \frac{G(\beta)}{\sin\theta_0} \left\{ \begin{array}{c} -\sin\phi \\ \cos\phi \end{array} \right\} \frac{1}{2^{\nu_1-2}} \frac{\sqrt{\pi}(jkr')^{\nu_1-1}}{\Gamma(\nu_1+1/2)L^1_{\nu_1}(\theta_0)} \tag{4.107}$$

where

$$G(\beta) = \left\{ \begin{array}{c} \frac{P^1_{\nu_1}(\cos\beta)}{\sin\beta} \\ \frac{d}{d\beta}P^1_{\nu_1}(\beta) \end{array} \right\} \tag{4.108}$$

and

$$L^1_\nu(\theta_0) = \frac{\partial^2}{\partial\nu\partial\theta} P^1_\nu(\cos\theta_0). \tag{4.109}$$

Combining these terms yields

$$\mathbf{J}_{\mathbf{s}}^{\substack{\theta' \\ \phi'}}(\mathbf{r}') = J_0(jkr')^{\nu_1-1}\left[\hat{r}'\left\{\begin{array}{c}\cos\phi' \\ \sin\phi'\end{array}\right\} + \hat{\phi}'\nu_1\sin\theta_0\left\{\begin{array}{c}-\sin\phi' \\ \cos\phi'\end{array}\right\}\right] \tag{4.110}$$

where

$$J_0 = Y_0\frac{G(\beta)}{\nu_1\sin\theta_0}\frac{1}{2^{\nu_1-2}}\frac{\sqrt{\pi}}{\Gamma(\nu_1+1/2)}\frac{1}{\sin\theta_0 L_{\nu_1}^1(\theta_0)}. \tag{4.111}$$

The normalization integral, given in Appendix D, for this set of eigenvalues is given by

$$I_\nu^1(\theta_0) = \frac{-\sin\theta_0}{2\nu+1}P_\nu^1(\cos\theta_0)L_\nu^1(\theta_0). \tag{4.112}$$

Therefore, one can write

$$\sin\theta_0 L_\nu^1(\theta_0) = -\frac{(2\nu+1)I_\nu^1(\theta_0)}{P_\nu^1(\cos\theta_0)}. \tag{4.113}$$

Substituting this into the expression for the current (4.110) yields

$$\mathbf{J}_{\mathbf{s}}^{\substack{\theta' \\ \phi'}}(\mathbf{r}') = J_1(jkr')^{\nu_1-1}\mathbf{f}_{\mathbf{e}}(\phi') \tag{4.114}$$

where

$$\mathbf{f}_{\mathbf{e}}(\phi') = \sin\theta_0\begin{cases}\hat{x}(\cos^2\phi' + \nu_1\sin^2\phi') + \hat{y}(1-\nu_1)\sin\phi'\cos\phi' & \\ \quad +\hat{z}\cot\theta_0\cos\phi' & \hat{\theta}' \text{ incidence} \\ \hat{x}(1-\nu_1)\sin\phi'\cos\phi' + \hat{y}(\sin^2\phi' + \nu_1\cos^2\phi') & \\ \quad +\hat{z}\cot\theta_0\sin\phi' & \hat{\phi}' \text{ incidence}\end{cases} \tag{4.115}$$

is the vector for the exact current, and

$$J_1 = -Y_0\frac{G(\beta)}{\nu_1(2\nu_1+1)}\frac{1}{2^{\nu_1-2}}\frac{\sqrt{\pi}}{\Gamma(\nu_1+1/2)}\frac{P_{\nu_1}^1(\cos\theta_0)}{\sin\theta_0}\frac{1}{I_\nu^1(\theta_0)}. \tag{4.116}$$

The GO current is given by

$$\mathbf{J}_{\mathbf{go}}(r',\phi') = 2Y_0 e^{jkr'\cos\gamma}\mathbf{f}_{\mathbf{go}}(\phi') \tag{4.117}$$

where

$$\mathbf{f_{go}}(\phi') = \begin{cases} \hat{x}\sin\theta_0 + \hat{z}\cos\theta_0\cos\phi' & \hat{\theta}' \text{ incidence} \\ \hat{x}\cos\theta_0\sin\beta\sin\phi' + \hat{z}\cos\theta_0\cos\beta\sin\phi' & \hat{\phi}' \text{ incidence} \\ \quad +\hat{y}\left(\sin\theta_0\cos\beta - \cos\theta_0\sin\beta\cos\phi'\right) & \end{cases} \tag{4.118}$$

and

$$\cos\gamma = \sin\alpha\sin\beta\cos\phi' + \cos\theta_0\cos\beta \tag{4.119}$$

For cone angles in the range given by $90° < \theta_0 < 180°$, $\nu_1 \approx 1$. If one evaluates these expressions for axial incidence ($\beta = 0$) and $\nu_1 \approx 1$, then

$$\mathbf{f_e}(\phi') = \begin{cases} \hat{x}\sin\theta_0 + \hat{z}\cos\theta_0\cos\phi' & \hat{\theta}' \text{ incidence} \\ \hat{y}\sin\theta_0 + \hat{z}\cos\theta_0\sin\phi' & \hat{\phi}' \text{ incidence} \end{cases} \tag{4.120}$$

and

$$\mathbf{f_{go}}(\phi') = \begin{cases} \hat{x}\sin\theta_0 + \hat{z}\cos\theta_0\cos\phi' & \hat{\theta}' \text{ incidence} \\ \hat{y}\sin\theta_0 + \hat{z}\cos\theta_0\sin\phi' & \hat{\phi}' \text{ incidence.} \end{cases} \tag{4.121}$$

Hence, one can define

$$\mathbf{f}(\phi') = \mathbf{f_e}(\phi') = \mathbf{f_{go}}(\phi'). \tag{4.122}$$

Moreover,

$$G(0) = \frac{\nu_1(\nu_1+1)}{2} \approx 1 \tag{4.123}$$

$$\frac{\sqrt{\pi}}{\Gamma(\nu_1+1/2)} \approx 2 \tag{4.124}$$

$$\frac{P^1_{\nu_1}(\cos\theta_0)}{\sin\theta_0} \approx -1 \tag{4.125}$$

$$I^1_\nu(\theta_0) \approx 1 \tag{4.126}$$

$$\cos\gamma = \cos\theta_0 \tag{4.127}$$

Lastly, investigating the first few terms in the eigenfunction expansion with the knowledge that for the given range of angles

$$\nu_1 \approx 1 \tag{4.128}$$

$$\nu_2 \approx 2 \tag{4.129}$$

$$\gamma_1 \approx \nu_2 - 1 \approx 1 \tag{4.130}$$

$$I^1_{\nu_1}(\theta_0) \approx 1 \tag{4.131}$$

$$I^1_{\nu_2}(\theta_0) \approx 2 \tag{4.132}$$

$$I^1_{\gamma_1}(\theta_0) \approx 1, \tag{4.133}$$

one can see that the series is that of an exponential given by

$$\sum \approx C[1 + jkr' \cos\theta_0 \cos\beta + \ldots]. \tag{4.134}$$

Therefore, for axial incidence, this exponential is

$$\sum \approx e^{jkr' \cos\theta_0}. \tag{4.135}$$

This is exactly the same phase as that given for the GO current. The two currents may be written as,

$$\mathbf{J_{go}}(r', \phi') = 2Y_0 e^{jkr' \cos\theta_0} \mathbf{f}(\phi') \tag{4.136}$$

and

$$\mathbf{J_e}(r', \phi') = \frac{4}{3} Y_0 (jkr')^{\nu_1 - 1} e^{jkr' \cos\theta_0} \mathbf{f}(\phi'). \tag{4.137}$$

The $(jkr')^{\nu_1 - 1}$ has been kept in tact to preserve the singularity at the tip.

The behavior of these two currents is very similar for the axial incidence case; therefore, it is felt that the matching of the current $\mathbf{J_e}$ near the tip, to the current $\mathbf{J_{go}}$ far from the tip, could provide a very good approximation to the actual current. It is proposed as a part of future research, that this matching be found in terms of the transition function F from (3.30) with a proper argument. Such a current representation is expected to be more accurate than the one based on PO. Once this more refined approximation for the current is found, one could calculate the tip diffracted field using the asymptotic methods in Chapter III.

In the next section, reciprocity is invoked to determine the far fields of a circumferential slot on the cone using the Green's function derived in this work.

4.7 RADIATION FROM CIRCUMFERENTIAL SLOT ANTENNAS

The Lorentz Reciprocity Theorem as shown in [34] relates the fields from one set of sources to those of another set of sources. That theorem is used here to find the far zone fields of a slot in a cone in terms of the reciprocal problem of determining the current induced on the cone surface by a distant electric current point source; the electric current point source is located where the far field of the slot is to be evaluated, and the slot is replaced by an equivalent magnetic surface current distribution over the slot aperture with the slot short–circuited. It is noted that the solution to the reciprocal problem of determining the current induced on the cone by the distant electric point source can be found from the previous two sections. In this case, these fields radiate in the presence of a perfectly conducting semi–infinite cone. Reciprocity states that

$$\int\int\int_{V_b} [\mathbf{E_a} \cdot \mathbf{J_b} - \mathbf{H_a} \cdot \mathbf{M_b}]\, dv = \int\int\int_{V_a} [\mathbf{E_b} \cdot \mathbf{J_a} - \mathbf{H_b} \cdot \mathbf{M_a}]\, dv \qquad (4.138)$$

where $(\mathbf{E_a}, \mathbf{H_a})$ and $(\mathbf{E_b}, \mathbf{H_b})$ are the fields radiated in the presence of the cone by sources $(\mathbf{J_a}, \mathbf{M_a})$ and $(\mathbf{J_b}, \mathbf{M_b})$ respectively. This is specialized such that we have either an electric or a magnetic source. Let $(\mathbf{E_m}, \mathbf{H_m})$ be the fields radiated by $\mathbf{M}$, and let $(\mathbf{E_e}, \mathbf{H_e})$ be the fields radiated by $\mathbf{J}$. Therefore,

$$\mathbf{J_a} = 0 \qquad (4.139)$$

$$\mathbf{J_b} = \mathbf{J} \qquad (4.140)$$

$$\mathbf{M_a} = \mathbf{M} \qquad (4.141)$$

$$\mathbf{M_b} = 0 \qquad (4.142)$$

$$V_a = V_e \tag{4.143}$$

$$V_b = V_m \tag{4.144}$$

In this case, the reciprocity integral yields

$$\int\int\int_{V_e} \mathbf{E_m}(\mathbf{R}') \cdot \mathbf{J}(\mathbf{R}')dV' = -\int\int\int_{V_m} \mathbf{H_e}(\mathbf{R}') \cdot \mathbf{M}(\mathbf{R}')dV' \tag{4.145}$$

Defining the electric current as

$$\mathbf{J}(\mathbf{R}') = \mathbf{p_e}(\mathbf{R})\delta(\mathbf{R} - \mathbf{R}') \tag{4.146}$$

then

$$\mathbf{E_m}(\mathbf{R}) \cdot \mathbf{p_e}(\mathbf{R}) = -\int\int\int_{V_m} \mathbf{H_e}(\mathbf{R}') \cdot \mathbf{M}(\mathbf{R}')dV'. \tag{4.147}$$

The Green's function given previously is for electric sources. From Equation (4.16),

$$\mathbf{E_e}(\mathbf{R}') = jkZ_c\overline{\overline{\mathbf{\Gamma}}}(\mathbf{R}', \mathbf{R}) \cdot \mathbf{p_e}(\mathbf{R}). \tag{4.148}$$

Applying Maxwell's equation yields

$$\mathbf{H_e}(\mathbf{R}') = -\nabla' \times \overline{\overline{\mathbf{\Gamma}}}(\mathbf{R}', \mathbf{R}) \cdot \mathbf{p_e}(\mathbf{R}). \tag{4.149}$$

Substituting into Equation (4.147) yields

$$\mathbf{E_m}(\mathbf{R}) \cdot \mathbf{p_e}(\mathbf{R}) = \int\int\int_{V_m} \nabla' \times \overline{\overline{\mathbf{\Gamma}}}(\mathbf{R}', \mathbf{R}) \cdot \mathbf{p_e}(\mathbf{R}) \cdot \mathbf{M}(\mathbf{R}')dV' \tag{4.150}$$

In [32], it is given that

$$\nabla' \times \overline{\overline{\mathbf{\Gamma}}}(\mathbf{R}', \mathbf{R}) \cdot \mathbf{p_e}(\mathbf{R}) = \mathbf{p_e}(\mathbf{R}) \cdot \nabla' \times \widetilde{\overline{\overline{\mathbf{\Gamma}}}}(\mathbf{R}', \mathbf{R}) \tag{4.151}$$

but

$$\nabla' \times \widetilde{\overline{\overline{\mathbf{\Gamma}}}}(\mathbf{R}', \mathbf{R}) = \nabla \times \overline{\overline{\mathbf{\Gamma}}}(\mathbf{R}, \mathbf{R}'). \tag{4.152}$$

We can write Equation (4.150) as

$$\mathbf{p_e}(\mathbf{R}) \cdot \mathbf{E_m}(\mathbf{R}) = \mathbf{p_e}(\mathbf{R}) \cdot \int\int\int_{V_m} \nabla \times \overline{\overline{\mathbf{\Gamma}}}(\mathbf{R}, \mathbf{R}') \cdot \mathbf{M}(\mathbf{R}')dV'. \tag{4.153}$$

The dipole moment $\mathbf{p_e}(\mathbf{R})$ was arbitrary; therefore, (dropping the m subscript for convenience)

$$\mathbf{E}(\mathbf{R}) = \int\int\int_{V_m} \nabla \times \overline{\overline{\Gamma}}(\mathbf{R},\mathbf{R}') \cdot \mathbf{M}(\mathbf{R}')dV'. \tag{4.154}$$

Now specialize this volume current $\mathbf{M}$ to a surface current $\mathbf{M_s}$. Letting an $\mathbf{E}$ field exist only within the slot, the voltage can be written by $V = -\mathbf{E}\cdot d\mathbf{R}$. This voltage only exists at $R' = a$; therefore,

$$\mathbf{E_{slot}}(\mathbf{R}') = -\hat{R}V\delta(R'-a). \tag{4.155}$$

But the equivalent magnetic surface current, $\mathbf{M_s}$, is needed. This is given by

$$\mathbf{M_s}(\mathbf{R}') = -\mathbf{E_{slot}}(\mathbf{R}') \times \hat{\theta} = V\delta(R'-a)\hat{\phi}' \tag{4.156}$$

and $dS = R'\sin\theta_0 dR'd\phi'$. Therefore,

$$\mathbf{E}(\mathbf{R}) = \int\int_S \nabla \times \overline{\overline{\Gamma}}(\mathbf{R},\mathbf{R}') \cdot V\delta(R'-a)\hat{\phi}'R'\sin\theta_0 dR'd\phi'. \tag{4.157}$$

Our excitation is symmetric; hence, there is no ϕ variation. This means that $m = 0$. Therefore,

$$\mathbf{E}(\mathbf{R}) = 2\pi V a \sin\theta_0 \nabla \times \overline{\overline{\Gamma}}(\mathbf{R},\mathbf{R}') \cdot \hat{\phi}'\Big]_{R'=a,\theta'=\theta_0,m=0} \tag{4.158}$$

The next step is to look at the Green's function which is given by

$$\overline{\overline{\Gamma}}(\mathbf{R},\mathbf{R}') = \begin{cases} \sum_p \dfrac{\mathbf{M}_p^{(1)}(\mathbf{R})\mathbf{M}_p^{(4)}(\mathbf{R}')}{\Omega_p} + \sum_q \dfrac{\mathbf{N}_q^{(1)}(\mathbf{R})\mathbf{N}_q^{(4)}(\mathbf{R}')}{\Upsilon_q} & R < R' \\ \sum_p \dfrac{\mathbf{M}_p^{(4)}(\mathbf{R})\mathbf{M}_p^{(1)}(\mathbf{R}')}{\Omega_p} + \sum_q \dfrac{\mathbf{N}_q^{(4)}(\mathbf{R})\mathbf{N}_q^{(1)}(\mathbf{R}')}{\Upsilon_q} & R > R' \end{cases} \tag{4.159}$$

We need $\nabla \times \overline{\overline{\Gamma}}(\mathbf{R},\mathbf{R}')$, where ∇ operates on the unprimed variables. Recalling that $\nabla \times \mathbf{M} = k\mathbf{N}$ and $\nabla \times \mathbf{M} = k\mathbf{N}$, yields

$$\nabla \times \overline{\overline{\Gamma}}(\mathbf{R},\mathbf{R}') = \begin{cases} k\sum_p \dfrac{\mathbf{N}_p^{(1)}(\mathbf{R})\mathbf{M}_p^{(4)}(\mathbf{R}')}{\Omega_p} + k\sum_q \dfrac{\mathbf{M}_q^{(1)}(\mathbf{R})\mathbf{N}_q^{(4)}(\mathbf{R}')}{\Upsilon_q} & R < R' \\ k\sum_p \dfrac{\mathbf{N}_p^{(4)}(\mathbf{R})\mathbf{M}_p^{(1)}(\mathbf{R}')}{\Omega_p} + k\sum_q \dfrac{\mathbf{M}_q^{(4)}(\mathbf{R})\mathbf{N}_q^{(1)}(\mathbf{R}')}{\Upsilon_q} & R > R' \end{cases} \tag{4.160}$$

Next, performing the dot product with $\hat{\phi}'$ yields

$$\mathbf{M}_p^{(1)}(\mathbf{R}') \cdot \hat{\phi}'\Big]_{R'=a,\theta'=\theta_0,m=0} = -j_\nu(ka)\frac{d}{d\theta}P_\nu(\cos\theta_0) \tag{4.161}$$

$$\mathbf{N}_q^{(1)}(\mathbf{R}') \cdot \hat{\phi}'\Big]_{m=0} = 0 \tag{4.162}$$

Therefore, there is only a value for p. It is given by

$$p = e0\nu. \tag{4.163}$$

An important thing to note is that p is determined by satisfying the boundary condition given by

$$\hat{\theta} \times \nabla \times \bar{\bar{\Gamma}}(\mathbf{R}, \mathbf{R}') = 0 \tag{4.164}$$

which yields

$$\hat{\theta} \times \mathbf{N}_{e0\nu}^{(4)}(\mathbf{R}) = 0. \tag{4.165}$$

Therefore, ν is determined from the solutions to

$$P_\nu(\cos\theta_0) = 0. \tag{4.166}$$

Hence, the electric field is given by,

$$\mathbf{E}(\mathbf{R}) = 2\pi V ka \sin\theta_0 \sum_\nu \frac{\mathbf{N}_{e0\nu}^{(4)}(\mathbf{R})}{\Omega_{0\nu}}[-j_\nu(ka)]\frac{d}{d\theta}P_\nu(\cos\theta_0). \tag{4.167}$$

We are interested in the far field. Therefore, only the transverse components are needed. These are given by

$$\mathbf{N}_{e0\nu}^{(4)}(\mathbf{R}) \cdot (\bar{\bar{I}} - \hat{R}\hat{R}) = \hat{\theta}\frac{(kRh_\nu^{(2)}(kR))'}{kR}\frac{d}{d\theta}P_\nu(\cos\theta). \tag{4.168}$$

For these boundary conditions, the normalization factor is given by

$$\Omega_{0\nu} = \sin\theta_0 \frac{2\pi}{jk}\frac{\nu(\nu+1)}{2\nu+1}\frac{d}{d\theta}P_\nu(\cos\theta_0)\frac{d}{d\nu}P_\nu(\cos\theta_0). \tag{4.169}$$

Evaluating the large argument form of the Hankel function according to the results given by Equations (4.72)-(4.73). and recalling that

$$j_\nu(x) = \sqrt{\frac{\pi}{2x}} J_{\nu+1/2}(x), \tag{4.170}$$

and after making the appropriate substitutions, the expression becomes

$$E_\theta(R) = E_0 \sum_\nu j^\nu \frac{2\nu+1}{\nu(\nu+1)} J_{\nu+1/2}(ka) \frac{\frac{d}{d\theta} P_\nu(\cos\theta)}{\frac{d}{d\nu} P_\nu(\cos\theta_0)} \tag{4.171}$$

where

$$E_0 = Vka\sqrt{\frac{\pi}{2ka}} \frac{e^{-jkR}}{jR}. \tag{4.172}$$

This expression matches that given in both in [3] and [34]. A pattern has been calculated for $ka = \pi, \theta_0 = 165°$ which duplicates that given in [3]. The comparison of the previous result with that found using the present work is shown in Figure 25. In addition, a radiation pattern has been plotted for the case when $ka = 10$ and $\theta_0 = 170°$. This plot agrees with that given in [35] and therefore supports their contention that some of the figures shown in [3] are in error. The comparison of the previous result and that found using the present work is shown in Figure 26.

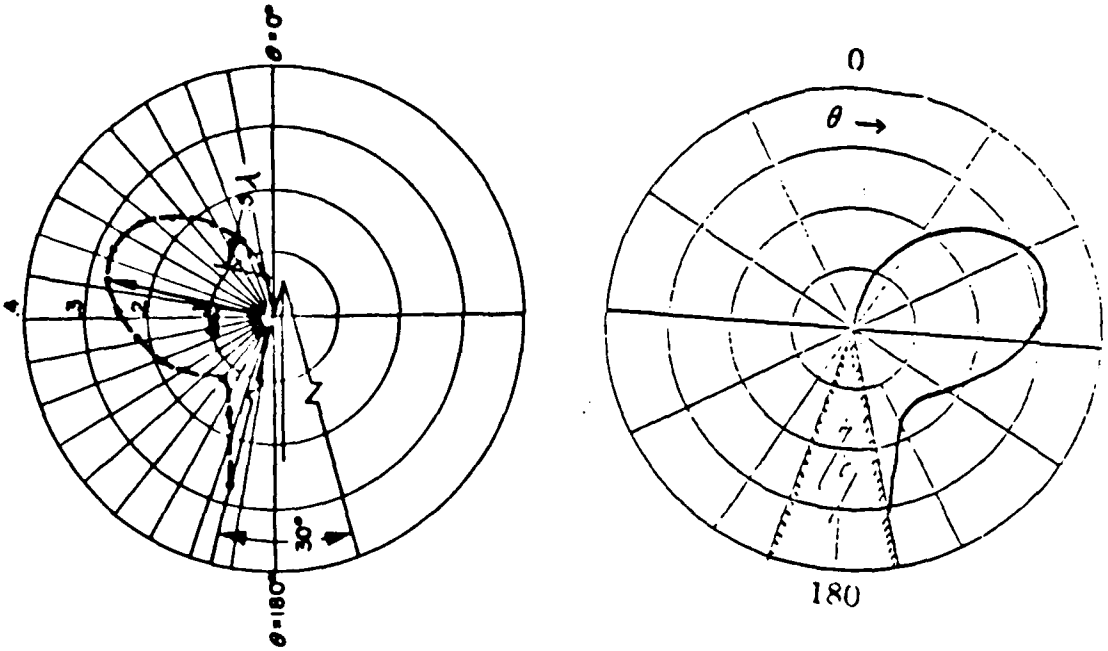

Figure 25: Comparison of Radiation Pattern for Circumferential Slot at $ka = \pi$ and $\theta_0 = 165°$ from [3]

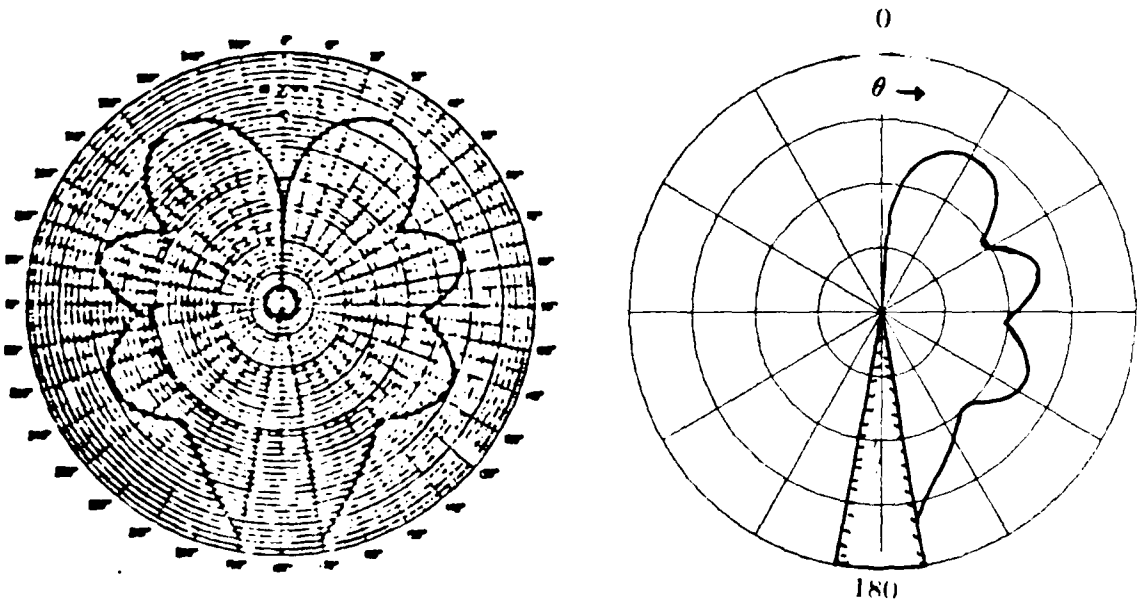

Figure 26: Comparison of Radiated Pattern for Circumferential Slot at $ka = 10$ and $\theta_0 = 170°$ from [35]

CHAPTER V

SUMMARY AND CONCLUSIONS

This dissertation has endeavored to determine an expression for the plane wave fields scattered by a fully illuminated, semi-infinite, perfectly conducting cone such that it remains valid throughout the region exterior to the cone. To this end, a uniform asymptotic representation based on the physical optics (PO) approximation was developed. Using these expressions, a UTD tip diffracted field was determined. With the use of PO, however, comes the inherent shortfalls. Namely, the fact that PO does not satisfy the proper boundary conditions, and that it does not properly model the tip discontinuity. In spite of these shortcomings, the results are very accurate as seen in comparison with the rigorous asymptotic solution for the narrow angle cone given in [5]. Although the present analysis was performed for the semi-infinite cone, it is also valid for the finite cone since high frequency diffraction is a local phenomenon. Recall that the previous GTD solution for the RCS of the flat-backed cone [10] had not accounted for the tip-base interaction. To verify the validity of the UTD tip diffracted field given in the present work, it is shown that when it is included in the previous GTD solution for the RCS of a finite flat-backed cone [10], then it serves to correct the long-standing discrepancy between calculation and measurement. Although the application of the UTD tip diffracted field was concentrated on the scattering problem, it is intimately related to the radiation problem through reciprocity. It could be used

equally well to determine the fields radiated by an antenna on the cone surface.

For the case of axial incidence, the actual tip current and the GO based current were compared and it was shown that the two currents are very similar in this case. Since the dominant term from the eigenfunction expansion for the current exhibits the proper singularity at the tip, and the GO current dominates far from the tip, it is felt that the matching of these two currents in their respective regions by a transition function with a proper agrument could provide a better model for the actual current. The fields from this current could be evaluated using the method given in Chapter III.

The necessary computer routines for determining the eigenvalues associated with the exact eigenfunction solution for the cone problem, as well as the computer routines needed to calculate the associated Legendre polynomials evaluated at these eigenvalues have been written and tested by computing the far fields radiated by a circumferential slot on the cone. In performing this check, the results were used to verify that some of the plots previously published in [3] are in error.

There are several recommendations for future research. Now that the form of the tip surface wave is better understood, a hybrid MM/GTD analysis could be undertaken to further refine the tip diffraction mechanism along the cone surface. Also, ways to modify the PO solution to enforce the boundary conditions could be investigated. The case when the cone is not fully illuminated needs to be investigated also. In this case, the creeping wave in the shadowed region of the surface needs to be accounted for, and the range of PO integration which is dictated by the limits of the lit region on the surface must be modified via Fock theory. In addition, the PO correction based on the dominant term of the exact eigenfunction could be tested and improved upon. The availability of the computer routines required to calculate the exact eigenfunction solution enlarges the possibilities for

AD-A172 838 A HIGH FREQUENCY ANALYSIS OF ELECTROMAGNETIC PLANE WAVE 2/2
SCATTERING BY A F (U) AIR FORCE INST OF TECH
WRIGHT-PATTERSON AFB OH K D TROTT 1986
UNCLASSIFIED AFIT/CI/NR-86-186D F/G 20/6 NL

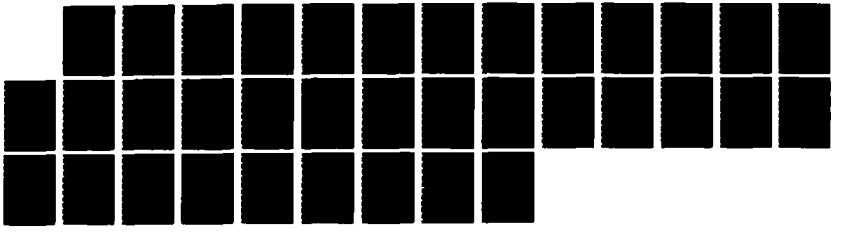

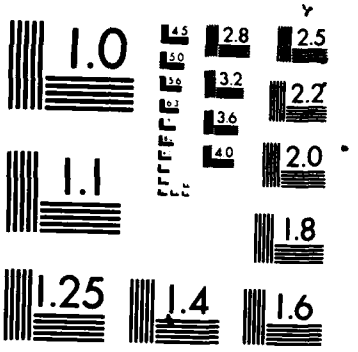

research that integrates this eigenfunction solution with high frequency techniques. Last, but not least, the asymptotic evaluation over the azimuth variable (ϕ') in the development of a UTD solution as in Chapter III should be investigated. This was investigated in a cursory manner; however, there were some problems, and due to time constraints, not completed. One should be able to determine the stationary phase contribution that is the source of the reflected field.

APPENDIX A

EVALUATION OF TERMS IN THE UNIFORM SADDLE POINT INTEGRATION

A.1 INTRODUCTION

In this appendix, the terms required to evaluate the uniform saddle point integral are shown.

A.2 DERIVATION AND EVALUATION OF TERMS

Transforming to the steepest descent path required that

$$G(s) = \mathbf{f}(r', \phi')\frac{dr'}{ds}. \tag{A.1}$$

This must be evaluated at s=0 and $s = s_a$. For s=0

$$G(0) = \mathbf{f}(r_s, \phi')\frac{dr'}{ds}\,]_{r'=r_s}, \tag{A.2}$$

and for $s = s_a$

$$G(s_a) = \mathbf{f}(0, \phi')\frac{dr'}{ds}\,]_{r'=0}, \tag{A.3}$$

but

$$\mathbf{f}(0, \phi') = 0. \tag{A.4}$$

Hence,

$$G(s_a) = 0. \tag{A.5}$$

Turning to H(s), recall that

$$H(s) = \frac{d}{ds}\left[\frac{G(s) - G(0)}{s}\right] = \frac{sG'(s) - G(s) + G(0)}{s^2}. \qquad (A.6)$$

Evaluating this at $s = 0$, yields $\frac{0}{0}$. Applying L'Hospital's rule yields

$$H(0) = \frac{G''(0)}{2}. \qquad (A.7)$$

When evaluated at $s = s_a$,

$$H(s_a) = \frac{s_a G'(s_a) + G(0)}{{s_a}^2}. \qquad (A.8)$$

In general,

$$G'(s) = \mathbf{f}(r', \phi')\frac{d^2r'}{ds^2} + \mathbf{f}'(r', \phi')(\frac{dr'}{ds})^2 \qquad (A.9)$$

$$G''(s) = \mathbf{f}(r', \phi')\frac{d^3r'}{ds^3} + 3\mathbf{f}'(r', \phi')\frac{d^2r'}{ds^2}\frac{dr'}{ds} + \mathbf{f}''(r', \phi')(\frac{dr'}{ds})^3 \qquad (A.10)$$

The next task is to determine the expressions for the differentials above. Recall that the transformation was given by

$$q(r', \phi') = q(r_s, \phi') - s^2 \qquad (A.11)$$

This is used to derive the expressions for the differentials in terms of q and its derivatives. For now, the explicit r' and ϕ' dependence will be dropped.

Starting with this expression and taking derivatives, a system of equations is set up that can be solved for the required differentials. This system will be used differently depending upon whether it is evaluated at $r' = 0$ or $r' = r_s$.

$$-2s = q'\frac{dr'}{ds} \qquad (A.12)$$

$$-2 = q''(\frac{dr'}{ds})^2 + q'\frac{d^2r'}{ds^2} \qquad (A.13)$$

$$0 = q'''(\frac{dr'}{ds})^3 + 3q''\frac{dr'}{ds}\frac{d^2r'}{ds^2} + q'\frac{d^3r'}{ds^3} \qquad (A.14)$$

$$0 = q^{iv}(\frac{dr'}{ds})^4 + 6q'''(\frac{dr'}{ds})^2\frac{d^2r'}{ds^2} + q''\left[3(\frac{d^2r'}{ds^2})^2 + 4\frac{dr'}{ds}\frac{d^3r'}{ds^3}\right] + q'\frac{d^4r'}{ds^4} \qquad (A.15)$$

Recall that $q'(r_s, \phi') = 0$, evaluating these for $r' = r_s$, yields

$$\frac{dr'}{ds}\,]_{r=r_s} = \sqrt{\frac{-2}{q''(r_s)}} \tag{A.16}$$

$$\frac{d^2r'}{ds^2}\,]_{r=r_s} = \frac{2}{3}\frac{q'''(r_s)}{[q''(r_s)]^2} \tag{A.17}$$

$$\frac{d^3r'}{ds^3}\,]_{r=r_s} = \frac{1}{2[q''(r_s)]^2}\sqrt{\frac{-2}{q''(r_s)}}\left[q^{iv} - \frac{5}{3}\frac{[q'''(r_s)]^2}{q''(r_s)}\right] \tag{A.18}$$

These are then used in the expressions for G(0) and H(0). These are now given by

$$G(0) = \mathbf{f}(r_s)\sqrt{\frac{-2}{q''(r_s)}} \tag{A.19}$$

and

$$H(0) = \frac{1}{2}\left(\frac{-2}{q''(r_s)}\right)^{3/2}\left[\mathbf{f}''(r_s) - \mathbf{f}'(r_s)\frac{q'''(r_s)}{q''(r_s)} + \frac{1}{4}\mathbf{f}(r_s)\left[\frac{5}{3}\left[\frac{q'''(r_s)}{q''(r_s)}\right]^2 - \frac{q^{iv}(r_s)}{q''(r_s)}\right]\right]. \tag{A.20}$$

Turning to those evaluated at s_a, one obtains

$$\frac{dr'}{ds}\,]_{r'=0} = \frac{-2s_a}{q'(0)}. \tag{A.21}$$

It has already been shown that $G(s_a) = 0$, Next, $G'(s_a)$ is determined. Recall

$$G'(s) = \mathbf{f}(r', \phi')\frac{d^2r'}{ds^2} + \mathbf{f}'(r', \phi')(\frac{dr'}{ds})^2, \tag{A.22}$$

and since $\mathbf{f}(0) = 0$,

$$G'(s_a) = 4\frac{\mathbf{f}'(0){s_a}^2}{[q'(0)]^2}. \tag{A.23}$$

Lastly,

$$G''(s_a) = \mathbf{f}''(0, \phi')(\frac{dr'}{ds})^3 + 3\mathbf{f}'(0, \phi')\frac{d^2r'}{ds^2}\frac{dr'}{ds} \tag{A.24}$$

where the differentials are also evaluated at $r' = 0$. Therefore, expressions are needed for this case. One should note that if the function q is expanded in a

Taylor series about r_s, it can be shown that as $r_s \to 0$, the differentials for the $r' = 0$ case, which are shown below, reduce to those given for $r' = r_s$.

$$\frac{dr'}{ds}\Big|_{r'=0} = -\frac{2s_a}{q'(0)} \tag{A.25}$$

$$\frac{d^2r'}{ds^2}\Big|_{r'=0} = -\frac{2}{[q'(0)]^3}\left\{2{s_a}^2 q''(0) + [q'(0)]^2\right\} \tag{A.26}$$

$$\frac{d^3r'}{ds^3}\Big|_{r'=0} = \frac{4}{[q'(0)]^3}\left\{2{s_a}^3\frac{q'''(0)}{q'(0)} - 6{s_a}^3\left[\frac{q''(0)}{q'(0)}\right]^2 - 3s_a q''(0)\right\} \tag{A.27}$$

Expressions for the phase functions used in the differentials are needed. Moreover, the expressions for $\mathbf{f}$, $\mathbf{f}'$, and $\mathbf{f}''$ are needed. Beginning with the phase functions. These are given by

$$q(r') = r'\cos\gamma - \sqrt{r^2 + r'^2 - 2rr'\cos\varsigma} \tag{A.28}$$

$$q'(r') = \cos\gamma - \frac{r' - r\cos\varsigma}{\sqrt{r^2 + r'^2 - 2rr'\cos\varsigma}} \tag{A.29}$$

$$q''(r') = \frac{-r^2(1-\cos^2\varsigma)}{(r^2 + r'^2 - 2rr'\cos\varsigma)^{3/2}} \tag{A.30}$$

$$q'''(r') = \frac{3r^2(r' - r\cos\varsigma)(1-\cos^2\varsigma)}{(r^2 + r'^2 - 2rr'\cos\varsigma)^{5/2}} \tag{A.31}$$

$$q^{iv}(r') = \frac{3r^2(1-\cos^2\varsigma)}{(r^2 + r'^2 - 2rr'\cos\varsigma)^{7/2}}\left[r^2(1 - 5\cos^2\varsigma) + 8rr'\cos\varsigma - 4r'^2\right] \tag{A.32}$$

Evaluating these at $r' = 0$ and $r' = r_s$ yields

$$q(0) = -r \tag{A.33}$$

$$q(r_s) = r\cos(\varsigma + \gamma) \tag{A.34}$$

$$q'(0) = \cos\varsigma + \cos\gamma \tag{A.35}$$

$$q'(r_s) = 0 \tag{A.36}$$

$$q''(0) = -\frac{\sin^2\varsigma}{r} \tag{A.37}$$

$$q''(r_s) = -\frac{1}{r}\frac{\sin^3\gamma}{\sin\varsigma} \tag{A.38}$$

$$q'''(0) = -3\frac{\cos\varsigma\sin^2\varsigma}{r^2} \tag{A.39}$$

$$q'''(r_s) = \frac{3}{r^2}\frac{\cos\gamma\sin^4\gamma}{\sin^2\varsigma} \tag{A.40}$$

$$q^{iv}(r_s) = \frac{-3}{r^3}\frac{\sin^5\gamma}{\sin^3\varsigma}[4\cos^2\gamma - \sin^2\gamma] \tag{A.41}$$

These could also be found by noting that when $r_s = 0$, then $\varsigma + \gamma = \pi$. Substituting this into the equations for $r' = r_s$ the values reduce to those shown for $r = 0$.

To find G(0) and H(0) we need

$$\frac{q'''(r_s)}{q''(r_s)} = -3\cos\gamma\frac{\sin\gamma}{r\sin\varsigma} \tag{A.42}$$

and

$$\frac{q^{iv}(r_s)}{q''(r_s)} = 3\frac{\sin^2\gamma}{r^2\sin^2\varsigma}[4\cos^2\gamma - \sin^2\gamma] \tag{A.43}$$

Therefore G(0) and H(0) are given by

$$G(0) = \mathbf{f}(r_s)\sqrt{\frac{2r\sin\varsigma}{\sin^3\gamma}} \tag{A.44}$$

and

$$H(0) = \frac{1}{2}\left(\frac{2r\sin\varsigma}{\sin^3\gamma}\right)^{3/2}\left[\mathbf{f}''(r_s) + 3\cos\gamma\frac{\sin\gamma}{r\sin\varsigma}\mathbf{f}'(r_s) + \frac{3}{4}\frac{\sin^2\gamma}{r^2\sin^2\varsigma}\mathbf{f}(r_s)\right]. \tag{A.45}$$

The remaining task is the derivation of the expressions for f and its derivatives. Recall that

$$\mathbf{f}(r',\phi') = -r'\frac{Y_0\sin\alpha}{2\pi R}(jk + \frac{1}{R})\hat{R}\times(\hat{x}\sin\alpha - \hat{z}\cos\alpha\cos\phi'). \tag{A.46}$$

Since

$$\hat{R} = \frac{\mathbf{R}}{R}, \tag{A.47}$$

we write

$$\mathbf{f}(r',\phi') = \mathbf{g}(r') \times \mathbf{h}(\phi'), \tag{A.48}$$

where

$$\mathbf{g}(r') = p(r')\mathbf{R}, \tag{A.49}$$

with

$$p(r') = -r' \frac{Y_0 \sin\alpha}{2\pi R^2}(jk + \frac{1}{R}), \tag{A.50}$$

and

$$\mathbf{h}(\phi') = \hat{x}\sin\alpha - \hat{z}\cos\alpha\cos\phi'. \tag{A.51}$$

Taking derivatives of $\mathbf{f}$ requires

$$\mathbf{f}'(r',\phi') = \frac{d}{dr'}\left[\mathbf{g}(r') \times \mathbf{h}(\phi')\right] \tag{A.52}$$

and

$$\mathbf{f}''(r',\phi') = \frac{d^2}{dr'^2}\left[\mathbf{g}(r') \times \mathbf{h}(\phi')\right]. \tag{A.53}$$

Since $\mathbf{h}(\phi')$ is not a function of r',

$$\mathbf{f}'(r',\phi') = \mathbf{g}'(r') \times \mathbf{h}(\phi'). \tag{A.54}$$

Similarly,

$$\mathbf{f}''(r',\phi') = \mathbf{g}''(r') \times \mathbf{h}(\phi'). \tag{A.55}$$

Recall that

$$\mathbf{g}(r') = p(r')\mathbf{R}. \tag{A.56}$$

Therefore,

$$\mathbf{g}'(r') = p'(r')\mathbf{R} + p(r')\frac{\partial \mathbf{R}}{\partial r'} \tag{A.57}$$

and

$$\mathbf{g}''(r') = p''(r')\mathbf{R} + 2p'(r')\frac{\partial \mathbf{R}}{\partial r'} + p(r')\frac{\partial^2 \mathbf{R}}{\partial r'^2}, \tag{A.58}$$

where

$$\frac{\partial \mathbf{R}}{\partial r'} = -\frac{\partial \mathbf{r}'}{\partial r'} = -\hat{r'} \tag{A.59}$$

and

$$\frac{\partial^2 \mathbf{R}}{\partial r'^2} = 0. \tag{A.60}$$

Also recall that

$$\mathbf{R} = \mathbf{r} - \mathbf{r}' = r\hat{r} - r'\hat{r'}. \tag{A.61}$$

Hence,

$$\mathbf{g}(r') = rp(r')\hat{r} - r'p(r')\hat{r'} \tag{A.62}$$

$$\mathbf{g}'(r') = rp'(r')\hat{r} - [p(r') + r'p'(r')]\hat{r'} \tag{A.63}$$

and

$$\mathbf{g}''(r') = rp''(r')\hat{r} - [2p'(r') + r'p''(r')]\hat{r'}. \tag{A.64}$$

Combining these quantities yields

$$\mathbf{f}(r', \phi') = rp(r')\mathbf{V_1} + r'p(r')\mathbf{V_2} \tag{A.65}$$

$$\mathbf{f}'(r', \phi') = rp'(r')\mathbf{V_1} + [p(r') + r'p'(r')]\mathbf{V_2} \tag{A.66}$$

$$\mathbf{f}''(r', \phi') = rp''(r')\mathbf{V_1} + [2p'(r') + r'p''(r')]\mathbf{V_2} \tag{A.67}$$

where

$$\mathbf{V_1} = \hat{r} \times \mathbf{h}(\phi') \tag{A.68}$$

$$\mathbf{V_2} = -\hat{r'} \times \mathbf{h}(\phi') \tag{A.69}$$

and

$$-\hat{r'} = -\hat{x}\sin\alpha\cos\phi' - \hat{y}\sin\alpha\sin\phi' + \hat{z}\cos\alpha. \tag{A.70}$$

After performing the vector operations

$$\mathbf{V_1} = \hat{\theta}\sin\alpha\sin\phi + \hat{\phi}\left[\sin\alpha\cos\theta\cos\phi + \cos\alpha\sin\theta\cos\phi'\right] \tag{A.71}$$

and

$$\begin{aligned}\mathbf{V_2} &= \hat{r}\left[\sin^2\alpha\cos\theta\sin\phi' + \sin\alpha\cos\alpha\sin\theta\left(\sin\phi - \cos\phi'\sin(\phi-\phi')\right)\right] \\ &\quad \hat{\theta}\left[-\sin^2\alpha\sin\theta\sin\phi' + \sin\alpha\cos\alpha\cos\theta\left(\sin\phi - \cos\phi'\sin(\phi-\phi')\right)\right] \\ &\quad \hat{\phi}\sin\alpha\cos\alpha\left[\cos\phi - \cos\phi'\cos(\phi-\phi')\right] \qquad \text{(A.72)}\end{aligned}$$

Now the expressions for p and its derivatives are shown. These will be evaluated at the saddle point $r' = r_s$, and the end point $r' = 0$.

$$p(0) = 0 \qquad \text{(A.73)}$$

$$p(r_s) = -Y_0\frac{\sin\alpha}{2\pi}r_s\frac{\sin^2\gamma}{r^2\sin^2\varsigma}\left[jk + \frac{\sin\gamma}{r\sin\varsigma}\right] \qquad \text{(A.74)}$$

$$p'(0) = -Y_0\frac{\sin\alpha}{2\pi r^2}\left[jk + \frac{1}{r}\right] \qquad \text{(A.75)}$$

$$\begin{aligned}p'(r_s) &= -Y_0\frac{\sin\alpha}{2\pi}\frac{\sin^2\gamma}{r^2\sin^2\varsigma}\left\{\left[jk + \frac{\sin\gamma}{r\sin\varsigma}\right]\right. \\ &\quad \left. -r_s\cos\gamma\frac{\sin\gamma}{r\sin\varsigma}\left[2jk + 3\frac{\sin\gamma}{r\sin\varsigma}\right]\right\} \qquad \text{(A.76)}\end{aligned}$$

$$p''(0) = -Y_0\frac{\sin\alpha}{\pi r^3}\left[2jk + \frac{3}{r}\right]\cos\varsigma \qquad \text{(A.77)}$$

$$\begin{aligned}p''(r_s) &= -Y_0\frac{\sin\alpha}{2\pi}\frac{\sin^3\gamma}{r^3\sin^3\varsigma}\left\{-\left[2jk + 3\frac{\sin\gamma}{r\sin\varsigma}\right]\left[2\cos\gamma + r_s\frac{\sin\gamma}{r\sin\varsigma}\sin^2\gamma\right]\right. \\ &\quad \left. +3r_s\left[2jk + 4\frac{\sin\gamma}{r\sin\varsigma}\right]\cos^2\gamma\frac{\sin\gamma}{r\sin\varsigma}\right\} \qquad \text{(A.78)}\end{aligned}$$

As with the phase functions, when $r_s = 0$, then $\varsigma + \gamma = \pi$. Under this condition, the expressions evaluated at $r' = r_s$ yield the expressions for those evaluated at $r = 0$.

The expressions in this appendix were used to program the results of Chapter III for the uniform PO solution.

APPENDIX B

VECTOR WAVE FUNCTIONS

B.1 INTRODUCTION

In this appendix the derivation for the vector wave functions in the general case is shown. This is then specialized to the conical geometry.

B.2 GENERAL CASE

In a source–free region of space, both **E** and **H** fields satisfy the vector Helmholtz equation given by

$$\nabla \times (\nabla \times \left\{ \begin{array}{c} \mathbf{E} \\ \mathbf{H} \end{array} \right\}) - k^2 \left\{ \begin{array}{c} \mathbf{E} \\ \mathbf{H} \end{array} \right\} = 0 \qquad (B.1)$$

As shown in [8,20,21], the vector wave functions are also solutions to the vector Helmholtz equation and are defined by

$$\mathbf{M}_q = \nabla \times \psi_q \mathbf{f} = \frac{1}{k} \nabla \times \mathbf{N}_q \qquad (B.2)$$

$$\mathbf{N}_q = \frac{1}{k} \nabla \times \mathbf{M}_q \qquad (B.3)$$

where ψ_q is the solution to the scalar wave equation

$$(\nabla^2 + k^2)\psi_q = 0 \qquad (B.4)$$

and **f** is a vector function to be determined. Substituting Equation (B.2) into Equation (B.1) yields

$$\nabla \times (\nabla \times \nabla \times \psi \mathbf{f} - k^2 \psi \mathbf{f}) = 0 \qquad (B.5)$$

By definition, $\nabla \times \nabla u = 0$; therefore, we define

$$\nabla \times \nabla \times \psi \mathbf{f} - k^2 \psi \mathbf{f} = \nabla u \tag{B.6}$$

Using a vector identity, yields

$$\nabla \times (\nabla \times \psi \mathbf{f}) = \nabla \times (\nabla \psi \times \mathbf{f} + \psi \nabla \times \mathbf{f}) \tag{B.7}$$

Looking at each term separately, it can be seen that

$$\nabla \times (\nabla \psi \times \mathbf{f}) = (\mathbf{f} \cdot \nabla) \nabla \psi - \nabla^2 \psi \mathbf{f} - \nabla \psi \cdot \nabla \mathbf{f} + \nabla \psi (\nabla \cdot \mathbf{f}) \tag{B.8}$$

and

$$\nabla \times (\psi \nabla \times \mathbf{f}) = \nabla \psi \times (\nabla \times \mathbf{f}) + \psi (\nabla \times \nabla \times \mathbf{f}) \tag{B.9}$$

After expanding Equation (B.9), adding it to Equation (B.8), and performing a fair amount of vector algebra

$$\nabla \times (\nabla \times \psi \mathbf{f}) = \nabla (\nabla \cdot \psi \mathbf{f}) - \mathbf{f} \nabla^2 \psi - \psi \nabla^2 \mathbf{f} - 2 (\nabla \psi \cdot \nabla) \mathbf{f} \tag{B.10}$$

Manipulating Equation (B.6) a little further, yields

$$-\psi \nabla^2 \mathbf{f} - 2 (\nabla \cdot \nabla) \mathbf{f} - \mathbf{f} (\nabla^2 \psi + k^2 \psi) = \nabla (u - \nabla \cdot \psi \mathbf{f}) \tag{B.11}$$

Recall that ψ satisfies the scalar wave equation given in Equation (B.4); therefore,

$$\psi \nabla^2 \mathbf{f} + 2 (\nabla \psi \cdot \nabla) \mathbf{f} = \nabla U \tag{B.12}$$

where

$$U = \nabla \cdot \psi \mathbf{f} - u \tag{B.13}$$

is another scalar function.

In order to arbitrarily satisfy the boundary conditions for different ψ, ψ and $\mathbf{f}$ must be independent. Since ψ and $\mathbf{f}$ must be independent, closer examination of Equation (B.12) yields two equations

$$\nabla^2 \mathbf{f} = 0 \tag{B.14}$$

and

$$2(\nabla\psi \cdot \nabla)\mathbf{f} = \nabla U \tag{B.15}$$

Equation (B.15) can be expanded for the x component of **f** as

$$\frac{\partial\psi}{\partial x}\frac{\partial f_x}{\partial x} + \frac{\partial\psi}{\partial y}\frac{\partial f_x}{\partial y} + \frac{\partial\psi}{\partial z}\frac{\partial f_x}{\partial z} = \frac{1}{2}\frac{\partial U}{\partial x} \tag{B.16}$$

The expansions for f_y and f_z follow similarly. For independence we need f_x to be only a function of x, f_y to be only a function of y, and f_z to be only a function of z. Also needed is $U = 2c\psi$. Enforcing the preceeding conditions leaves

$$\frac{\partial f_x}{\partial x} = c \tag{B.17}$$

$$\frac{\partial f_y}{\partial y} = c \tag{B.18}$$

$$\frac{\partial f_z}{\partial z} = c \tag{B.19}$$

The solutions to these equations yields

$$f_x = cx + a_1 \tag{B.20}$$

$$f_y = cy + a_2 \tag{B.21}$$

$$f_z = cz + a_3 \tag{B.22}$$

Combined into vector notation, this yields

$$\mathbf{f} = c(x\hat{x} + y\hat{y} + z\hat{z}) + a_1\hat{x} + a_2\hat{y} + a_3\hat{z} \tag{B.23}$$

which can be written

$$\mathbf{f} = c\mathbf{R} + a\hat{a} \tag{B.24}$$

It can be shown that

$$\nabla \times \mathbf{f} = 0 \tag{B.25}$$

$$\nabla \cdot \mathbf{f} = 3c \tag{B.26}$$

and

$$(\nabla\psi \cdot \nabla)\mathbf{f} = c\nabla\psi \tag{B.27}$$

These relationships, along with Equations (B.4) and (B.24) yield the general form of the vector wave functions as

$$\mathbf{M} = -\mathbf{f} \times \nabla\psi \tag{B.28}$$

$$\mathbf{N} = k\psi\mathbf{f} + \frac{1}{k}\nabla(c\psi + \mathbf{f} \cdot \nabla\psi) \tag{B.29}$$

In the next section, the general result is specialized to spherical coordinates and the spherical vector wave functions are used to form the conical vector wave functions.

B.3 CONICAL VECTOR WAVE FUNCTIONS

The cone can be described in the spherical coordinate system; therefore, we specialize the vector wave functions to spherical coordinates. For this case $\mathbf{f} = \mathbf{R}$; therefore, $c = 1$ and $a = 0$. The spherical vector wave functions form the basis for the conical vector wave functions [32]. There are a few differences. One is that the degree of the Legendre polynomials is fractional and determined by the boundary conditions of the cone. Another is the orthogonality relationships of the auxiliary vector wave functions. The vector wave functions for this case have the form

$$\mathbf{M_q} = -\mathbf{R} \times \nabla\psi_q \tag{B.30}$$

$$\mathbf{N_q} = k\nabla\mathbf{R} + \frac{1}{k}\nabla(\psi_q + \mathbf{R} \cdot \nabla\psi_q) \tag{B.31}$$

In [22], it is shown that the ψ_q that satisfies the scalar wave equation in spherical coordinates when the origin is included is given by

$$\psi_q^{(l)}(\rho) = z_\nu^{(l)}(\rho)Y_q(\theta, \phi) \tag{B.32}$$

where $\rho = kR$ and $q = \begin{matrix} e \\ o \end{matrix} m\nu$.

The $Y_q(\theta,\phi)$ are called the tesseral or sectoral harmonics and are defined by

$$Y_q(\theta,\phi) = P_\nu^m(\cos\theta)\left\{ \begin{matrix} \cos m\phi \\ \sin m\phi \end{matrix} \right\} \tag{B.33}$$

where the $P_\nu^m(\cos\theta)$ are the associated Legendre polynomials of degree ν, and order m. The $z_\nu^{(l)}(\rho)$ are given by

$$z_\nu^{(l)}(\rho) = \begin{cases} j_\nu(\rho) & \text{spherical Bessel function} \quad ; \text{l=1} \\ y_\nu(\rho) & \text{spherical Neuman function} \quad ; \text{l=2} \\ h_\nu^{(1)}(\rho) & \text{spherical Hankel function, 1st kind} \quad ; \text{l=3} \\ h_\nu^{(2)}(\rho) & \text{spherical Hankel function, 2nd kind} \quad ; \text{l=4} \end{cases} \tag{B.34}$$

The e and o refer to even or odd behavior in the ϕ variation described by the bracketed terms. The e goes with the top term and the o with the bottom.

Substituting Equations (B.32) and (B.33) into Equations (B.30) and (B.31) and performing a wealth of manipulations, we finally have the form of the conical vector wave functions given by

$$\mathbf{M}_q^{(l)}(\rho) = z_\nu^{(l)}(\rho)\mathbf{m}_q(\theta,\phi) \tag{B.35}$$

$$\mathbf{N}_q^{(l)}(\rho) = \frac{z_\nu^{(l)}(\rho)}{\rho}\mathbf{l}_q(\theta,\phi) + \frac{(\rho z_\nu^{(l)}(\rho))'}{\rho}\hat{R}\times\mathbf{m}_q(\theta,\phi) \tag{B.36}$$

where $\rho = kR$, $q = \begin{matrix} e \\ o \end{matrix} m\nu$ and

$$\mathbf{l}_q(\theta,\phi) = \nu(\nu+1)Y_q(\theta,\phi)\hat{R} \tag{B.37}$$

$$\mathbf{m}_q(\theta,\phi) = \mp m\frac{P_\nu^m(\cos\theta)}{\sin\theta}\left\{ \begin{matrix} \sin m\phi \\ \cos m\phi \end{matrix} \right\}\hat{\theta} - \frac{d}{d\theta}P_\nu^m(\cos\theta)\left\{ \begin{matrix} \cos m\phi \\ \sin m\phi \end{matrix} \right\}\hat{\phi} \tag{B.38}$$

The $\mathbf{l}_q$, $\mathbf{m}_q$, and $\hat{R}\times\mathbf{m}_q$ are called the auxiliary vector wave functions. These functions exhibit surface orthogonality over a spherical sector. That is, for the spherical sector defined by $d\Omega = \sin\theta d\theta d\phi$ and $\Omega = \left\{ \begin{matrix} 0 \le \phi \le 2\pi \\ 0 \le \theta \le \theta_0 \end{matrix} \right\}$ we have integrals of the form

$$\int_0^{2\pi}\int_0^{\theta_0}\left[\frac{m^2}{\sin^2\theta}P_\nu^m(\cos\theta)P_{\nu'}^m(\cos\theta)\left\{ \begin{matrix} \sin^2 m\phi \\ \cos^2 m\phi \end{matrix} \right\}\right.$$
$$\left. + \frac{d}{d\theta}P_\nu^m(\cos\theta)\frac{d}{d\theta}P_{\nu'}^m(\cos\theta)\left\{ \begin{matrix} \cos^2 m\phi \\ \sin^2 m\phi \end{matrix} \right\}\right]\sin\theta d\theta d\phi \tag{B.39}$$

Due to the orthogonality of the Legendre polynomials (shown in Appendix D), there is only a value when $\nu = \nu'$. This yields

$$\frac{2\pi}{\epsilon_m}\int_0^{\theta_0}\left\{\left[\frac{m}{\sin\theta}P_\nu^m(\cos\theta)\right]^2+\left[\frac{d}{d\theta}P_\nu^m(\cos\theta)\right]^2\right\}\sin\theta d\theta=\frac{2\pi}{\epsilon_m}\nu(\nu+1)I_{m\nu} \tag{B.40}$$

where

$$I_{m\nu}=\int_0^{\theta_0}[P_\nu^m(\cos\theta)]^2\sin\theta d\theta \tag{B.41}$$

and

$$\epsilon_m=\begin{cases}1 & m=0\\ 2 & m\neq 0\end{cases} \tag{B.42}$$

The relation used in (B.40) was found in [32]. Using the integrals above, the following orthogonality relationships hold for the auxiliary conical wave functions:

$$\int\int_\Omega \mathbf{m}_{p'}\cdot\mathbf{m}_p d\Omega =$$

$$\int\int_\Omega(\hat{R}\times\mathbf{m}_{p'})\cdot(\hat{R}\times\mathbf{m}_p)d\Omega=\begin{cases}0 & p\neq p'\\ \frac{2\pi}{\epsilon_m}\nu(\nu+1)I_{m\nu} & p=p'\end{cases} \tag{B.43}$$

and

$$\int\int_\Omega \mathbf{l}_{p,}\cdot\mathbf{l}_p d\Omega=\begin{cases}0 & p\neq p'\\ \frac{2\pi}{\epsilon_m}\nu^2(\nu+1)^2I_{m\nu} & p=p'\end{cases} \tag{B.44}$$

Moreover, these functions are vectorially orthogonal; therefore, they are mutually orthogonal. That is, any integral of two distinct auxiliary vector wave functions over a spherical sector is zero.

As described in [21,23], the vector wave functions, as shown, are complete with respect to **E** and **H** in a source-free region. If a volume source density were to be included, the $\mathbf{L}_q$ functions would be needed to be included [21]; however, these will not be discussed in this paper.

In general,

$$\mathbf{E}=\sum_p a_p\mathbf{M}_p+\sum_q b_q\mathbf{N}_q \tag{B.45}$$

Using $\nabla \times \mathbf{E} = -j\omega\mu\mathbf{H}$ along with Equations (B.2) and (B.3) yields

$$\mathbf{H} = jY_0 \sum_p a_p \mathbf{N}_p + jY_0 \sum_q b_q \mathbf{M}_q \qquad (B.46)$$

From these, the representations for the surface currents can be found as well.

In the next appendix, the dyadic Green's function for conical systems will be derived in terms of these vector wave functions.

APPENDIX C

DYADIC GREEN'S FUNCTION

C.1 INTRODUCTION

In this appendix the dyadic Green's function is derived and shown how it is applied in deriving the solution.

C.2 DERIVATION OF DYADIC GREEN'S FUNCTION

The most general way to relate vector fields to vector sources is with the dyadic Green's function. The dyadic Green's function satisfies the inhomogenous vector differential equation shown below.

$$\nabla \times \nabla \times \overline{\overline{\Gamma}}(\mathbf{R},\mathbf{R}') - k^2\overline{\overline{\Gamma}}(\mathbf{R},\mathbf{R}') = -\overline{\overline{I}}\delta(\mathbf{R}-\mathbf{R}') \qquad (C.1)$$

where $\overline{\overline{I}}$ is the identity dyad. Letting $\overline{\overline{\Gamma}}(\mathbf{R},\mathbf{R}') \cdot \hat{a} = \mathbf{G}(\mathbf{R},\mathbf{R}')$ to simplify the derivation of Equation (C.1), we have the following equation,

$$\nabla \times \nabla \times \mathbf{G}(\mathbf{R},\mathbf{R}') - k^2\mathbf{G}(\mathbf{R},\mathbf{R}') = -\hat{a}\delta(\mathbf{R}-\mathbf{R}') \qquad (C.2)$$

Recall, the vector wave functions are orthogonal functions that form a complete set over the solutions to source- free vector wave equation. As in [24], surfaces as shown in Figure 27 are defined.

For $R > R'$, outgoing waves that will satisfy the radiation condition on Σ, the surface at ∞ are needed. Therefore,

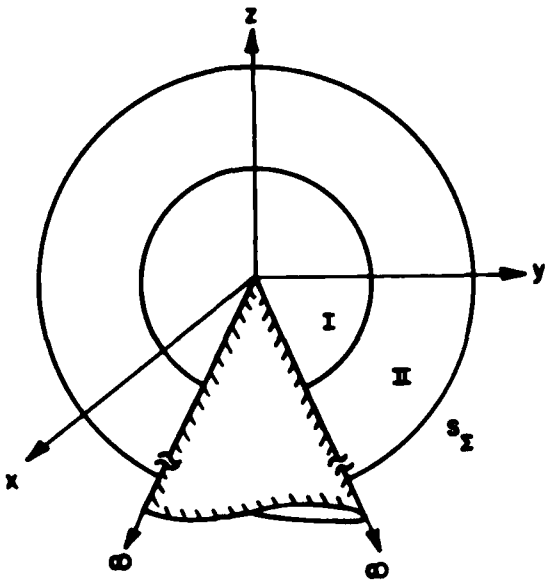

Figure 27: Geometry used in Derivation of Vector Wave Function

$$\mathbf{G^{II}}(\mathbf{R},\mathbf{R}') = \sum_p \mathbf{a_p^M}(\mathbf{R}')\mathbf{M}_p^{(4)}(\mathbf{R}) + \sum_q \mathbf{a_q^N}(\mathbf{R}')\mathbf{N}_q^{(4)}(\mathbf{R})$$
$$R > R' \qquad \text{(C.3)}$$

where the (4) implies that the radial behavior is described by the spherical Hankel function. This function satisfies the radiation condition for the time convention $(e^{j\omega t})$.

Green's second identity for vectors is given via the Divergence Theorem as

$$\int_V \{\mathbf{A}\cdot(\nabla\times\nabla\times\mathbf{B}) - \mathbf{B}\cdot(\nabla\times(\nabla\times\mathbf{A})\}dV$$
$$= \int_{S+\Sigma}\{\mathbf{B}\times(\nabla\times\mathbf{A}) - \mathbf{A}\times(\nabla\times\mathbf{B})\}\cdot\hat{n}dS \qquad \text{(C.4)}$$

As discussed, functions will be chosen such they that satisfy the radiation condition on Σ; that is, the integral over the surface Σ at ∞ will go to zero.

Substituting $\mathbf{B} = \mathbf{M}_{p'}^{(1)}$ and $\mathbf{A} = \mathbf{G}^{II}$ into Equation (C.4) with $\mathbf{R}''$ as a dummy variable yields

$$\begin{aligned}
&\int_V \{\mathbf{G}^{\mathbf{I/II}}(\mathbf{R}'',\mathbf{R}') \cdot (\nabla'' \times \nabla'' \times \mathbf{M}_{p'}^{(1)}(\mathbf{R}'')) \\
&-\mathbf{M}_{p'}^{(1)}(\mathbf{R}'') \cdot (\nabla'' \times \nabla'' \times \mathbf{G}^{\mathbf{I/II}}(\mathbf{R}'',\mathbf{R}'))\} dV'' \\
&= \int_S \{\mathbf{M}_{p'}^{(1)}(\mathbf{R}'') \times \nabla'' \times \mathbf{G}^{\mathbf{II}}(\mathbf{R}'',\mathbf{R}') \\
&-\mathbf{G}^{\mathbf{II}}(\mathbf{R}'',\mathbf{R}') \times \nabla'' \times \mathbf{M}_{p'}^{(1)}(\mathbf{R}'')\} \cdot \hat{R} dS'' \qquad \text{(C.5)}
\end{aligned}$$

Note, in the volume integral, both $\mathbf{G}^{\mathbf{I}}$ and $\mathbf{G}^{\mathbf{II}}$ appear. The volume integrand can be simplified since $\mathbf{M}_{p'}^{(1)}(\mathbf{R}'')$ satisfies the vector Helmholtz equation. Therefore, the left hand side becomes

$$-\int_V \mathbf{M}_{p'}^{(1)}(\mathbf{R}'') \cdot \{\nabla'' \times \nabla'' \times \mathbf{G}^{\mathbf{I/II}}(\mathbf{R}'',\mathbf{R}') - k^2 \mathbf{G}^{\mathbf{I/II}}(\mathbf{R}'',\mathbf{R}')\} dV'' \qquad (C.6)$$

but by Equation (C.3), the bracketed term can be replaced by $\hat{a}\delta(\mathbf{R}'' - \mathbf{R}')$ and

$$\int_V \mathbf{M}_{p'}^{(1)}(\mathbf{R}'') \cdot \hat{a}\delta(\mathbf{R}'' - \mathbf{R}') dV'' = \mathbf{M}_{p'}^{(1)}(\mathbf{R}') \cdot \hat{a} \qquad (C.7)$$

by the sifting property of the delta function. Since $R < R'$ includes the origin, we chose $\mathbf{M}_{p'}^{(1)}(\mathbf{R}')$ which is finite there since the (1) implies that the radial behavior is described by a spherical Bessel function which is bounded at the origin. Equation (C.5) can be rewritten as

$$\begin{aligned}
&\int_S \{\mathbf{M}_{p'}^{(1)}(\mathbf{R}'') \times \nabla'' \times \mathbf{G}^{\mathbf{II}}(\mathbf{R}'') - \mathbf{G}^{\mathbf{II}}(\mathbf{R}'') \times \nabla'' \times \mathbf{M}_{p'}^{(1)}(\mathbf{R}'')\} \cdot \hat{R} dS'' \\
&= \mathbf{M}_{p'}^{(1)}(\mathbf{R}') \cdot \hat{a} \qquad \text{(C.8)}
\end{aligned}$$

Substituting the series representation of $\mathbf{G}^{\mathbf{II}}$ from (C.3), and recalling the relationship between $\mathbf{M}$ and $\mathbf{N}$ given in Equations (B.2) and (B.3) where ∇'' operates only on double primed variables, yields

$$k \sum_p \int_S \mathbf{a}_{\mathbf{p}}^{\mathbf{M}}(\mathbf{R}') \{\mathbf{M}_{p'}^{(1)}(\mathbf{R}'') \times \mathbf{N}_p^{(4)}(\mathbf{R}'') - \mathbf{M}_p^{(4)}(\mathbf{R}'') \times \mathbf{N}_{p'}^{(1)}(\mathbf{R}'')\} \cdot \hat{R} dS''$$

$$+k\sum_q \int_S \mathbf{a}_\mathbf{q}^\mathbf{N}(\mathbf{R}')\{\mathbf{M}_{p'}^{(1)}(\mathbf{R}'') \times \mathbf{M}_q^{(4)}(\mathbf{R}'') - \mathbf{N}_q^{(4)}(\mathbf{R}'') \times \mathbf{N}_{p'}^{(1)}(\mathbf{R}'')\} \cdot \hat{R} dS''$$
$$= \mathbf{M}_{p'}^{(1)}(\mathbf{R}') \cdot \hat{a} \qquad (C.9)$$

After expressing **M** and **N** functions in terms of their auxiliary wave functions, and performing the indicated dot and cross products, applying the orthogonality relationships what remains is

$$k\sum_p \int_S \mathbf{a}_\mathbf{p}^\mathbf{M}(\mathbf{R}')\{j_\nu(\rho)\frac{(\rho h_\nu^{(2)}(\rho))'}{\rho} - h_\nu^{(2)}(\rho)\frac{(\rho j_\nu(\rho))'}{\rho}\}\mathbf{m}_{p'} \cdot \mathbf{m}_p R^2 d\Omega'' \qquad (C.10)$$

The terms within the bracket that involve the spherical Hankel and Bessel functions can be rewritten as

$$j_\nu(\rho)h_\nu^{(2)'}(\rho) - h_\nu^{(2)}(\rho)j_\nu'(\rho) = W(j_\nu(\rho), h_\nu^{(2)}(\rho)) = -\frac{j}{\rho^2} \qquad (C.11)$$

where W is the Wronskian of those two functions. Recall that $\rho = kR$, therefore Equation (C.10) becomes

$$-\frac{j}{k}\sum_p a_p^M \int_{\Omega''} \mathbf{m}_{p'} \cdot \mathbf{m}_p d\Omega'' = \mathbf{M}_{p'}^{(1)}(\mathbf{R}') \cdot \hat{a} \qquad (C.12)$$

For $p = \begin{matrix} e \\ o \end{matrix} m\nu$ this yields

$$a_p^M \frac{2\pi\nu(\nu+1)}{jk\epsilon_m} I_{m\nu} = \mathbf{M}_p^{(1)}(\mathbf{R}') \cdot \hat{a} \qquad (C.13)$$

From this, $\mathbf{a}_\mathbf{p}^\mathbf{M}(\mathbf{R}')$ can be solved for and given by

$$\mathbf{a}_\mathbf{p}^\mathbf{M}(\mathbf{R}') = \frac{jk\epsilon_m}{2\pi\nu(\nu+1)I_{m\nu}} \mathbf{M}_p^{(1)}(\mathbf{R}') \cdot \hat{a} \qquad (C.14)$$

To find the expression for $\mathbf{a}_\mathbf{q}^\mathbf{N}(\mathbf{R}')$, we would proceed in a similar manner using $\mathbf{N}_{q'}^{(1)}(\mathbf{R}'')$ in Equation (C.5) with $q = \begin{matrix} e \\ o \end{matrix} m\gamma$. This yields

$$\mathbf{a}_\mathbf{q}^\mathbf{N}(\mathbf{R}') = \frac{jk\epsilon_m}{2\pi\gamma(\gamma+1)I_{m\gamma}} \mathbf{N}_q^{(1)}(\mathbf{R}') \cdot \hat{a} \qquad (C.15)$$

Substituting this into Equation (C.3), we get the representation for $\mathbf{G}^{\mathbf{II}}$ from which we can easily see the form of $\overline{\overline{\Gamma}}$ as

$$\overline{\overline{\Gamma}}(\mathbf{R},\mathbf{R}') = \sum_p \frac{\mathbf{M}_p^{(4)}(\mathbf{R})\mathbf{M}_p^{(1)}(\mathbf{R}')}{\Omega_p} + \sum_q \frac{\mathbf{N}_q^{(4)}(\mathbf{R})\mathbf{N}_q^{(1)}(\mathbf{R}')}{\Upsilon_q} \qquad R > R' \qquad \text{(C.16)}$$

Moreover, due to symmetry of the Green's function,

$$\overline{\overline{\Gamma}}(\mathbf{R},\mathbf{R}') = \sum_p \frac{\mathbf{M}_p^{(1)}(\mathbf{R})\mathbf{M}_p^{(4)}(\mathbf{R}')}{\Omega_p} + \sum_q \frac{\mathbf{N}_q^{(1)}(\mathbf{R})\mathbf{N}_q^{(4)}(\mathbf{R}')}{\Upsilon_q} \qquad R < R' \qquad \text{(C.17)}$$

where

$$\Omega_p = \frac{2\pi}{jk\epsilon_m}\nu(\nu+1)I_{m\nu} \qquad (C.18)$$

$$\Upsilon_q = \frac{2\pi}{jk\epsilon_m}\gamma(\gamma+1)I_{m\gamma} \qquad (C.19)$$

and $I_{m\alpha}$ is defined by Equation (B.41) in Appendix B. Note, the notation above is defined in the following way,

$$\mathbf{M}_p^{(l)}(\mathbf{R})\mathbf{M}_p^{(l)}(\mathbf{R}') = \mathbf{M}_{em\nu}^{(l)}(\mathbf{R})\mathbf{M}_{em\nu}^{(l)}(\mathbf{R}') + \mathbf{M}_{om\nu}^{(l)}(\mathbf{R})\mathbf{M}_{om\nu}^{(l)}(\mathbf{R}') \qquad (C.20)$$

and similarly for $\mathbf{N}_q^{(l)}(\mathbf{R})\mathbf{N}_q^{(l)}(\mathbf{R}')$.

Equations (C.16) and (C.17) combine to define the dyadic Green's function for all R. The indexes p and q are assumed to be distinct. This is required to satisfy the boundary conditions on the cone. The Green's function was chosen such that

$$\hat{n}' \times \overline{\overline{\Gamma}}(\mathbf{R}',\mathbf{R})\Big]_{\theta=\theta_0} = -\hat{\theta} \times \overline{\overline{\Gamma}}(\mathbf{R}',\mathbf{R})\Big]_{\theta=\theta_0} = 0 \qquad (C.21)$$

Since p and q are distinct,

$$\hat{\theta} \times \mathbf{M}_p^{()}(\mathbf{R})\Big]_{\theta=\theta_0} = \hat{\theta} \times \mathbf{N}_q^{()}(\mathbf{R})\Big]_{\theta=\theta_0} = 0 \qquad (C.22)$$

where $p = \begin{matrix} e \\ o \end{matrix} m\nu$ and $q = \begin{matrix} e \\ o \end{matrix} m\gamma$. Evaluating these, it can be seen that

$$\hat{\theta} \times \mathbf{M}_p^{()}(\mathbf{R})\Big]_{\theta_0} = 0 \tag{C.23}$$

requires

$$\frac{d}{d\theta} P_\nu^m(\cos\theta)\Big]_{\theta=\theta_0} = 0 \tag{C.24}$$

and that

$$\hat{\theta} \times \mathbf{N}_q^{()}(\mathbf{R})\Big]_{\theta=\theta_0} = 0 \tag{C.25}$$

requires

$$P_\gamma^m(\cos\theta_0) = 0 \tag{C.26}$$

The ν and γ are the theta eigenvalues. Their determination is an important part of the problem. Appendix D discusses this problem.

In the next section, the procedure for using dyadic Green's functions to determine the solution is discussed.

C.3 SOLUTION WITH DYADIC GREEN'S FUNCTIONS

The next step is to show how the dyadic Green's function is used in the solution. As in [25], beginning with the equation

$$\nabla' \times \nabla' \times \mathbf{E}(\mathbf{R}') - k^2\mathbf{E}(\mathbf{R}') = -j\omega\mu\mathbf{J}_\mathbf{v}(\mathbf{R}') \tag{C.27}$$

We introduce $\overline{\overline{\Gamma}}$ that satisfies the primed version of equation (C.1) and is given by

$$\nabla' \times \nabla' \times \overline{\overline{\Gamma}}(\mathbf{R}', \mathbf{R}) - k^2\overline{\overline{\Gamma}}(\mathbf{R}', \mathbf{R}) = -\hat{a}\delta(\mathbf{R}' - \mathbf{R}) \tag{C.28}$$

Green's second identity for tensors is then applied. This yields

$$\begin{aligned} \int_V \{\mathbf{E}(\mathbf{R}') \cdot (\nabla' \times \nabla' \times \overline{\overline{\Gamma}}(\mathbf{R}', \mathbf{R})) - (\nabla' \times \nabla' \times \mathbf{E}(\mathbf{R}')) \cdot \overline{\overline{\Gamma}}(\mathbf{R}', \mathbf{R})\} dV' \\ = \oint_{S+\Sigma} \{\hat{n}' \times (\nabla' \times \mathbf{E}(\mathbf{R}')) \cdot \overline{\overline{\Gamma}}(\mathbf{R}', \mathbf{R}) dS' \\ + \oint_{S+\Sigma} (\hat{n}' \times \mathbf{E}(\mathbf{R}')) \cdot (\nabla' \times \overline{\overline{\Gamma}}(\mathbf{R}', \mathbf{R}))\} dS' \end{aligned} \tag{C.29}$$

Solving for $\nabla' \times \nabla' \times \overline{\overline{\Gamma}}(\mathbf{R}', \mathbf{R})$ using Equation (C.28) and using Equation (C.27), to solve for $\nabla' \times \nabla' \times \mathbf{E}(\mathbf{R}')$ and substituting into the volume integral yields

$$-\int_V \mathbf{E}(\mathbf{R}')\delta(\mathbf{R}' - \mathbf{R})dV' + j\omega\mu \int_V \mathbf{J_v}(\mathbf{R}') \cdot \overline{\overline{\Gamma}}(\mathbf{R}', \mathbf{R})dV' \qquad (C.30)$$

Also used are the following relationships

$$\nabla' \times \mathbf{E}(\mathbf{R}') = -j\omega\mu\mathbf{H}(\mathbf{R}') \qquad (C.31)$$

$$\hat{n'} \times \mathbf{H}(\mathbf{R}') = \mathbf{J_s}(\mathbf{R}') \qquad (C.32)$$

$$\hat{n'} \times \mathbf{E}(\mathbf{R}') = -\mathbf{K_s}(\mathbf{R}') \qquad (C.33)$$

The integrals over Σ vanish since $\mathbf{E}(\mathbf{R}')$ and $\overline{\overline{\Gamma}}(\mathbf{R}', \mathbf{R})$ satisfy the radiation condition. Using the sifting property of the delta function, and the above relationships Equation (C.29) can be written as

$$\left.\begin{array}{ll} \mathbf{R} & \text{in V} \\ \mathbf{R} & \text{not in V} \end{array} \quad \begin{array}{l} \mathbf{E}(\mathbf{R}) \\ 0 \end{array}\right\} = j\omega\mu \int_V \mathbf{J_v}(\mathbf{R}') \cdot \overline{\overline{\Gamma}}(\mathbf{R}', \mathbf{R})dV'$$
$$+j\omega\mu \oint_S \mathbf{J_s}(\mathbf{R}') \cdot \overline{\overline{\Gamma}}(\mathbf{R}', \mathbf{R})dS' + \oint_S \mathbf{K_s}(\mathbf{R}') \cdot (\nabla' \times \overline{\overline{\Gamma}}(\mathbf{R}', \mathbf{R}))dS' \qquad (C.34)$$

The form of the equation can be modified depending upon the material boundary conditions, and the symmetry properties of the Green's function. This is described in many places, particularly in [21,25,26]. The Green's function satisfies the following symmetry relation

$$\tilde{\overline{\overline{\Gamma}}}(\mathbf{R}', \mathbf{R}) = \overline{\overline{\Gamma}}(\mathbf{R}, \mathbf{R}') \qquad (C.35)$$

In some applications the volume integral is treated as, $\mathbf{E^i}$, the incident field. For that case, the expression for the scattered field, $\mathbf{E^s}$, is given in terms of the induced surface currents $\mathbf{J_s}(\mathbf{R})$ and $\mathbf{K_s}(\mathbf{R})$.

In the next appendix, the derivations of the associated Legendre polynomial expressions used to program these functions are discussed.

APPENDIX D

ASSOCIATED LEGENDRE POLYNOMIALS

D.1 INTRODUCTION

In order to compute the exact solution to the cone problem using the tesseral or sectoral harmonics, we need to be able to calculate the associated Legendre polynomials $P_\nu^m(x)$ for non–integer degree ν. Moreover, in order to determine the required degrees, the solution to the following are required

$$P_\gamma^m(\cos\theta_0) = 0 \tag{D.1}$$

$$\frac{d}{d\theta}P_\nu^m(\cos\theta_0) = 0 \tag{D.2}$$

with $\theta_0 = \pi - \alpha$; where α is the cone half–angle. These are solved as functions of γ and ν respectively. For the case of the cone, these are generally non–integer. This is why a special effort was required to determine a method to evaluate the Legendre polynomials. In this appendix, Γ represents the well known gamma function. We will begin by disscussing the integral representation for the Legendre polynomial.

D.2 INTEGRAL REPRESENTATION

The solution of boundary value problems in the spherical system gives rise to the following differential equation

$$(1-x^2)y'' - 2xy' + \{\nu(\nu+1) - \frac{m^2}{1-x^2}\}y = 0 \tag{D.3}$$

for which one solution is $P_\nu^m(x)$, the associated Legendre polynomial. Many papers have been published that tabulate these for certain values. References used include Hobson [27], Snow [28], Siegel [2], Abramowitz and Stegun [29], McDonald [30], Carrus and Treuenfels [31], Lebedev[18], and the Bateman Manuscript Project [17].

From [17], the following integral is the starting point

$$P_\nu^m(\cos\theta) = \frac{2^m}{\sqrt{\pi}} \frac{1}{(\sin\theta)^m \Gamma(1/2-m)} \int_0^\pi \frac{(\cos\theta + j\sin\theta\cos t)^{\nu+m}}{(\sin t)^{2m}} dt \qquad (D.4)$$

next performing a change of variables and letting

$$e^{jx} = \cos\theta + j\sin\theta\cos t \qquad (D.5)$$

This yields

$$dt = -\frac{e^{jx}}{\sin\theta\sin t} dx \qquad (D.6)$$

and changes the limits from $0 \rightarrow \pi$ to $\theta \rightarrow -\theta$. Solving for $\cos^2 t$, it can be found that $\sin t = \sqrt{1-\cos^2 t}$ and it is given by

$$\sin t = e^{jx/2} \frac{\sqrt{2\cos x - 2\cos\theta}}{\sin\theta} \qquad (D.7)$$

Putting this into equation (D.4) with

$$(\cos\theta + j\sin\theta\cos t)^{\nu+m} = e^{jx(\nu+m)} \qquad (D.8)$$

and noting that $\int_\theta^{-\theta} = -\int_{-\theta}^{\theta}$, yields

$$P_\nu^m(\cos\theta) = \frac{1}{\sqrt{2\pi}} \frac{(\sin\theta)^m}{\Gamma(1/2-m)} \int_{-\theta}^{\theta} \frac{e^{jx(\nu+1/2)}}{(\cos x - \cos\theta)^{m+1/2}} dx \qquad (D.9)$$

This can be simplified further since it is over a symmetric interval. That is, $\int_{-\theta}^{\theta} e^{jx} dx$ goes to $2\int_0^\theta \cos x dx$ since $\int_{-\theta}^{\theta} \sin x dx = 0$. Therefore

$$P_\nu^m(\cos\theta) = \sqrt{\frac{2}{\pi}} \frac{(\sin\theta)^m}{\Gamma(1/2-m)} \int_0^\theta \frac{\cos(\nu+1/2)x}{(\cos x - \cos\theta)^{m+1/2}} dx$$
$$\text{for } 0 < \theta < \pi, \text{ m an integer, } \nu \text{ real.} \qquad (D.10)$$

which is Equation (27) in [17]. However, this integral will have convergence problems for $m > 0$. An improper integral of the form $\int_a^b \frac{1}{x^p} dx$ will converge for $p < 1$, and diverge for $p \geq 1$. In order to avoid this problem, the expression is evaluated at $m = -m$ which yields

$$P_\nu^{-m}(\cos\theta) = \sqrt{\frac{2}{\pi}} \frac{1}{(\sin\theta)^m \Gamma(m+1/2)} \int_0^\theta \frac{\cos(\nu+1/2)x}{(\cos x - \cos\theta)^{1/2-m}} dx \qquad (D.11)$$

but

$$P_\nu^m(\cos\theta) = (-1)^m \frac{\Gamma(\nu+m+1)}{\Gamma(\nu-m+1)} P_\nu^{-m}(\cos\theta) \qquad (D.12)$$

So, in conclusion

$$P_\nu^m(\cos\theta) =$$
$$\sqrt{\frac{2}{\pi}} \frac{\Gamma(\nu+m+1)}{\Gamma(\nu-m+1)} \frac{(-1)^m}{\Gamma(m+1/2)(\sin\theta)^m} \int_0^\theta \frac{\cos(\nu+1/2)x}{(\cos x - \cos\theta)^{1/2-m}} dx$$
$$\text{for } 0 < \theta < \pi, \text{ m an integer, } \nu \text{ real.} \qquad (D.13)$$

which is the expression in [18]. This integral has no convergence problems. When $m = 0$, the exponent is $1/2$, which meets the criteria for convergence. When $m > 0$, the denominator moves into the numerator and it is no longer an improper integral. Although the $m = 0$ case converges, it is slow. To avoid this, a recursion formula found in [18] is used with $m = 0$. This yields

$$P_\nu^0(\cos\theta) = \frac{-1}{\nu(\nu+1)} \left[2\frac{\cos\theta}{\sin\theta} P_\nu^1(\cos\theta) + P_\nu^2(\cos\theta) \right] \qquad (D.14)$$

Another important recursion relation is

$$\frac{d}{d\theta} P_\nu^m(\cos\theta) = \frac{(\nu-m+1)P_{\nu+1}^m(\cos\theta) - (\nu+1)\cos\theta P_\nu^m(\cos\theta)}{\sin\theta} \qquad (D.15)$$

which expresses the derivative of the Legendre polynomial in terms of the polynomials themselves. This expression is used in the determination of the eigenvalues that satisfy Equation (D.2).

In the next section, orthogonality is proven, and the incomplete Legendre integrals is evaluated.

D.3 ORTHOGONALITY AND NORMALIZATION

The cone presents a special problem in terms of the orthogonality relations. As seen in Appendix B,

$$\int_0^{\theta_0} [P_\nu^m(\cos\theta)]^2 \sin\theta d\theta \qquad (D.16)$$

The first thing to do is to prove the original statement of orthogonality that was made in Appendix B. To this end, we begin with the original differential equation for different ν and μ. We will work with the form in terms of the variable x, and then convert to $\cos\theta$. This yields

$$\frac{d}{dx}\left[(1-x^2)\frac{d}{dx}P_\nu^m(x)\right] + \left\{\nu(\nu+1) - \frac{m^2}{1-x^2}\right\} P_\nu^m(x) = 0 \qquad (D.17)$$

and

$$\frac{d}{dx}\left[(1-x^2)\frac{d}{dx}P_\mu^m(x)\right] + \left\{\mu(\mu+1) - \frac{m^2}{1-x^2}\right\} P_\mu^m(x) = 0 \qquad (D.18)$$

After multiplying each equation by the other solution and subtracting, what remains is

$$P_\nu^m(x)P_\mu^m(x) = \frac{d}{dx}\frac{\left[(1-x^2)\left(P_\nu^m(x)\frac{d}{dx}P_\mu^m(x) - P_\mu^m(x)\frac{d}{dx}P_\nu^m(x)\right)\right]}{(\nu-\mu)(\nu+\mu+1)} \qquad (D.19)$$

Next, if integrating from 1 to x_0 in x (equivalent to 0 to θ_0 in theta) yields

$$\int_1^{x_0} P_\nu^m(x)P_\mu^m(x)dx = (1-x^2)\frac{\left(P_\nu^m(x)\frac{d}{dx}P_\mu^m(x) - P_\mu^m(x)\frac{d}{dx}P_\nu^m(x)\right)}{(\nu-\mu)(\nu+\mu+1)}\Bigg]_1^{x_0} \qquad (D.20)$$

When $\nu \neq \mu$, the integral goes to zero at the lower limit because of the $(1-x^2)$ term, and it goes to zero at the upper limit due the boundary conditions. Therefore, orthogonality has been shown.

When $\nu = \mu$ we have a $\frac{0}{0}$ condition. Applying L'Hospital's rule in ν yields

$$\int_1^{x_0} [P_\nu^m(x)]^2 dx = \lim_{\mu \to \nu} (1 - x_0^2) \frac{\left[\frac{\partial}{\partial \nu} P_\nu^m(x_0) \frac{\partial}{\partial x} P_\mu^m(x_0) - P_\mu^m(x_0) \frac{\partial^2}{\partial \nu \partial x} P_\nu^m(x_0) \right]}{2\nu + 1} \tag{D.21}$$

Now performing a change of variables such that

$$x = \cos\theta \tag{D.22}$$

then

$$dx = -\sin\theta \tag{D.23}$$

and

$$\frac{d}{dx} = \frac{-1}{\sin\theta} \frac{d}{d\theta} \tag{D.24}$$

The expressions for the integral are different depending upon which eigenvalues are used. This depends upon which type of boundary condition is satisfied. After performing the substitutions above, the integrals have two forms. When

$$P_\gamma^m(\cos\theta_0) = 0 \tag{D.25}$$

then

$$\int_0^{\theta_0} [P_\gamma^m(\cos\theta_0)]^2 \sin\theta d\theta = \frac{\sin\theta_0}{2\gamma + 1} \frac{\partial}{\partial \gamma} P_\gamma^m(\cos\theta_0) \frac{\partial}{\partial \theta} P_\gamma^m(\cos\theta_0) \tag{D.26}$$

However, when

$$\frac{d}{d\theta} P_\nu^m(\cos\theta_0) = 0 \tag{D.27}$$

the normalization integral becomes

$$\int_0^{\theta_0} [P_\nu^m(\cos\theta)]^2 \sin\theta d\theta = \frac{-\sin\theta_0}{2\nu + 1} P_\nu^m(\cos\theta_0) \frac{\partial^2}{\partial \nu \partial \theta} P_\nu^m(\cos\theta_0) \tag{D.28}$$

For future notational simplicity, define

$$L_\gamma^m(\theta_0) = \frac{\partial}{\partial \gamma} P_\gamma^m(\cos\theta_0) \tag{D.29}$$

$$L_\nu^m(\theta_0) = \frac{\partial^2}{\partial\nu\partial\theta} P_\nu^m(\cos\theta_0) \qquad (D.30)$$

The derivative with respect to theta was done using recursion formulas; however, the derivative with respect to the degree was done using a double precision library subroutine. The expressions are the same as those given in [33]. Moreover, the results check with the tables given in [1].

In the next section, the approach used to determine the particular eigenvalues ν and γ will be discussed.

D.4 EIGENVALUES

The determination of the zeros as shown in Equations (D.1) and (D.2) is a very important aspect of the solution to the cone problem. The solutions to these problems determines over what values the series is summed. There have been several articles published on this subject. In [31], there are tables for both $P_\gamma^m(\cos\theta)$ and $\frac{d}{d\theta}P_\nu^m(\cos\theta)$. The results obtained in this derivation compare very well with those published. Also, in [2], the values of ν and γ that were used in their solution compare very well with ours. To find the zeros begin with Equation (D.13). The leading coefficients will not be zero in the specified range. Therefore, finding the zeros of $P_\gamma^m(\cos\theta)$ amounts to determining where the integral goes to zero. That is,

$$f(\nu, m, \theta) = \int_0^\theta \frac{\cos(\nu + 1/2)x}{(\cos x - \cos\theta)^{1/2-m}} dx = 0 \qquad (D.31)$$

as a function of ν, for a given m and θ.

The determination of the zeros of $\frac{d}{d\theta}P_\nu^m(\cos\theta)$ employs the recursion formula in Equation (D.15). The integral forms from Equation (D.13) were substituted into the recursion expression. After manipulating the integral forms, applying several

gamma function identities and factoring out all common terms, what remains is

$$\frac{d}{d\theta}P_\nu^m(\cos\theta) = \frac{1}{(\sin\theta)^{m+1}}\sqrt{\frac{2}{\pi}}\frac{\Gamma(\nu+m+1)}{\Gamma(\nu-m+1)\Gamma(m+1/2)} \times[(\nu+m+1)I_1-(\nu+1)\cos\theta I_0]=0 \qquad \text{(D.32)}$$

where

$$I_0=\int_0^\theta \frac{\cos(\nu+1/2)x}{(\cos x-\cos\theta)^{1/2-m}}dx \qquad (D.33)$$

$$I_1=\int_0^\theta \frac{\cos(\nu+3/2)x}{(\cos x-\cos\theta)^{1/2-m}}dx \qquad (D.34)$$

As before, the leading coefficients are not zero; therefore, finding the zeros required the solution of

$$(\nu+m+1)I_1-(\nu+1)\cos\theta I_0=0 \qquad (D.35)$$

as a function of ν, for a given m and θ. These results also compared very well with the published values. All of the preceeding integrals were performed using a 32 point Gaussian quadrature routine. The roots were found using existing library subroutines.

In the last section, the method employed to verify the validity of the Legendre function routines is discussed.

D.5 VERIFICATION

In [33], a Wronskian result is given. A more general form of this expression is

$$P_\nu^m(\cos\theta_1)\sin\theta_2\tfrac{d}{d\theta_2}P_\nu^m(\cos\theta_2)-P_\nu^m(\cos\theta_2)\sin\theta_1\tfrac{d}{d\theta_1}P_\nu^m(\cos\theta_1) = \tfrac{2}{\pi}\sin[(\nu-m)\pi]\tfrac{\Gamma(\nu+m+1)}{\Gamma(\nu-m+1)} \qquad \text{(D.36)}$$

Letting $\theta_2=\pi-\theta_1$, then

$$\frac{d}{d\theta_2}P_\nu^m(\cos\theta_2)=-\frac{d}{d\theta_1}P_\nu^m(-\cos\theta_1) \qquad (D.37)$$

Therefore, Equation (D.36) becomes

$$P_\nu^m(\cos\theta_1)\frac{d}{d\theta_1}P_\nu^m(-\cos\theta_1) + P_\nu^m(-\cos\theta_1)\frac{d}{d\theta_1}P_\nu^m(\cos\theta_1)$$
$$= -\frac{2}{\pi}\frac{\sin[(\nu-m)\pi]}{\sin\theta_1}\frac{\Gamma(\nu+m+1)}{\Gamma(\nu-m+1)} \qquad \text{(D.38)}$$

The routines were checked against existing tabulated results; however, for angles and degrees that were not tabulated, Equation (D.38) was used to verify the routines. This, in effect, checked both the routine for $P_\gamma^m(\cos\theta)$ and the routine for $\frac{d}{d\theta}P_\nu^m(\cos\theta)$ simultaneously.

REFERENCES

[1] Siegel, K.M., H.A. Alperin, "Studies in Radar Cross- Sections-III; Scattering by a Cone," UMM 87, Willow Run Research Center, University of Michigan, Jan, 1952.

[2] Siegel, K.M., H.A. Alperin, J.W. Crispin, H.E. Hunter, R.E. Kleinman, W.C. Orthwein, and C.E. Schensted, "Comparison Between Theory and Experiment of Cross- Section of a Cone," UMM 92, Willow Run Research Center, University of Michigan, Feb, 1953.

[3] Bailin, L.L. and Samuel Silver, "Exterior Electromagnetic Boundary Value Problems for Spheres and Cones," *IRE Trans. Antennas and Propagat.*, Vol AP-4, pp. 5-16, Jan, 1956.

[4] Felsen, L.B., "Alternative Representations in Regions Bounded by Spheres, Cones, and Planes," *IRE Trans. Antennas and Propagat.*, Vol AP-5, pp. 109-121, Jan, 1957.

[5] Felsen, L.B., "Plane Wave Scattering by Small Angle Cones," *IRE Trans. Antennas and Propagat.*, Vol AP-5 pp. 121-129, Jan, 1957.

[6] Felsen, L.B., "Asymptotic Expansion of the Diffracted Wave for a Semi-Infinite Cone," *IRE Trans. Antennas and Propagat.*, Vol AP-5, pp. 402-404, Oct, 1957.

[7] Schultz, F.V., G.M. Ruckgaber, J.K. Schindler, and C.C. Rogers, "The Theoretical and Numerical Determination of Radar Cross Section of a Finite Cone," *Proceedings IEEE*, Vol 53, No. 8, pp.1065-1067, August 1965.

[8] Bechtel, M.E., "Application of Geometric Diffraction Theory to Scattering from Cones and Disks," *Proceedings IEEE*, Vol 53, No. 8, pp. 877-882, August 1965.

[9] Senior, T.B.A., P.L.E. Uslenghi, "High Frequency Backscattering from a Finite Cone," *Radio Science*, Vol 6, No. 3, pp. 393-406, Mar 1971.

[10] Burnside, W.D., L.Peters, Jr., "Axial-Radar Cross Section of Finite Cones by the Equivalent Current Concept with Higher Order Diffraction," *Radio Science*, Vol 7, No. 10, pp. 943-948, Oct 1972.

[11] Kouyoumjian, R.G., "The High Frequency Target Strength of Cone Shaped Scatterers, Part I-Flat Backed Cone," Tech Report ESL 4720-1, Aug 1977.

[12] Chan, K.K., L.B. Felsen, A. Hessel, J. Shmoys, "Creeping Waves on a Perfectly Conducting Cone," *IEEE Trans. on Antennas and Propagat.*, Vol AP-25, No. 5, Sept 1977.

[13] Chan, K.K., L.B. Felsen, "Transient and Time Harmonic Diffraction by a Semi-Infinite Cone," *IEEE Trans. on Antennas and Propagat.*, Vol AP-25, No. 6, pp. 802-804, Nov 1977.

[14] Chan, K.K., L.B. Felsen, "Transient and Time Harmonic Dyadic Green's Functions for a Perfectly Conducting Cone," *IEEE Trans. on Antennas and Propagat.*, Vol AP-27, No. 1, Jan 1979.

[15] Wang, D.S., L.N. Medgyesi-Mitschang, "Electromagnetic Scattering from Finite Circular and Elliptical Cones," *IEEE Trans. on Antennas and Propagat.*, Vol Ap-33, No. 5, May 1985.

[16] Mathematical Tables Project, *Tables of Associated Legendre Functions*, New York, Columbia University Press, 1945.

[17] Bateman Manuscript Project, *Higher Transcendental Functions*, Vol I, McGraw-Hill, 1953.

[18] Lebedev, N.N., R.A. Silverman (Ed), *Special Functions and Their Applications*, New York, Dover Pub. Co., 1972.

[19] Kouyoumjian,R.G., and P.H. Pathak, "A Uniform Geometrical Theory of Diffraction for an Edge in a Perfectly Conducting Surface," *Proceedings of the IEEE*, Vol 62, No. 11, Nov, 1974.

[20] Kouyoumjian, R.G., "The Importance of Vector Wave Functions," unpublished notes.

[21] Stratton, J.A., *Electromagnetic Theory*, New York, McGraw-Hill, 1941.

[22] Kouyoumjian, R.G., "Introduction to Vector Wave Functions for Electromagnetic Fields," unpublished notes

[23] Kouyoumjian, R.G., "Spherical Vector Wave Functions," unpublished notes.

[24] Kouyoumjian, R.G., "Solutions for the Dyadic Green's Function," unpublished notes.

[25] Kouyoumjian, R.G.,"Solutions with Dyadic Green's Function," unpublished notes.

[26] Kouyoumjian, R.G.,"Symmetry Properties of Dyadic Green's Function," unpublished notes.

[27] Hobson, E.W., *Spherical and Ellipsoidal Harmonics*, Cambridge University Press, Cambridge England, 1939.

[28] Snow, C., *Hypergeometric and Legendre Functions with Applications to Potential Theory* (NBS Applied Math Series No. 55) Washington, D.C., NBS, 1964.

[29] Abramowitz, M. and I. Stegun, *Handbook of Mathematical Functions* (NBS Applied Math Series No. 55) Washington, D.C., NBS, 1964.

[30] MacDonald, H.M., "Zeros of the Spherical Harmonic $P_n^m(\mu)$ Considered as a Function of n," Proceedings of London Mathematical Society, Vol XXXI, May 1899.

[31] Carrus, P. and C.G. Treuenfels, "Tables of Roots and Incomplete Integrals of Associated Legendre Functions of Fractional Order," Journal of Mathematics and Physics, Vol XXIX, 1950.

[32] Tai, C.T., *Dyadic Green's Function in Electromagnetic Theory*, Intext Educational Pub, 1971.

[33] Bowman, J.J., T.B.A. Senior, P.L.E. Uslenghi (Editors), *Electromagnetic and Acoustic Scattering By Simple Shapes*, Chap. 18, North Holland Pub. Co., Amsterdam, 1969.

[34] Harrington, R.F., *Time-Harmonic Electromagnetic Fields*, McGraw-Hill, New York, 1961.

[35] Pridmore-Brown, D.C., and G.E. Stewart, "Radiation from Slot Antennas on Cones," *IEEE Trans. on Antennas and Propagat.*, Vol AP-20, No. 1, Jan 1972.

[36] Felsen, L.B., and N. Marcuvitz, *Radiation and Scattering of Waves*, Prentice-Hall, New Jersey, 1973.

[37] Goryainov, A.S., "Diffraction of a Plane Electromagnetic Wave Propagating along the Axis of a Cone", Radio Eng Electron No 6, 1961.

[38] Gradshteyn, I.S., and I.M. Ryzhik, *Table of Integrals, Series, and Products*, Academic Press, Inc., New York, 1980.

[39] Molinet, F., Personal Communication.

[40] Pathak, P.H.,"Techniques for High Frequency Problems", Chapter IV in *Handbook of Antenna Theory and Design*, Eds., Y.T. Lo and S.W. Lee, to be published by ITT-Howard W. Sams and Co., Inc.

END

11-86

DTIC